2017-08-01

Miniaturization of Linear Ion Traps and Ion Motion Study in a Toroidal Ion Trap Mass Analyzer

Ailin Li
Brigham Young University

Miniaturization of Linear Ion Traps and Ion Motion Study in a Toroidal Ion Trap Mass Analyzer

Ailin Li

A dissertation submitted to the faculty of
Brigham Young University
in partial fulfillment of the requirements for the degree of

Doctor of Philosophy

Daniel E. Austin, Chair
Matthew C. Asplund
David V. Dearden
Steven R. Goates
Jaron C. Hansen

Department of Chemistry and Biochemistry

Brigham Young University

ABSTRACT

Miniaturization of Linear Ion Traps and Ion Motion Study in a Toroidal Ion Trap Mass Analyzer

Ailin Li
Department of Chemistry and Biochemistry, BYU
Doctor of Philosophy

I describe the miniaturization of a linear-type ion trap mass spectrometer for possible applications in portable chemical analysis, and demonstrate the advantages of using lithographically patterned electrode plates in realizing an ion trap with dimension r_0 less than 1 mm. The focus of the work was to demonstrate the viability and feasibility of the patterned electrode approach to trap miniaturization, and also to discover potential obstacles to its use. Planar ceramic substrates were patterned with metal electrodes using photolithography. Plates that were originally used in a linear trap with a half-spacing (r_0) of 2.19 mm were positioned much closer together such that r_0 = 0.95 mm. A capacitive voltage divider provided different radiofrequency (RF) amplitudes to each electrode, and the capacitor values were adjusted to provide the correct electric field at this closer spacing. Electron ionization mass spectra of toluene and dichloromethane demonstrate instrument performance with better than unit mass resolution. Compared with the larger plate spacing, the signal intensity is reduced, corresponding to the reduced trapping capacity of the smaller device, but the mass resolution of the larger device is retained. A further miniaturized linear ion trap with a half-spacing of 362 μm was designed and tested. A series of obstacles and troubleshooting on ion source, analytical method, and electronics were present. These experiments show promise for further miniaturization using patterned ceramic plates and provide a guide for the ion trap miniaturization. The feasibility of a wire linear ion trap was also demonstrated. Unit mass resolution was obtained, indicating a promise for further optimization and miniaturization of the wire linear ion trap.

In addition to the practical experiments on the miniaturized linear ion traps, I theoretically studied ion motion in the toroidal ion trap using SIMION simulations, which show classical chaotic behavior of single ions. The chaotic motion is a result of the non-linear components of the electric fields as established by the trap electrodes, and not by Coulombic interaction from other ions. The chaotic behavior was observed specifically in the ejection direction of ions located in non-linear resonance bands within and adjacent to the region of stable trapping. The non-linear bands crossing through the stability regions correspond to hexapole resonance conditions, while the chaotic ejection observed immediately adjacent to the stable trapping region corresponds to a “fuzzy” ejection boundary. Fractal-like patterns were obtained in a series of zoomed-in regions of the stability diagram.

Keywords: linear ion trap, miniaturization, toroidal ion trap, non-linear field, chaotic motion, ion trajectory simulation

ACKNOWLEDGEMENTS

I would like to express gratitude to those that have been instrumental to the success in my study and career. In particular, I am grateful for the support of my advisor, Dr. Daniel E. Austin. It has been a precious opportunity for me to be advised by him as an excellent and knowledgeable scientist. His mentorship and advice have been vital in guiding me through my career as a student and researcher.

I also would like to express thanks to my graduate committee members, Dr. Matthew C. Asplund, Dr. David V. Dearden, Dr. Steven R. Goates and Dr. Jaron C. Hansen, for their critical evaluation and high standards during my research and study. They have all aided my education and progress. I am grateful for their willingness to provide assistance to me.

I would like to thank Dr. Aaron R. Hawkins and Dr. Stephen A. Lammert for their enlightened instruction to my research. Dr. Hawkins has helped guide me in learning all I know about ion trap microfabrication. Dr. Lammert provided appreciated consultation and support to my research on ion trap instrumentation and mechanisms. I am grateful for the opportunities for learning and growth that they provided me. They have given me invaluable support and guidance as I have progressed in my career.

I have been fortunate to work with several valued colleagues in this endeavor. These include Dr. Brett J. Hansen, Dr. Qinghao Wu, Dr. Brandon L. Barney, Jessica M. Higgs, Yuan Tian, Sara Pratt, Junting Wang, Andrew T. Powell, Justin Sorensen, Derek Andrew, Trevor Decker, and other friends in both Dr. Austin's group and other groups. Working with these individuals has given me valuable team experience and friendship that always encourage me

during my work and study.

I also would like to thank the staff in the instrument shop in the Department of Chemistry and Biochemistry at Brigham Young University for helping me repair the electric circuits and accessories in the ion trap system. Thanks also to the department for giving me this precious opportunity and support.

Finally, I am particularly grateful for my parents and my husband Zhe Yang. They have been constantly supportive and encouraging during this important time of my life. Their help gives me the focus and motivation to finish this work. This dissertation is dedicated to my parents and my husband.

TABLE OF CONTENTS

LIST OF FIGURES

LIST OF TABLES

1 THEORY, DEVELOPMENT AND MINIATURIZATION OF ION TRAPS

1.1 Quadrupole Ion Traps

The quadrupole ion trap is an extraordinary device that can trap, store and analyze ions using a radiofrequency (RF) electric field. In 1956, the quadrupole ion trap was created by Wolfgang Paul for ion storage use.[1,2] Subsequently, it functioned as a mass analyzer for mass spectrometry, and a variety of improvements were discovered that significantly increased the ion trap performance.[3] In 1984, the ion trap mass spectrometer was commercialized by Finnigan.[4] Commercialized ion traps have been evolving since then, offering many advantages in size, cost, sensitivity, precision, as well as tandem mass spectrometry capabilities.[5,6]

1.1.1 Theory of Quadrupole Ion Trap

The quadrupole ion trap can be used as both an ion storage device and as a mass spectrometer providing considerable mass range and resolution.[7] For instance, as an ion storage device, the quadrupole ion trap can confine charged particles into an electric field for a period of time, allowing the study of ion chemistry and structure elucidation. As a mass spectrometer, the quadrupole ion trap can be used to measure the mass-to-charge ratio of the confined ions for compound identification.

A quadrupole ion trap consists of three electrodes – one ring electrode and two identical end-cap electrodes (Figure 1-1 (a)). The end-cap electrodes contain an aperture on each

electrode center for ion injection and ejection. The electrodes are hyperboloidal with a radial r_0 and axial z_0 dimension, respectively (Figure 1-1 (b)); r_0 is the inner radius of the ring electrode and z_0 is the distance from the trapping center to one of the end-cap electrodes. Ideally, the relationship between the radial and axial dimension should be: $r_0 = 2z_0^2$ (1-1)

(a)

(b)

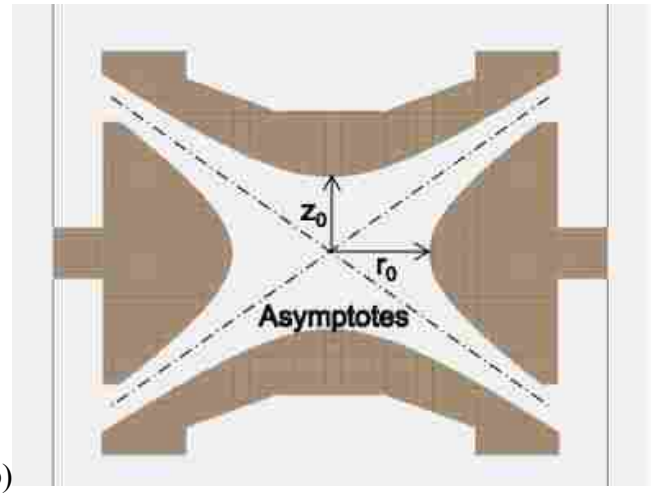

Figure 1-1: (a) Quadrupole ion trap consists of three hyperboloidal electrodes; (b) cross section of quadrupole ion trap (Adapted from Peng, Y. Novel ion trap made using lithographically patterned plates. 2011, BYU Dissertation)

Theoretically, an ideal quadrupole ion trap with perfect quadrupole electric field would have infinite electrodes that ultimately meet infinite asymptotes. However, making unlimited electrodes is impractical.

In quadrupole ion trap operation, a radiofrequency (RF) waveform and DC offset voltage are applied on the ring electrode to create a time-varying electric field. In addition, an alternating current (AC) waveform, or ground could be applied on the end-cap electrodes depending on the analysis method. Consequently, ions are trapped in the trapping region due to a pseudopotential well. In the simplest mass analysis mode, the parameters of the trap (such as RF voltage) are scanned such that ions are sequentially ejected based on the mass-to-charge ratio (m/z). This trapping and analysis are analogous to a bowl filled with layers of liquids of different densities.[8] Upon tilting the bowl, the upper layer liquid, corresponding to the ions of lowest mass-to-charge ratio is poured first from the bowl (Figure 1-2). Continuing with the analogy, the bowl continues to be tilted by ramping the RF amplitude, so that the ions with different mass-to-charge ratio are ejected out of the trap to the detector at different times. Lastly, ion signals are recorded as a mass spectrum.

The ion motion, which is determined by the electric fields, in the quadrupole ion trap is critical to ion storage and mass analysis. The electric field created by the applied RF amplitude results in a set of time-dependent forces that affect the motion of ions. Ions in the quadrupole ion trap experience a strong focusing force. The focusing force increases to restore the ions back to the center region, when ions deviate from the trapping center. The ion motion is generally described by the solutions to the Mathieu equation.[9]

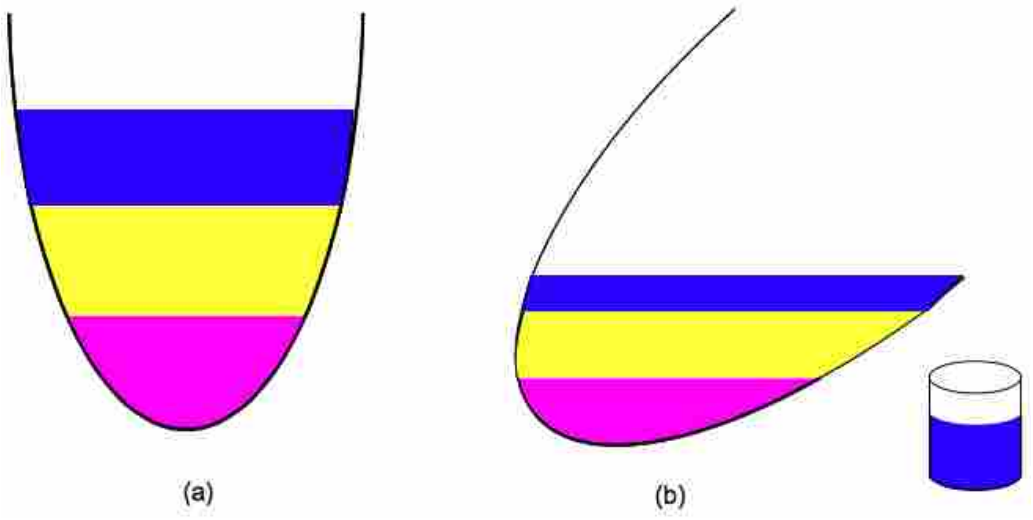

Figure 1-2: (a) A potential well is described by a bowl containing three layers of liquids with different densities, which represents ions with three different *m/z*; (b) ions are mass selectively ejected out of the ion trap (Adapted from March, R. E., An introduction to quadrupole ion trap mass spectrometry. J. Mass Spectrom. 1997, 32, 351-369)

Mathieu equation is

$$\frac{d^2u}{d\xi^2} + (a_u - 2q_u \cos 2\,\xi)\mathrm{u} = 0 \qquad (1\text{-}2)$$

where u is a displacement, ξ is a dimensionless parameter equal to Ωt/2 such that Ω must be a frequency as t is time, and a_u and q_u are additional dimensionless stability parameters.[10]

Essential information concerning ion behavior and trapping conditions is linked to solutions to the Mathieu equation. Additionally, a stability diagram can be plotted showing the limits of trajectory stability. In the equation, a_u and q_u are two dimensionless parameters. In the quadrupole ion trap, ions are ejected in the axial direction (z-direction), so the a_u and q_u can be expressed as a_z and q_z in the Mathieu equation:

$$a_z = \frac{-8eU}{mr_0^2\Omega^2}; \qquad q_z = \frac{4eV}{mr_0^2\Omega^2} \qquad (1\text{-}3)$$

Where e is the electric charge, U is the DC voltage on the end-cap electrodes, m is the mass of the ion in kg, Ω is the frequency of the RF (in rad s^{-1}), and V is the RF amplitude on the ring electrodes ($V_{0\text{-}p}$). The parameters a_z and q_z are plotted in Figure 1-3 as a stability diagram.

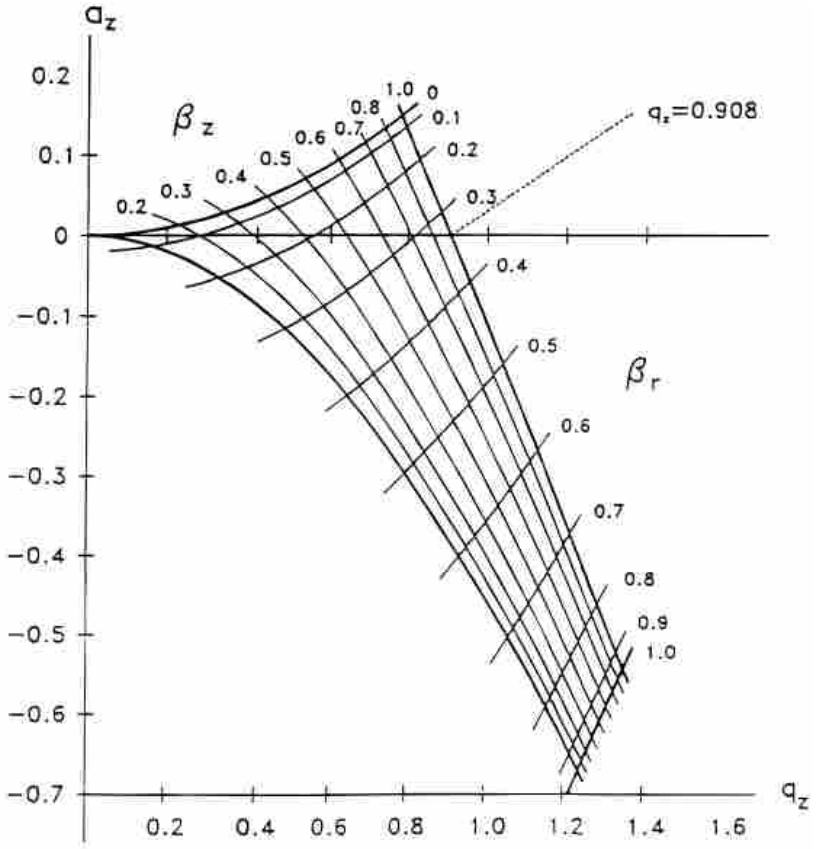

Figure 1-3: Stability diagram in a_z, q_z in the z-direction of 3D quadrupole ion trap. (Adapted from March, R. E., An introduction to quadrupole ion trap mass spectrometry. J. Mass Spectrom. 1997, 32, 351-369)

Although the ideal quadrupole ion trap contains a perfect quadrupole field, a small portion of higher order nonlinear field components exist in any practical quadrupole ion trap for several reasons including electrode truncation, the edge effect of any ejection apertures, and

roughness of the electrode surface.[10-12] To reduce the impact of nonlinear fields on ion trap performance, many modifications on the electrode geometry and placement have been studied. The first modified quadrupole ion trap was made by increasing the distance between end-cap electrodes by 10.6%, which demonstrated a significantly improved mass resolution.[13] In this way, the relationship between r_0 and z_0 is not $r_0 = 2z_0^2$. The a and q solutions to the Mathieu equation can be expressed as:

$$a_z = \frac{-16eU}{m(r_0^2+2z_0^2)\Omega^2}; \qquad q_z = \frac{8eV}{m(r_0^2+2z_0^2)\Omega^2} \tag{1-4}$$

In mass analysis using an ion trap, the trapped ions can be ejected using two methods: mass-selective instability mode and mass-selective resonant ejection mode. In mass-selective instability mode, all the parameters in equation 1-4 are constant for a given ion except the RF amplitude. When the RF amplitude increases linearly, the ion will move to the right boundary of the stability region. Consequently, the ion will be ejected at the boundary, due to its moving out of the stability region, with a fixed q_z value. This mode is also called boundary ejection. Thus, ions are ejected at different times according to their mass-to-charge ratio. However, this method has some limitations, which are limited mass range and somewhat reduced mass resolution compared with resonant ejection.

These conditions can be improved by another scan method: the mass-selective resonant ejection. In the mass-selective resonant ejection, a linearly increasing RF amplitude is applied, similar to the mass-selective instability mode. However, an additional supplementary AC amplitude with a constant frequency is applied to the end-cap electrodes to resonantly excite the ions. When this applied frequency is equal to the natural oscillation frequency of the trapped ions (called the secular frequency), the ion can be ejected resonantly at any value of q. Another

way to operate the mass-selective resonant ejection mode is to use constant RF amplitude with a swept AC frequency. Herein, the q_z value of the ion is constant on the stability diagram, while the AC ejection point moves closer to the ion until resonant excitation occurs. The mass-selective resonant ejection mode greatly increases the mass resolution, but it still has drawbacks. In the ramped RF with constant AC frequency scan, a low-mass-cut-off (LMCO) effect occurs because the ions with small mass-to-charge ratio between the AC resonant point and the boundary would never be able to reach the resonant point. Thus, these low-mass ions are cut-off by the AC resonant line.

An additional scan mode is the reverse scan, which linearly decreases the RF amplitude that moves the ions to the left in the stability region. The reverse scan can only be used in mass-selective resonant ejection mode, since the boundary scan cannot trap the ions out of the boundary at the starting high RF amplitude. In the AC excitation mode, the low-mass-cut-off problem turns into a high-mass-cut-off problem. The reverse scan is not as commonly used as the forward scan.

1.1.2 Ion Trap Development

To improve ion trap performance and meet specific requirements, ion traps have been studied and developed over many decades. Ion trap development has progressed, starting from small trapping capacities, complex and difficult fabrication to large trapping capacity, simple and easy fabrication (Figure 1-4).[14]

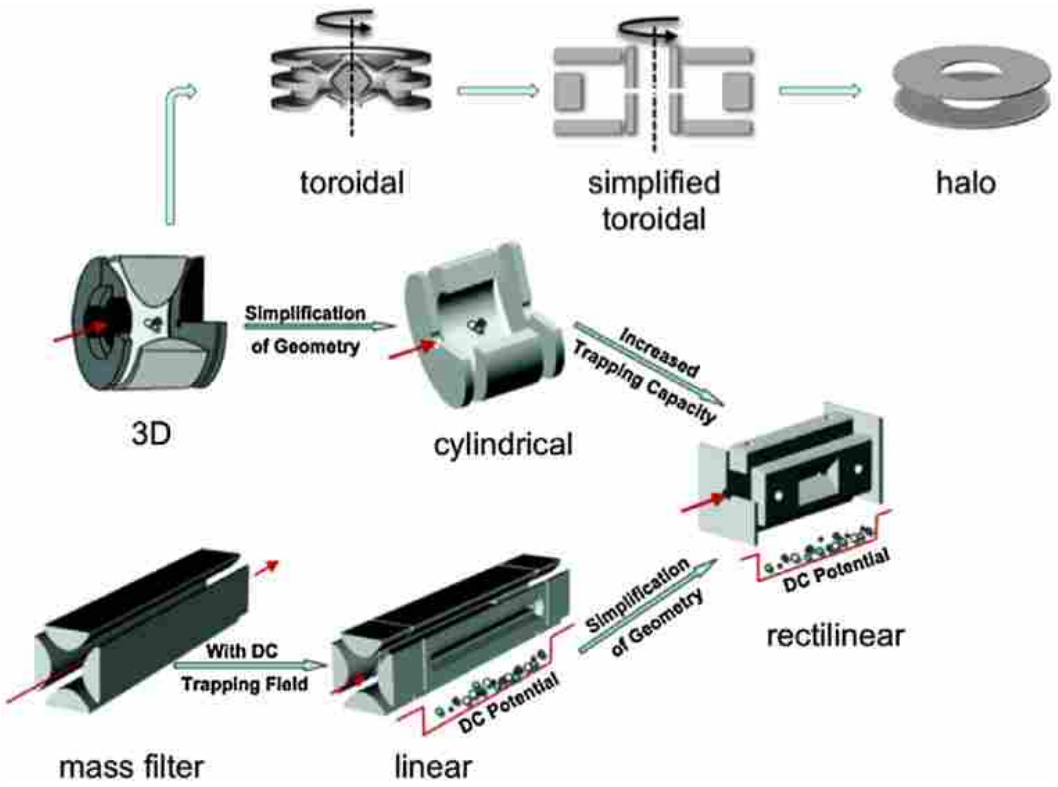

Figure 1-4: Development of ion trap geometry (Adapted from D.T. Snyder, C.J. Pulliam, Z. Ouyang, R.G. Cooks, Miniature and fieldable mass spectrometers: recent advances, Anal. Chem. 2016, 88, 2–29.)

The quadrupole ion trap created by Wolfgang Paul in 1956, consists of three hyperboloid electrodes. It was first used as an ion storage that constant RF amplitude applied on the ring electrode. Subsequently, Todd et al.[15] and March et al.[16] turned a quadrupole ion trap into a mass analyzer. The ion ejection methods used were boundary ejection and resonant ejection.[17] Ions were ejected at different times according to their mass-to-charge ratio by varying the RF or AC waveform where a mass spectrum was obtained from the signal of ion ejection. In addition, tandem mass analysis has been developed using collision-induced dissociation (CID) for further fragmentation of the target ions which provides a way for compound identification.[18]

Based on the 3D quadrupole ion trap (QIT), researchers developed the cylindrical ion trap (CIT) by simplifying the electrode geometry from hyperbolic to a cylindrical shape.[19,20] The ring electrode is cylindrical and the two end-cap electrodes are flat, which are considerably easier to machine, especially at small dimensions.[21-24] However, the electric fields are not as close to quadrupolar, so the CIT has somewhat reduced performance compared with the QIT.

In the ion trap developmental process, the quadrupole mass filter plays an important role as the origin of the linear ion trap.[25,26] The quadrupole mass filter is used for ion guiding and transmission, and consists of four rod-shaped or hyperboloidal electrodes applied with a pair of opposite RF and DC voltages. Therefore, ions of a selected mass range will be able to pass through the mass filter, while ions out of the mass range will be filtered. Since the quadrupole mass filter could not trap nor store the ions, researchers modified the geometry of the mass filter by adding axial DC trapping and created a linear ion trap (LIT).[27,28] Two end-caps were added to two sides of the quadrupole mass filter as a linear ion trap with the purpose of trapping, storing and analyzing mass of ions. Ions are confined to the trapping region with a proper DC voltage applied on the end-caps. Additionally, the RF amplitude was applied to four trapping electrodes for ion trapping as well as an AC waveform for resonant excitation. Two ion ejection slits were fabricated on opposite electrodes for axial ion ejection. In addition, Hager et al.[29] described another ion ejection method for mass analysis using the linear ion trap that can eject ions axially by controlling the voltage on the two end-cap electrodes. Compared with the cylindrical ion trap, the linear ion trap has a long trapping dimension that allows ions to be trapped along a line rather than a small spherical volume as in a 3D ion trap. Therefore, the LIT significantly increases the trapping capacity, intensity, and resolution of mass analysis, and the

space-charge effects are reduced. However, the trapping electrodes are still hyperbolic which may limit reduced-size fabrication.

Ouyang et al. developed the rectilinear ion trap (RIT)[30,31] by simplifying the geometry of the linear ion trap. The hyperbolic electrodes are modified to be planar, and the two end-cap electrodes are replaced using two planar electrodes with a sample inlet/outlet hole on each side, so that the RIT consists of four x-, y-facing electrodes and two facing end-cap electrodes along the z-axis. The RIT has the advantages of both simplicity of CIT and large trapping capacity of LIT. Compared with the CIT, the trapping capacity is 40-fold greater than that of a CIT in the same size scale.[35]

Another trap, the toroidal ion trap was developed from the quadrupole ion trap by rotating the QIT cross section by 360 degrees along an axis outside of the trapping region.[32] The toroidal ion trap has a larger trapping capacity than the 3D QIT, because ions are trapped in the larger toroidal region compared to the center of the quadrupole ion trap, thus, the space charge effect is greatly reduced in mass analysis. Since the electrode geometry of the toroidal ion trap is curved, it provides a compact mass analyzer. A portable gas chromatography-mass spectrometer (GC-MS) has been commercialized by Torion Technologies with good performance.[33] However, the electrode field is complicated due to the curvature in the toroidal ion trap which creates many non-linear electric fields.

1.2 Ion Trap Miniaturization

1.2.1 Significance of Ion Trap Miniaturization

The mass spectrometer is one of the most powerful analytical tools due to its high sensitivity, precision, and compatibility with chromatography.[34-38] Although a mass spectrometer in the laboratory can provide high performance, such instruments are fragile, costly, and are not portable. With the need for rapid analysis in many areas of study, miniaturized mass spectrometers have become more desirable. Portable mass spectrometers significantly enhance the efficiency of compound analysis when an on-site rapid analysis is required, and provide good performance and fast results with low per-sample cost. In addition, portable mass spectrometers are able to analyze samples in harsh environments due to their convenient and robust properties.

A good mass spectrometry system requires both portability, high specificity, and sensitivity. Developing a miniaturized mass spectrometer with good portability and performance is a significant undertaking. One of the most effective ways to miniaturize mass spectrometers is to start by reducing the size of the mass analyzer. By reducing the size of the mass analyzer, a smaller mean free path allows a higher operating pressure with a smaller pump. Smaller dimensions of the mass analyzer allow a smaller detector and vacuum chamber, and a reduced gas load for a lower-power pump. Since the RF trapping voltage is directly proportional to the square of the analyzer radial dimension, a modest decrease in analyzer size results in a large reduction in operating voltage. Thus, lower power requirements can be provided using a smaller battery in the mass spectrometer system.

Several types of mass analyzers are used in mass spectrometers. Much of the effort to make mass spectrometers more portable has focused on ion trap mass analyzers because they

have high sensitivity, throughput and resolution; they are already smaller and can operate at higher pressure than other mass analyzers, and have the advantages of tandem capabilities and ion-molecule reactions for in-field identification of compounds.[39] Many trap geometries have unique capabilities, because electric field shape is defined and constrained by electrode shape.

1.2.2 Methods for Ion Trap Miniaturization

Although the mass analyzer is only a part of the overall mass spectrometer system, smaller analyzers are expected to operate at higher pressures and lower voltages, resulting in smaller, lighter vacuum and power systems.

Many approaches have been taken to miniaturize ion trap mass analyzers because the ion trap is one of the most preferable mass analyzers to miniaturize as mentioned above. One of the methods is to use conventional machining to make miniaturized electrodes, which is called top-down. However, the electrode precision and surface roughness are challenges in this approach.

Significant development has been done on miniaturization using microfabrication, including microelectromechanical systems (MEMS) techniques.[40-47] The microfabrication method is a bottom-up approach to make a miniaturized ion trap. In the ion trap miniaturization, some designs simplified electrode geometries for easier machining and alignment of the smaller electrodes, and other designs have increased trapping capacity in the mass analyzer to achieve a larger ion storage region.

1.2.3 Obstacles to Ion Trap Miniaturization

Ion trap miniaturization is essential in the developmental progress to make portable mass spectrometers. However, many obstacles came up with the miniaturization process. One of the

most critical issues is making accurately shaped electric fields. Several problems could cause this issue, including machining or microfabrication difficulty, surface roughness, and electrode misalignment. Compared to large ion traps, any slight surface roughness, misalignment, or other imperfections have larger effects on the higher-order trapping field in smaller ion traps. The smaller the ion trap is, the more precise machining it will require to produce at a given level of field accuracy. Sometimes the microfabrication of a hole or slit on a miniaturized electrode requires micrometer or nanometer precision; otherwise the electric field would deviate from the optimal design. The electrode roughness is also related to the machining process. To solve this problem, high quality microfabrication is necessary. Although the machining problem may only make a tiny difference, the ion trap performance will be greatly impacted due to a slight change of the electric field.

In addition to the microfabrication problem, electrode alignment is also an important issue in terms of accuracy. Consider, for example, a linear ion trap (Figure 1-5 (a)(b)). Ions are trapped along the trapping region of the linear ion trap and will be ejected at different times due to their mass-to-charge ratio. If a misalignment is present between the ejection electrodes or ejection slits, the ions with different mass-to-charge ratio might be ejected at the same time, thus lowering the mass resolution. Other types of misalignment will also cause similar problems that can greatly reduce mass resolution and ion trap performance.

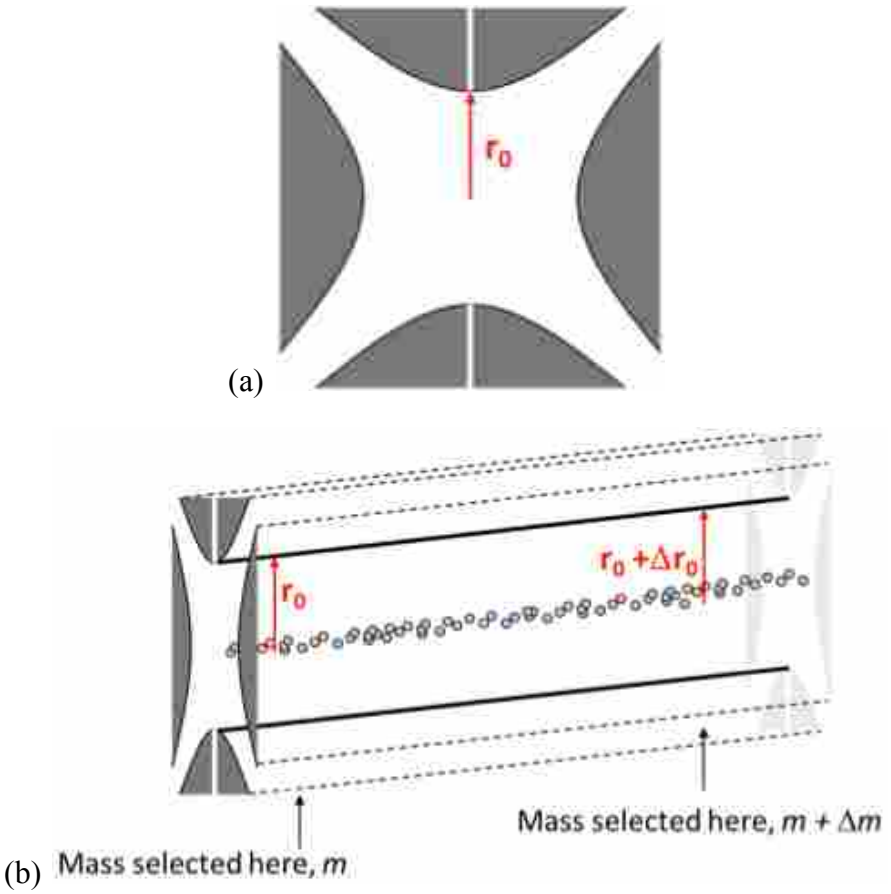

Figure 1-5: (a) Cross-section of linear ion trap with radial dimension r_0; (b) relationship between electrode misalignment and mass resolution. (Figure courtesy of D. Austin)

Other obstacles in ion trap miniaturization include getting sufficient numbers of ions into and out of the trap. With the reduction of trap size, the ion count in the ion trap is reduced, due to space-charge limits. The Coulombic interaction between ions cause a distortion of the local electric field that impacts mass resolution and accuracy. Further, since the ion trap is miniaturized, the trapping region may not be big enough to trap externally generated ions with relatively high efficiency. In addition, the ionization efficiency may also be greatly decreased due to the reduced ion access or ionizing radiation.

1.2.4 Microfabrication Approaches to Ion Trap Miniaturization

To overcome the obstacles of ion trap miniaturization, microfabrication is commonly used to effectively maintain accurate-shaped electric fields, which in turn provides precisely fabricated electrodes.[48] High precision in electrode shape is achieved by using lithographically patterned electrodes on planar surfaces with a very precise 2-dimensional fabrication yield. Our group has demonstrated the practicality of this patterned-electrode approach with a planar Paul trap,[49-51] toroidal ion trap,[52,53] coaxial ion trap,[54] and a linear-type ion trap.[55] Each of these traps is made using two ceramic substrates, with the trapping fields formed in the space between the substrates. Electrodes are patterned onto each substrate surface providing electric fields for trapping and analyzing ions. Higher-order terms in the trapping fields can be readily modified by changing the RF amplitudes applied to one or more of the patterned electrodes. This fabrication approach provides great advantages when seeking to miniaturize the ion trap.

Accurate fabrication with micron level precision is possible using standard photolithography techniques. This process (Figure 1-6) seems to be less prone to surface roughness issues seen when machining miniaturized electrodes.[12] In addition, planar ion traps only require the fabrication and alignment of two flat surfaces. There are fewer electrode "pieces" than those required by other traps, hence the alignment of the electrodes is simplified and allows for much higher alignment accuracy.

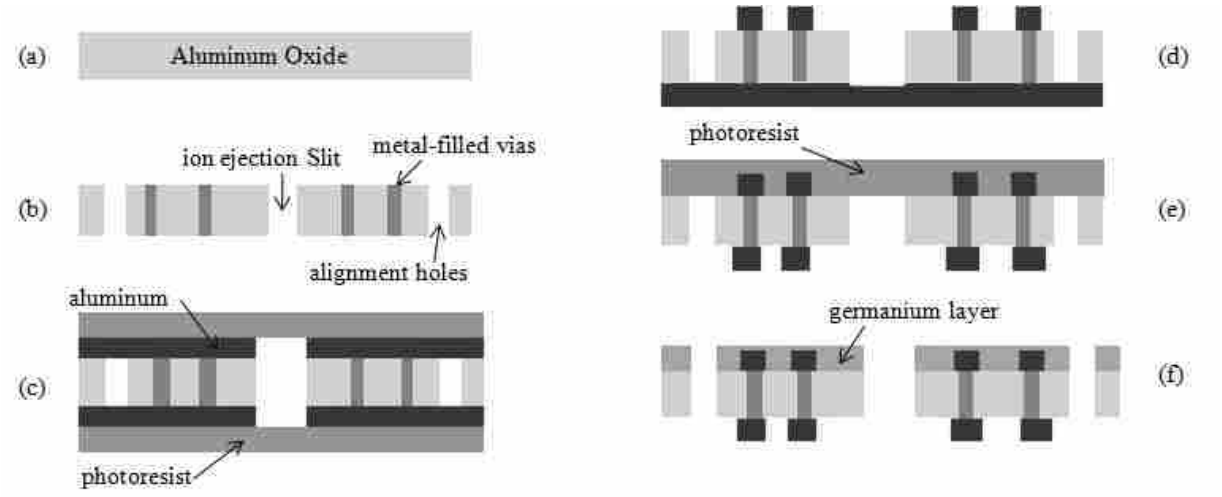

Figure 1-6: Cross-section view of the fabrication steps for planar electrode surfaces. (a) bare aluminum oxide substrate, (b) ejection slit, alignment holes, and metal-filled vias made by Hybrid-Tek (Clarksburg, NJ), (c) aluminum deposited on both sides of substrate, photoresist spun on top side and painted on bottom side, (d) top side patterned by photolithography and aluminum etching, (e) photoresist spun on bottom side, photoresist painted on already-patterned side, and bottom side is patterned and etched, (f) germanium layer deposited over top of trapping side of substrate. (Adapted from Hansen B.J.; Niemi, R.J.; Hawkins, A.R.; Lammert, S.A.; Austin, D.E. A lithographically patterned discrete planar electrode linear ion trap mass spectrometer. J. Microelectromech. Syst. 2013, 22, 876.)

Lithographically patterned substrates are a viable pathway to fabricate highly miniaturized ion traps for mass spectrometry. Experiments have demonstrated the possibility of significant reduction of an ion trap volume without physical modification of the electrodes and show a promising option for further miniaturization using assemblies of patterned ceramic plates.

1.2.5 Miniaturized Ion Traps

Many miniaturized ion traps are derived from the large-scale ion traps to fulfill the goal for portable mass spectrometry. A miniaturized cylindrical ion trap array was developed to increase the trapping capacity of CIT, (Figure 1-7).[56-62] A 0.25 cm^2 array was designed

consisting of 10^6 1-μm size CITs, which improved the trapping capacity limitation of CIT. However, some other problems were raised from the application and fabrication. In a normal sized CIT, the electron beam from the ion source is directed straight into the trapping area through the cap-electrode. The CITs in the array connect to each other in a distributed area and the electron beam may not reach every CIT for ionization, which causes ineffective ionization. The array also suffered from a large electrical capacitance.

Figure 1-7: Miniaturized cylindrical ion trap array. (Adapted from Austin, D.E.; Cruz, D.; Blain, M.G. Simulations of ion trapping in a micrometer-sized cylindrical ion trap. Int. J. Mass Spec. 2006, 3, 430-441.)

Two types of miniaturized RIT were published as RIT arrays to further increase trapping capacity. Fico et al. described a RIT array consisting of a round arrangement fabricated using stereolithography apparatus (SLA) method (Figure 1-8 (a)).[63] The RIT array consists of eight miniaturized RITs positioned as a circle. The ejection slit of each RIT faced to the center of the

circle, and detector received the ejected ions at the center. This device is feasible for both the separate ion source for each trap and single ion source for the entire array, which greatly increased the throughput. Li et al. reported another type of RIT array made using a printed circuit board (PCB) (Figure 1-8 (b)).[64]

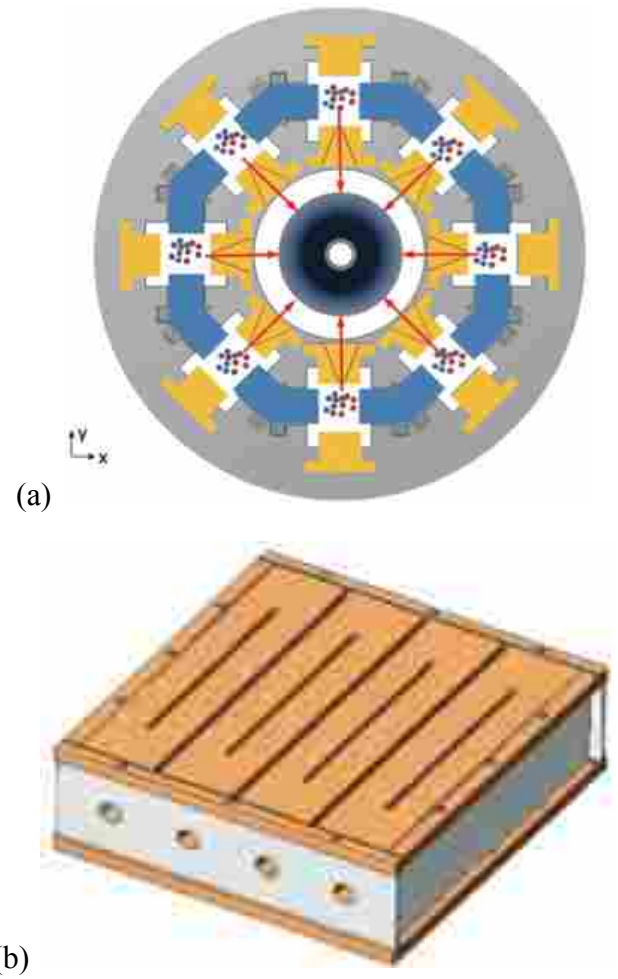

Figure 1-8: (a) Rectilinear ion trap array using stereolithography apparatus (SLA) method[63]; (b) rectilinear ion trap array made using printed circuit boards. [64]

The cylindrical toroidal ion trap (CTIT) was developed using simplified electrodes from the toroidal ion trap, which provides higher ejection efficiency and allows an easier fabrication

process (Figure 1-9).[65] Two main modifications were made in the CTIT. One is the hyperboloidal-shape electrodes were simplified to cylindrical, which reduced the difficulty of fabrication. The other modification was to change the ion ejection direction. In the original toroidal ion trap, ions are ejected out from the two circular end-cap electrodes at both up and down directions; this limits the ion detection with a detector at only one side. In addition, the curvature caused by the curved ring electrode deviated the trapping center, while the slit position was fabricated at the theoretical trapping center, so that the ion ejection trajectory did not exactly point to the slit. Therefore, the CTIT was designed with a switched ring and end-cap electrodes. The end-cap electrodes are applied with RF waveform for ion trapping without adding a slit, and the outer ring-electrode acts as an excitation end-cap electrode applied with AC waveform for resonant excitation of the ion to the detector at the center. There is a slit at the inner ring-electrode as a ground shielding for the detector. In this way, all the ions are ejected to the detector from different directions and the trapping center deviation does not affect the alignment between the slit and the ejection trajectory.

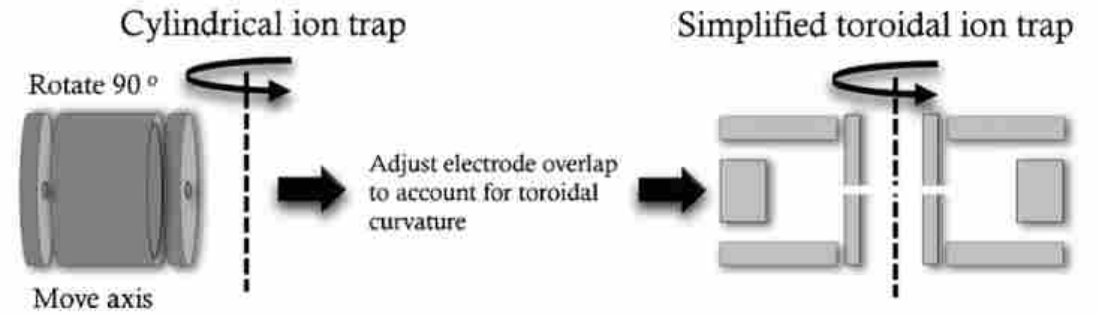

Figure 1-9: Simplified cylindrical toroidal ion trap originated from cylindrical ion trap with toroidal geometry.[32]

There are four types of planar ion traps fabricated using photolithography methods (Figure 1-10 (a)-(d)).[50,52,54,66] For the planar Paul trap, a central hole on each plate is used for ion ejection, and several electrode rings on the plate are lithographically arranged in a concentric pattern, each at an increasing distance from the central hole. The electric fields between the two plates are established by applying different radiofrequency potentials to each electrode ring. A printed circuit board (PCB) connected to the power supply contacts each plate and provides RF waveforms for the trap. The potential on each ring electrode can be independently optimized through varying the capacitors on the PCBs to provide an optimal trapping field. An electric field is generated between the two plates for mass analysis and ion ejection, which occurs through the center hole. Compared to the 3D quadrupole ion trap, the planar Paul trap has simpler geometry and high fabrication precision. However, the ion capacity should be further increased with future generation traps.

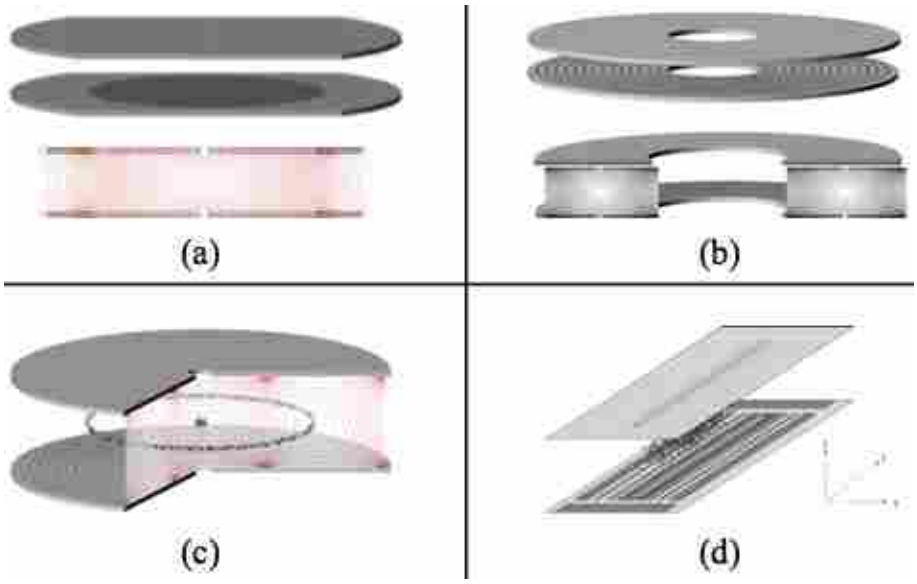

Figure 1-10: (a) Planar Paul trap; (b) planar toroidal ion trap; (c) coaxial ion trap; (d) planar linear ion trap.[54,56,58]

For the planar toroidal ion traps, the trapping capacity is enlarged to greater than that of the planar Paul trap due to its round-shaped electric field. Ions are trapped within the electric field, and then ejected to the center to be detected. The planar toroidal geometry provides a large trapping volume, which increases the trapping capacity and reduces the space charge effects. However, the electric field is still curved, so the curvature may affect the ion trap performance.

For the coaxial ion trap, both toroidal and quadrupolar trapping regions are created simultaneously. Ions are initially trapped in the toroidal region and mass-selectively ejected to the quadrupole region using an applied ac signal in the radial direction. In the quadrupole region, ions can either be fragmented by using CID for tandem mass analysis, or directly ejected from the quadrupolar region to a detector. Multiple transfer steps and mass analysis scans are possible on a single population of ions with good mass resolving power and sensitivity.

The planar-electrode linear ion trap (LIT) developed in this project was fabricated using photolithography techniques for easier and precise machining. Unlike the above types of planar ion traps, the LIT has a higher aspect ratio for an increased ion capacity due to its long trapping dimension. The electrode shape on the plate of the LIT is straight instead of toroidal. Compared to the other non-planar ion traps, the linear ion trap has several advantages, such as simplified geometry, simpler electric field, easier machining, and larger ion trapping capacity.

1.3 Conclusion

As one of the most widely used mass analyzers, ion traps play an important role in mass spectrometry miniaturization for portable use, which provides a convenient way to accomplish rapid on-site analysis. In addition, the tandem-in-time capability of an ion trap gives an effective way to precisely identify the compounds within a limited instrument space. Moreover,

combining with chromatography makes GC-MS a powerful analytical instrument to quantify and identify compounds more efficiently.

The mass analyzer is the center of the mass spectrometry system, similar to the central processing unit (CPU) of a computer. By reducing the size of the mass analyzer, the power system, vacuum system, and other parts of the mass spectrometer can be miniaturized as well. However, performance may be impacted by size reduction, just as laptop performance is usually not higher than that of a computer of the same configuration. However, just as developing a light-weight and highly efficient laptop is the trend of the market, there is a demand for portable mass spectrometry. In the exploration of ion traps, many different types of ion traps were created with modified geometry. The modification is driven by the same goal to make mass spectrometers simpler, smaller, and with maintained or even improved performance.

Miniaturizing ion traps is urgent in the current analytical environment because of the ability to analyze material in the native environment that cannot be analyzed otherwise. Much effort has been made on ion trap miniaturization including conventional fabrication and microfabrication (MEMS). Most ion traps are fabricated using these two methods. For instance, the planar ion traps referred to herein were microfabricated in a novel geometry with ceramic material.

The planar ion trap is a promising candidate for miniaturization. It has overcome several difficulties in the miniaturization process, such as high mechanical tolerance, excellent surface smoothness and easy fabrication process. In addition, the trapping capacity of planar toroidal ion trap and planar linear ion trap has been enhanced significantly.

1.4 Dissertation Overview

In this dissertation, Chapter 2 focuses on experiments of miniaturized linear ion traps, including two ion traps ―planar linear ion trap and wire linear ion trap. It describes the fabrication and assembly of the planar linear ion trap, germanium coating study on the trapping side of the plate, further miniaturization to 43% smaller than the original planar linear ion trap, sub-mm linear ion trap design, digital waveform ion trap and ion source design, respectively. Some of the sections related to planar linear ion traps are adapted from "Miniaturization of a planar-electrode linear ion trap mass spectrometer" (Li, A.; Hansen, B.J.; Powell, A.T.; Hawkins, A.R.; Austin, D.E., Rapid Commun. Mass Spectrom. 2014, 28, 1338-1344). In addition, the feasibility of a wire linear ion trap is also demonstrated by preliminary experiment, which contributed to the paper of "Miniaturized linear wire ion trap mass analyzer" (Wu, Q., Li, A., Tian, Y., Zare, R.N., Austin, D.E., Anal. Chem. 2016, 88, 7800-7806). A miniaturized planar linear ion trap with plate spacing of 4.38 mm is demonstrated with mass resolution 190 (m/Δm FWHM). Also, a 43% scale of further miniaturized ion trap with plate spacing of 1.90 mm is demonstrated with mass resolution 130 (m/Δm FWHM). A sub-mm planar linear ion trap with 724 μm plate spacing is designed with a digital waveform method. The ion source is also redesigned to improve the ionization efficiency in the sub-mm ion trap. In addition, a wire linear ion trap and the demonstration experiment are described.

Chapter 3 presents simulations of ion motion in the aforementioned cylindrical toroidal ion trap using SIMION 8.1. Much of this chapter is adapted from "Chaotic motion of single ions in a toroidal ion trap mass analyzer" (Li, A., Higgs, J.M., Austin, D.E, J. Am. Soc. Mass. Spectrom. 2017, in press). Theoretically, ion motion in a perfect quadrupole electric field is not chaotic. Simulations demonstrate that ions exhibit classical chaotic motion in the cylindrical

toroial ion trap due to the influence of higher order non-linear terms in the electric field. The chaotic motion is observed in the stability diagram. Figures with zoomed-in step voltage of the stability diagram show fractal (self-similar) behavior, which is a characteristic of chaos. In addition, the boundaries of the stability region in the diagram are diffuse. This phenomenon also demonstrates the chaotic behavior of ion motion. The ion starting condition is also studied to determine if the ion motion is sensitive to the ion initial conditions, which is applicable to all chaotic behavior. Ion motion in the experiment is studied as single ion trajectory, which excludes the Coulombic interaction and other influences between ions.

Chapter 4 describes the practical experiment of a miniaturized cylindrical toroidal ion trap, which is 1/3 size scale of the trap studied in chapter 3. This experiment is to demonstrate the feasibility of the miniaturized device with acceptable ion trap performance. The mass-selective instability scan mode is used for ion ejection. However, black canyons are found in the electric field that cause irregular non-linear ejections in the experiment.

Finally, the summary for the whole work during my PhD studies and future work are presented in Chapter 5.

1.5 References

1. Paul, W.; Steinwedel, H., German Patent 944,900, **1956**; U.S. Patent 2,939,952, 7 June **1960**.

2. Paul, W.; Reinhard, H.; Zahn, V. Z. *Phys*. **1959**, *156*, 1.

3. Fischer, E. Z. *Phys*. **1959**, *156*, 1.

4. Stafford, G.C.; Kelley, P.E.; Stephens, D.R., Method of mass analyzing a sample by use of a quadrupole ion trap. European Patent 0113207 A2, **1984**.

5. Henry, C., Building a better trap. *Anal. Chem*. **1998**, *70*, 533A-536A.

6. Ziegler, Z., Ion traps come of age - Software control helps these versatile mass spectrometers mature. *Anal. Chem*. **2002**, *74*, 489a-492a.

7. March, R.E.; Hughes, R.J.; Todd, J.F.J, Quadrupole storage mass spectrometry. *Wiley-interscience*, New York, (1989).

8. March, R. E., An introduction to quadrupole ion trap mass spectrometry. *J. Mass Spectrom*. **1997**, *32*, 351-369

9. Mathieu, E. *J. Math. Pure Appl . (J. Liouville)* **1868**, *13*, 137-203.

10. March, R.E.; Todd, J.F.J. (eds.) Practical aspects of ion trap mass spectrometry (Vol. IV), p. 393. CRC Press, Boca Raton, NY, (2010).

11. Gupta, A.; Rao, P.M., Numerical calculations of potential distribution in non-ideal quadrupole trap and simulations of anharmonic oscillations. *Pramana – J. Phys*. **2008**, *70*, 457-470.

12. Xu, W.; Chappell, W.J.; Cooks, R.G.; Ouyang, Z., Characterization of electrode surface roughness and its impact on ion trap mass analysis. *J. Mass Spectrom*. **2009**, *44*, 353-360.

13. Schwartz, J.C.; Senko, M.W.; Syka, J.E.P., A two-dimensional quadrupole ion trap mass spectrometer. *J. Am. Soc. Mass. Spectrom.* **2002**, *13*, 659-669.

14. Snyder, D.T.; Pulliam, C.J.; Ouyang, Z.; Cooks, R.G., Miniature and fieldable mass spectrometers: recent advances, *Anal. Chem*. **2016**, *88*, 2–29.

15. Mather, R. E.; Lawson, G.; Todd, J. F. J.; Bakker, J. M. B., Quadrupole Ion Storage Trap (Quistor) as a Low-Pressure Chemical Ionization Source for a Magnetic-Sector Mass-Spectrometer. *Int. J. Mass Spectrom.* **1978**, *28*, 347-364.

16. Fulford, J. E.; Hoa, D. N.; Hughes, R. J.; March, R. E.; Bonner, R. F.; Wong, G. J., Radio-Frequency Mass Selective Excitation and Resonant Ejection of Ions in a 3-Dimensional Quadrupole Ion Trap. *J. Vac. Sci. Technol*. **1980**, *17*, 829-835.

17. Stafford, G. C.; Kelley, P. E.; Syka, J. E. P.; Reynolds, W. E.; Todd, J. F. J., Recent Improvements in and Analytical Applications of Advanced Ion Trap Technology. *Int. J. Mass Spectrom*. **1984**, *60*, 85-98.

18. Louris, J. N.; Cooks, R. G.; Syka, J. E. P.; Kelley, P. E.; Stafford, G. C.; Todd, J. F. J., Instrumentation, Applications, and Energy Deposition in Quadrupole Ion-Trap Tandem Mass-Spectrometry. *Anal. Chem.* **1987**, *59*, 1677-1685.

19. Fulford, J. E.; March, R. E.; Mather, R. E.; Todd, J. F. J.; Waldren, R. M., The Cylindrical Ion Trap - a Theoretical and Experimental-Study. *Can. J. Spectrosc*. **1980**, *25*, 85-97.

20. Wells, J. M.; Badman, E. R.; Cooks, R. G., A quadrupole ion trap with cylindrical geometry operated in the mass selective instability mode. *Anal. Chem*. **1998**, *70*, 438-444.

21. Riter, L.S.; Peng, Y.; Noll, R.J.; Patterson, G.E.; Aggerholm, T.; Cooks, R.G., Analytical performance of a miniature cylindrical ion trap mass spectrometer. *Anal. Chem*. **2002**, *74*, 6154-6162.

22. Patterson, G.E.; Guymon, A.J.; Riter, L.S.; Everly, M.; Griep-Raming, J.; Laughlin, B.C.; Ouyang, Z.; Cooks, R.G., Miniature cylindrical ion trap mass spectrometer. *Anal. Chem*. **2002**, *74*, 6145.

23. Wu, G.; Cooks, R.G.; Ouyang, Z., Geometry optimization for the cylindrical ion trap: field calculations, simulations and experiments. *Int. J. Mass Spectrom*. **2005**, *241*, 119-132.

24. Yang, M.; Kim, T.; Hwang, H.; Yi, S.; Kim, D., Development of a palm portable mass spectrometer. *J. Am. Soc. Mass Spectrom.* **2008**, *19*, 1442-1448.

25. Miller, P.E.; Denton, M.B., The quadrupole mass filter: Basic operating concept. *J. Chem. Edu.* **1986**, *63*, 671-623.

26. Blaum, K.; Geppert, C.; Muller, P.; Nortershauser, W.; Otten, E.W.; Schmitt,; A.; Trautmann, N.; Wendt, K.; Bushaw, B.A., Properties and performance of a quadrupole mass filter used for resonance ionization mass spectrometry. *Int. J. Mass Spectrom*. **1998**, *181*, 67-87.

27. Douglas, D.J.; Frank, A.J.; Mao, D., Linear ion traps in mass spectrometry. *Mass Spectrom. Rev.* **2004**, *24*, 1-29.

28. Schwartz, J.C.; Senko, M.W.; Syka, J.E.P., A two-dimensional quadrupole ion trap mass spectrometer. *J. Am. Soc. Mass Spectrom*. **2002**, *13*, 659-669.

29. Hager, J.M., A new linear ion trap mass spectrometer. *Rapid Commun. Mass Spectrom*. **2002**, *16*, 512.

30. Song, Y.; Wu, G.; Song, Q.; Cooks, R.G.; Ouyang, Z.; Plass, W.R., Novel linear ion trap mass analyzer composed of four planar electrodes. *J. Am. Soc. Mass Spectrom*. **2006**, *17*, 631-639.

31. Ouyang, Z.; Wu, G.; Song, Y.; Li, H.; Plass, W.R.; Cooks, R.G., Rectilinear ion trap: concepts, calculations, and analytical performance of a new mass analyzer. *Anal. Chem*. **2004**, *76,* 4595.

32. Lammert, S.A.; Plass, W.R.; Thompson, C.V.; Wise, M.B., Design, optimization and initial performance of a toroidal rf ion trap mass spectrometer. *Int. J. Mass Spectrom*. **2001**, *212*, 25-40.

33. Contreras, J.A.; Murray, J.A.; Tolley, S.E.; Oliphant, J.L.; Tolley, H.D.; Lammert, S.A.; Lee, E.D.; Later, D.W.; Lee, M.L., Hand-portable gas chromatograph-toroidal ion trap mass spectrometer (GC-TMS) for detection of hazardous compounds. *J. Am. Soc. Mass. Spectrom.* **2008**, *19*, 1425-1434.

34. Takao, T.; Shimizu, T.; Ikegami, S.; Shimonishi, Y., High-sensitivity mass spectrometry for analysis of posttranslational modifications. *J. Protein Chem*. **1997**, *16*, 409-413.

35. Brand, W.A., High precision isotope ratio monitoring techniques in mass spectrometery, *J. Mass. Spectrom.* **1996**, *31*, 225-235.

36. Li, W.; Lundberg, J.; Dickin, A.P.; Ford, D.C.; Schwarcz, H.P.; Mcnutt, R.; Williams, D., High-precision mass-spectrometric uranium-series dating of cave deposits and implications for palaeoclimate studies. *Nature* **1989**, *339*, 534-536.

37. Thakur, S.S.; Geiger, T.; Chatterjee, B.; Bandilla, P.; Frohlich, F.; Cox, J.; Mann, M., Deep and Highly Sensitive Proteome Coverage by LC-MS/MS Without Prefractionation. *Mol. Cell. Proteomics* **2011**, M110.003699

38. Wittmann, C., Fluxome analysis using GC-MS. *Microb Cell Fact*. **2007**, 1-17.

39. Gao, L.; Song, Q.; Patterson, G.E.; Cooks, R.G.; Ouyang, Z., Handheld rectilinear ion trap mass spectrometer. *Anal. Chem*. **2006**, *78*, 5994-6002.

40. Malcolm, A.; Wright, S.; Syms, R.R.A.; Dash, N.; Schwab, M.-A.; Finlay, A., Miniature mass spectrometer systems based on a microengineered quadrupole filter. *Anal. Chem*. **2010**, *82*, 1751-1758.

41. Syms, R.R.A.; Tate, T.J.; Ahmad, M.M.; Taylor, S., Fabrication of a microengineered quadrupole electrostatic lens. *Electron. Lett.* **1996**, *32*, 2094-2095.

42. Syms, R.R.A.; Tate, T.J.; Ahmad, M.M.; Taylor, S., Design of a microengineered electrostatic quadrupole lens. *IEEE Trans. Electron Dev*. **1998**, *45*, 2304-2311.

43. Taylor, S.; Tindall, R.; Syms, R., Silicon based quadrupole mass spectrometry using microelectromechanical systems. *J. Vac. Sci. Tech. B*. **2001**, *19*, 557-562.

44. Taylor, S.; Tunstall, J.J.; Syms, R.R.A.; Tate, T.J.; Ahmad, M.M., Initial results for a quadrupole mass spectrometer with a silicon micromachined mass filter. *Electron. Lett.* **1998**, *34*, 546-547.

45. Geear, M.; Syms, R.R.A.; Wright, S.; Holmes, A.S., Monolithic MEMS quadrupole mass spectrometers by deep silicon etching. *J. Microelectromech. Syst*. **2005**, *14*, 1156-1166.

46. Velasquez-Garcia, L.F.; Akinwande, A.I., An out-of-plane MEMS quadrupole for a portable mass spectrometer. *Proceedings of the Solid State Sensors, Actuators and Microsystems Conference*, Cite Centre Des Congres Lyon, France, **2007**, pp. 2215-2320.

47. Velasquez-Garcia, L.F.; Cheung, K.; Akinwande, A.I., An application of 3-D MEMS packaging: out-of-plane quadrupole mass filters. *J. Microelectromech. Syst*. **2008**, *17*, 1430-1438.

48. Orient, O.J.; Chutjian, A., A compact, high-resolution Paul ion trap mass spectrometer with electron-impact ionization. *Rev. Sci. Instrum*. **2002**, *73*, 2157-2160.

49. Austin, D.E.; Peng, Y.; Hansen, B.J.; Miller, I.W.; Rockwood, A.L.; Hawkins, A.R.; Tolley, S.E., Novel ion traps using planar resistive electrodes: implications for miniaturized mass analyzers. *J. Am. Soc. Mass Spectrom*. **2008**, *19*, 1435-1441.

50. Zhang, Z.; Peng, Y.; Hansen, B.J.; Miller, I.W.; Wang, M.; Lee, M.L.; Hawkins, A.R.; Austin, D.E., Paul trap mass analyzer consisting of opposing microfabricated electrode plates. *Anal. Chem*. **2009**, *81*, 5241-5248.

51. Austin, D.E.; Hansen, B.J.; Peng, Y.; Zhang, Z., Multipole expansion in quadrupolar devices comprised of planar electrode arrays. *Int. J. Mass Spectrom*. **2010**, *295*, 153-158.

52. Austin, D.E.; Wang, M.; Tolley, S.E.; Maas, J.D.; Hawkins, A.R.; Rockwood, A.L.; Tolley, H.D.; Lee, E.D.; Lee, M.L., Halo ion trap mass spectrometer. *Anal. Chem*. **2007**, *79*, 2927-2932.

53. Wang, M.; Quist, H.E.; Hansen, B.J.; Peng, Y.; Zhang, Z.; Hawkins, A.R.; Rockwood, A.L.; Austin, D.E.; Lee, M.L., Performance of a halo ion trap mass analyzer with exit slits for axial ejection. *J. Am. Soc. Mass Spectrom*. **2011**, *22*, 369-378.

54. Peng, Y.; Hansen, B.J.; Quist, H.E.; Zhang, Z.; Wang, M.; Hawkins, A.R.; Austin, D.E., Coaxial ion trap mass spectrometer: concentric toroidal and quadrupolar trapping regions. *Anal. Chem*. **2011**, *83*, 5578-5584.

55. Hansen, B.J.; Niemi, R.J.; Hawkins, A.R.; Lammert, S.A.; Austin, D.E., A lithographically patterned discrete planar electrode linear ion trap mass spectrometer. *J. Microelectromech. Syst*. **2013**, *22*, 876-883.

56. Blain, M.G.; Riter, L.S.; Cruz, D.; Austin, D.E.; Wu, G.; Plass, W.R.; Cooks, R.G., Towards the hand-held mass spectrometer: design considerations, simulation, and fabrication of micrometer-scaled cylindrical ion traps. *Int. J. Mass Spectrom*. **2004,** *236*, 91-104.

57. Austin, D.E.; Cruz, D.; Blain, M.G., Simulations of ion trapping in a micrometer-sized cylindrical ion trap. *J. Am. Soc. Mass Spectrom*. **2006**, *17*, 430-441.

58. Ouyang, Z.; Badman, E.R.; Cooks, R.G., Characterization of a serial array of miniature cylindrical ion trap mass analyzers. *Rapid Commun. Mass Spectrom*. **1999**, *13*, 2444-2449.

59. Badman, E.R.; Johnson, R.C.; Plass, W.R.; Cooks, R.G., A miniature cylindrical quadrupole ion trap: simulation and experiment. *Anal. Chem*. **1998**, *70*, 4896-4901.

60. Tabert, A.M.; Griep-Raming, J.; Guymon, A.J.; Cooks, R.G., High-throughput miniature cylindrical ion trap array mass spectrometer. *Anal. Chem*. **2003**, *75*, 5656-5664.

61. van Amerom, F.H.W.; Chaudhary, A.; Cardenas, M.; Bumgarner, J.; Short, R.T., Microfabrication of cylindrical ion trap mass spectrometer arrays for handheld chemical analyzers. *Chem. Eng. Comm*. **2007**, *195*, 98-114.

62. Chaudhary, A.; van Amerom, F.; Short, R.T., Development of microfabricated cylindrical ion trap mass spectrometer arrays. *J. Microelectromech. Syst*. **2009**, *18*, 442-448.

63. Maas, J.D.; Hendricks, P.I.; Ouyang, Z.; Cooks, R.G.; Chappell, W.J., Miniature monolithic rectilinear ion trap arrays by stereolithography on printed circuit board. *J. Microelectromech. Syst*. **2010**, *19*, 951-960.

64. Li, X.; Jiang, G.; Luo, C.; Xu, F.; Wang, Y.; Ding, L.; Ding, C., Ion Trap Array Mass Analyzer: Structure and Performance. *Anal. Chem*. **2009**, *81*, 4840-4846.

65. Taylor, N.; Austin, D.E., A simplified toroidal ion trap mass analyzer. *Int. J. Mass Spectrom*. **2012,** *321-322*, 25-32.

66. Li, A.; Hansen, B.J.; Powell, A.T.; Hawkins, A.R.; Austin, D.E., Miniaturization of a Planar-Electrode Linear Ion Trap Mass Spectrometer. *Rapid Commun. Mass Spectrom*. **2014**, *28*, 1338-1344

2 MINIATURIZED PLANAR LINEAR ION TRAP MASS ANALYZER*

2.1 Introduction

Numerous applications now employ mass spectrometers based on radiofrequency (RF) quadrupole ion traps, including fields such as biology,[1] analytical chemistry,[2] forensics,[3,4] and space exploration.[5] There is considerable interest in many of these fields in making mass spectrometers portable. Much of the effort to make mass spectrometers more portable has focused on ion traps because they are already smaller and operate at higher pressure than other mass analyzers, and because of the advantages of tandem analysis for in-field identification of compounds.[6] A conventional ion trap is formed with facing hyperbolic electrodes in an arrangement that is symmetric both axially and radially.

Many approaches have been taken to miniaturize both ion trap mass analyzers and quadrupole mass filters. There has been significant development of miniaturized mass filters constructed with microelectromechanical system (MEMS) techniques.[7-14] MEMS has also been used to create linear ion traps for applications in quantum computing, although these devices do not operate as mass spectrometers.[15,16] Other approaches to miniaturization have used simplified electrode geometries for easier machining and alignment of the smaller electrodes. Such

* Section 2.1, 2.2 of this chapter came from a published paper "Li, A.; Hansen, B.J.; Powell, A.T.; Hawkins, A.R.; Austin, D.E., Miniaturization of a Planar-Electrode Linear Ion Trap Mass Spectrometer. *Rapid Commun. Mass Spectrom*. **2014**, *28*, 1338-1344.", in which I performed the experiments and obtained the results of 1.90 mm spacing LIT, except for the calculation of multipole coefficients.

approaches include the use of cylindrical ion traps,[17-20] cylindrical ion trap arrays,[21-27] rectilinear ion traps,[28-29] rectilinear ion trap arrays using stereolithography,[30] and linear ion traps using electrodes printed on the circuit board and metal-coated ceramic substrates.[31,32] Although the mass analyzer is only a part of the whole mass spectrometer system, smaller analyzers are expected to operate at higher pressures and lower voltages, resulting in smaller, lighter vacuum and lower power systems.[33-34]

An important issue in the miniaturization of ion traps is maintaining accurately shaped electric fields, which in turn requires high-precision fabrication of electrodes.[35] This is a particular issue in trap arrays (where every trap must be identical) or in higher-capacity traps, such as linear[36,37] or toroidal[38] traps that have an extended trapping dimension. Lithographically patterned electrodes on planar surfaces allow very precise two-dimensional fabrication processes that yield high precision in the electrode shape and alignment. Our group has demonstrated this patterned-electrode approach with a planar Paul trap,[39-41] a toroidal or 'halo' trap,[42,43] a hybrid Paul and toroidal trap, known as the coaxial trap,[44] and a linear-type ion trap.[45] Each of these traps is made using two patterned substrates, with the trapping fields formed in the space between the substrates. Electrodes patterned onto the facing surfaces of each substrate provide the electric fields for trapping and analyzing ions. Higher-order terms in the trapping fields can readily be modified by changing the RF amplitudes applied to one or more of the patterned electrodes. This approach provides great advantages when seeking to miniaturize the ion trap. Accurate fabrication on the micron and sub-micron level is possible using standard photolithography techniques. This process is also less prone to the surface roughness issues seen when machining miniaturized electrodes.[46] Furthermore, planar ion traps only require the fabrication and alignment of two flat surfaces. This is fewer electrode 'pieces' than those

required by other traps, thereby simplifying the alignment of the electrodes and allowing for much higher alignment accuracy.

Our group previously postulated that miniaturization of ion traps made using two patterned plates can readily be accomplished simply by moving the plates closer together.[39] With conventional electrodes, whether hyperbolic (as in the quadrupole ion trap) or flat (as in the cylindrical or rectilinear ion traps), changing the electrode spacing even a small amount results in significant distortions in the trapping field, which can compromise mass resolution. In contrast, consider two surfaces, each with quadratic potential distributions. The resulting potential between the surfaces will be quadratic. If the spacing between those surfaces is changed, the quadratic potential remains. This is illustrated in Figure 2-1. For the lithographically patterned plates discussed above, the surface potential is not exactly quadratic, but deviations from this ideal can be compensated for by optimizing the RF amplitudes applied to the electrode elements.

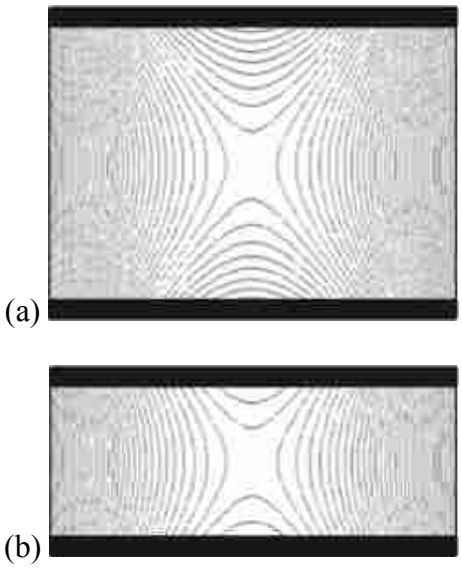

Figure 2-1: (a) Quadratic potential between two surfaces that has quadratically-varying potential; (b) The same plates moved closer together still produce a quadrupolar potential distribution between the plates.

Our group has demonstrated a planar linear ion trap (LIT) with a plate spacing of 4.38 mm.[45] The characteristic trapping dimension, which identifies the scale of ion motion within the trap, is half this value, or 2.19 mm. The germanium thickness coated on the inner side of the ceramic plate was studied. In the further miniaturization, the plate spacing was decreased to 43% of its original value without remaking the ceramic plates, resulting in a significantly smaller trapping region. The main benefit of the LIT over the Paul trap is in the increased ion storage capacity[47] but with simpler trapping fields than those of the toroidal trap.[43,48] The increased storage capacity of the planar LIT makes it an ideal candidate for initial exploration of the viability of planar ion traps as miniaturized mass analyzers.

2.2 Miniaturized Linear Ion Trap

2.2.1 Fabrication and Assembly of Planar Linear Ion Trap

The planar linear ion trap is comprised of two ceramic plates facing each other in a sandwich configuration, as shown in Figure 2-2. Each plate has lithographically patterned sets of aluminum electrodes, a laser-drilled slit for ion ejection, and other necessary electrical connections and mounting holes. A printed circuit board (PCB) attached the electrodes on the ceramic plate via pogo-pins. Quadrupolar potentials are created in the space between the plates as appropriate RF amplitudes are applied to each electrode via the capacitive voltage divider on the PCB. Higher-order terms in the trapping potential can be adjusted by careful selection of these RF amplitudes.[40-43] Electrodes at the ends (end bars) provide axial confinement of ions.

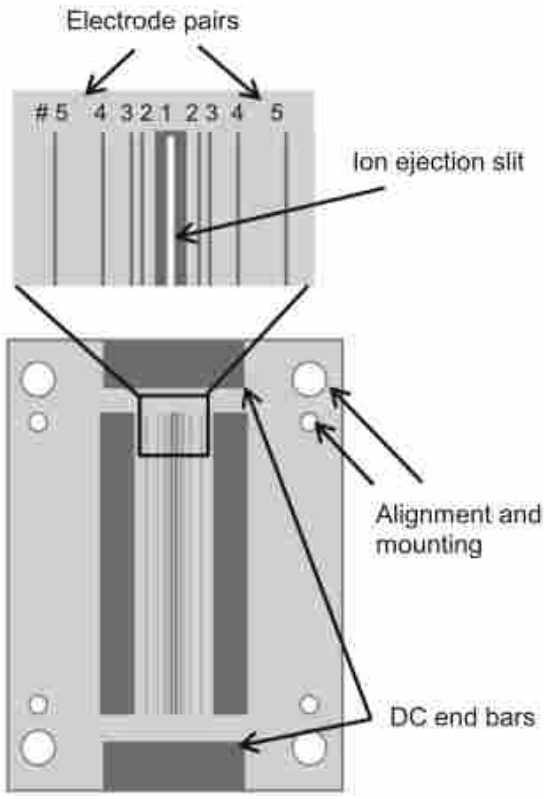

Figure 2-2: Schematic view of the electrode and hole layout of the planar electrode linear ion trap. Modified from Hansen et al.[45]

Several holes cut by laser in the substrate were used for alignment and mounting. Precision sapphire balls of 5.0 mm diameter (Swiss Jewel Co., Philadelphia, PA, USA) were placed in the holes for accurate alignment and precise spacing between the plates. Other holes, 125-µm diameter, were completely filled in with a gold-tungsten alloy to create vias, which are the electrical connections between the front and back sides of the plate. A slit with 500-µm width was cut in the middle of the plate for ion ejection. All the electrodes were patterned from 1-µm thick aluminum films thermally evaporated onto the substrate.

On the trapping side of the plates one electrode, 1-mm wide, was patterned to cover the entire ion ejection slit and overlap 250 microns onto the ceramic near the slit. Eight additional

electrodes – four on each side of the ejection slit – were patterned with a width of 25 μm each. The outermost electrodes were several millimeters wide. A thin layer of germanium was coated on the trapping side of the substrates after patterning the electrodes. The two end-bar electrodes were set at a voltage of 30 V. This choice of the bar electrode shape on the ends was made to try to emulate the axial trapping used in the rectilinear ion trap.[29]

The RF amplitudes applied to each electrode were produced using a capacitive voltage divider on a printed circuit board (PCB). A self-tuning RF power supply manufactured by Ardara Technologies (Ardara, PA, USA) provided the input RF to the voltage divider. A custom-made electronics box was used to provide the DC voltages for axial ion confinement, the detector voltage supply, electron gun control, and electron gate control. Ions were detected using an electron multiplier produced by DeTech (Palmer, MA, USA), located behind the slit of one of the plates. An electron gun from Torion Technologies (American Fork, UT, USA) was positioned so that 60 eV electrons passed through the length of the trapping region for ionization. The PCB and plate assembly, and photographs of the plates themselves, are shown in Figure 2-3.

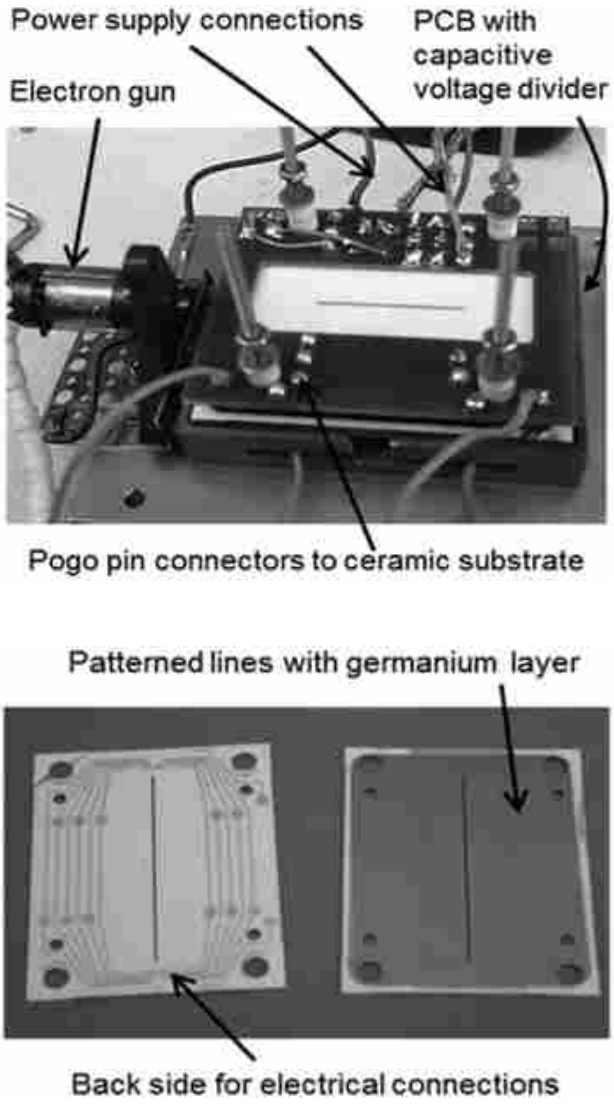

Figure 2-3: (a) Ceramic plate/PCB assembly used in ion trap mass analysis experiments; (b) Both sides of the patterned ceramic substrates, modified from Hansen et al.[45]

2.2.2 Germanium Coating Study

In the microfabrication process, a thin layer of germanium was coated on the facing surfaces of the plates using physical vapor deposition. This layer was intended to eliminate charge build-up and establish uniform potentials between electrodes. We found that the

germanium layer thickness might affect the ion trap performance in the experiment of the linear ion trap with larger spacing of r_0= 2.19 mm.

Mass analysis was performed using resonant ejection, which shows better-than-unit mass resolution. Toluene sample was ionized using an electron ionization (EI) source and analyzed by the r_0= 2.19 mm LIT. Different thicknesses of the germanium layer coated on the top of the electrode pattern were studied, which were 100 nm, 200 nm, 400 nm and 800 nm. The resolution increases between 100-nm to 400-nm thicknesses, and decreases at 800 nm thicknesses (Figure 2-4(a)-(d)). The mass resolution of m/z 91 reaches 190 (m/Δm FWHM). The reason that the resolution increases with the increasing thickness of Ge might be the dissipation of charge along the semi-conductive surfaces. However, if the Ge layer is too thick, the electric field is distorted due to the low-resistance in the circuit. Although the four mass spectra were obtained at identical parameter settings, the results might not be completely conclusive. Since the LIT was disassembled and reassembled using different plates each time, other differences such as plate alignment and pressure variations may also affect the resolution.

The mass scan method used in the planar LIT was a linear ramp of the RF amplitude with a constant additional AC signal. For the ion trap with larger spacing, the RF trapping voltage was 212 $V_{0\text{-}p}$ at a frequency of 2.4 MHz. The ionization time was 30 ms, and the cooling time was 144 ms. The RF voltage was ramped from 212 $V_{0\text{-}p}$ to 1088 $V_{0\text{-}p}$ over a time period of 200 ms. The AC signal was constant at a frequency of 560 kHz and had a magnitude of 1.1 $V_{0\text{-}p}$. The uncorrected pressure of sample gasses in the vacuum chamber was 6.0×10^{-6} Torr measured with an ion gauge, and the uncorrected pressure of background helium buffer gas was 4.0×10^{-3} Torr measured with a Pirani gauge. The compound studied was toluene.

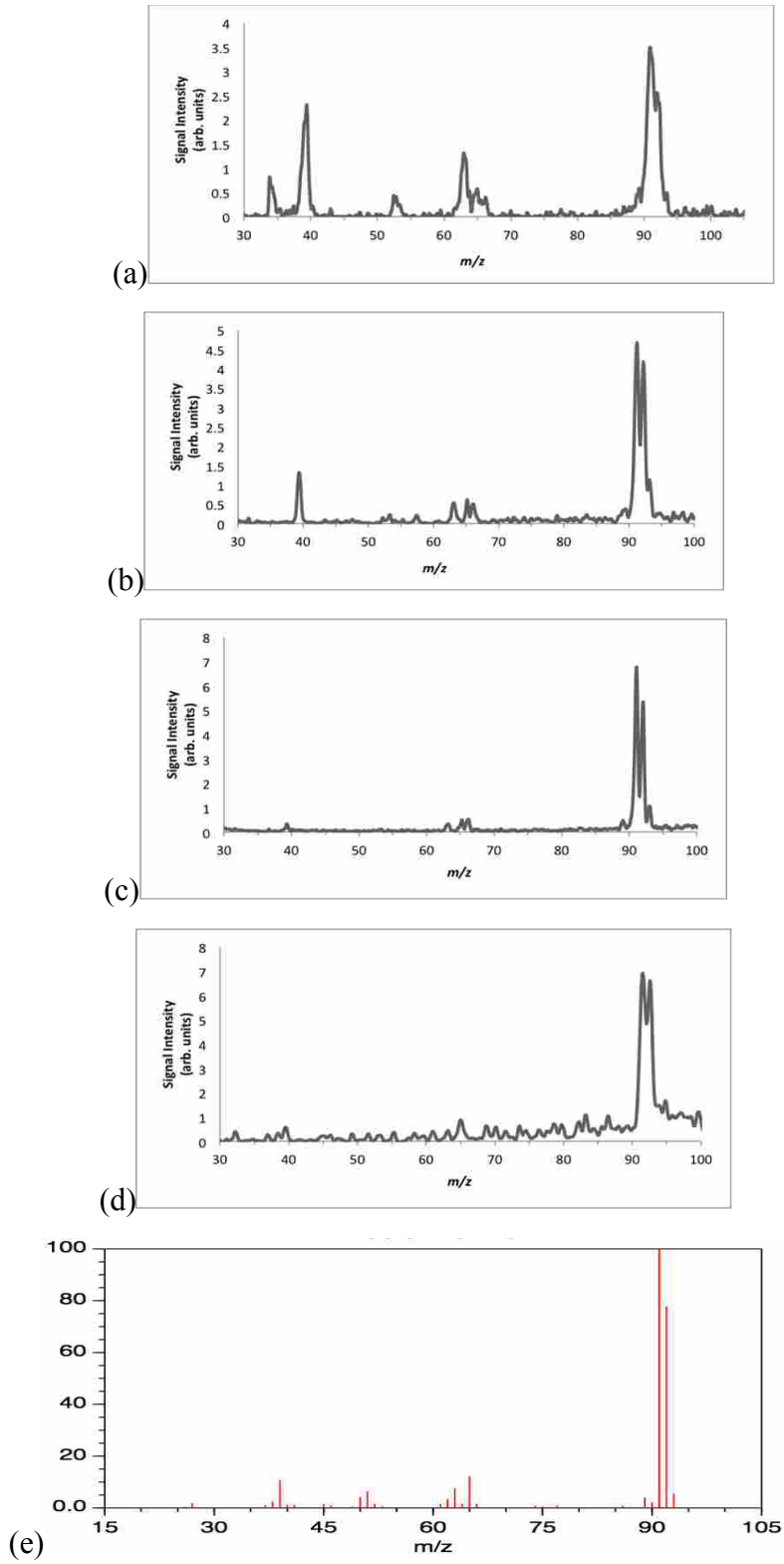

Figure 2-4: The mass spectra were obtained using LIT plates coated with different germanium thickness (a) 100 nm thickness; (b) 200 nm thickness; (c) 400 nm thickness; (d) 800 nm thickness; (e) EI mass spectrum of toluene from NIST database

2.2.3 Further Miniaturization

The linear ion trap was further miniaturized without remaking the plates. Only the capacitive voltage dividers on the PCBs were modified to create a suitable electric field for the miniaturized trap. The plate spacing of the trap (r_0 = 0.95 mm) has been decreased to 43% of its original value (r_0 = 2.19 mm), resulting in a significantly smaller trapping region but maintained good resolution. It provided the first experimental data of any LIT with trapping dimensions, r_0, less than 1 mm. The main benefit of the linear ion trap over the conventional Paul trap is the increased ion storage capacity,[47] and with simpler trapping fields than those of the toroidal trap.[43,48] The increased storage capacity of the planar linear ion trap makes it an ideal candidate for initial exploration of the viability of planar ion traps as miniaturized mass analyzers.

The electric potential in the space between the plates was calculated using SIMION 8.0 (Scientific Instrument Services, Ringoes, NJ, USA) and Matlab (Mathworks, Natick, MA, USA) using a previously published procedure.[41] The electrode patterns were made to be symmetric about the central ejection slit as shown in Figure 2-2. The pattern in the planar electrode LIT was a series of symmetric lines, numbered from line pairs closest to the slit going outward. The line pair closest to the slit is assigned as Line 1 (one on each side of the central, or slit electrode), and the line pair furthest from the slit is assigned as Line 5.

The mass-selective instability scan used in the planar electrode LIT employed a linear ramp of the RF amplitude with a constant additional AC signal. The RF trapping voltage was 230 $V_{0\text{-}p}$ at a frequency of 2.82 MHz. This RF frequency was chosen based on available power supplies and is higher than that used with the larger plate spacing reported previously. As discussed by Tian et al.[49] and Pau et al.,[33] higher RF frequencies are generally needed for smaller trapping dimensions due to the fundamental relationship between RF voltage, frequency, and

size of ion traps. The ionization time was 30 ms, and the cooling time was 40 ms. The RF voltage was ramped from 230 $V_{0\text{-}p}$ to 610 $V_{0\text{-}p}$ over a period of 200 ms. The AC signal was constant at a frequency of 1350 kHz and had a magnitude of 7.4 $V_{0\text{-}p}$. The ionization time, AC frequency, and AC magnitude were optimized experimentally to obtain the highest quality spectra. The signals from 100 scans were averaged to produce a single spectrum. The uncorrected pressure of sample gasses in the vacuum chamber was 1.0×10^{-4} Torr measured with an ion gauge, and the uncorrected pressure of background helium buffer gas was 2.8×10^{-3} Torr measured with a Pirani gauge. The timing of the control signals is shown in Figure 2-5. The headspace vapors were sampled using the same inlet and procedure described previously.[45]

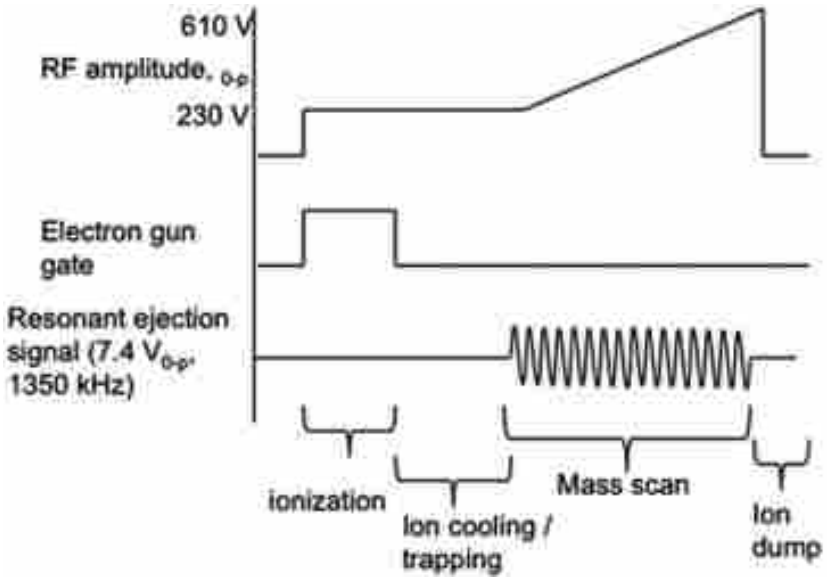

Figure 2-5: Control signals for the planar electrode linear ion trap experiment

Several electron ionization mass spectra of toluene were obtained using a linear ramp of RF amplitude and resonance ejection. The characteristics of the spectra showed some

dependence on the alignment of the two plates. As the plate assembly was disassembled and reassembled, the spectra showed variation, even under otherwise similar conditions. Figure 2.6 shows four such spectra. These four spectra were obtained under identical experimental conditions, but the ion trap was disassembled and reassembled between each. Schwartz et al.[37] demonstrated that LITs are particularly sensitive to the alignment of the electrodes, and the present observation appears to be a manifestation of that effect. Although the alignment of plates was verified using calipers after each assembly, small differences in alignment appear to be responsible for noticeable differences in spectra. Improved techniques to align the plates are the subject of ongoing research.

The molecular ion at m/z 92 and the fragment ion at m/z 91 appear in all spectra. Fragment ions at m/z 65, 63, and 39, which correspond to the cyclopentadienyl ion, its H_2 loss, and its ethyne loss, respectively, are observed in one spectrum, but are not observable in the others. The small features around m/z 50 could be due to a very small number of ions at m/z 50 and 51, which are known fragment ions of toluene; however, these peaks are below the detection limit. In the top spectrum, the signal intensity is greater, but the peaks are wider, possibly due to small differences in plate alignment, or to space charging. The different intensity might also be related to the different pattern of observed fragment ions. For the remaining spectra, the mass resolution (m/Δm FWHM) was measured to be 120–130 in the mass range of m/z 91 to 93, comparable with the resolution obtained using larger plate spacing.[45] However, the mass accuracy of the m/z 91 and 92 peaks was off by approximately one mass unit with a significant delay in the ejection of m/z 92. These shifted peaks might also be the result of space charging or non-linear fields.[50] Increasing the ionization time did not result in increased peak intensity; however, the peak intensity decreased when ionization times shorter than 30 ms were used.

These observations suggest that the trap was operating near a space-charge limit, but direct measurements of the number of trapped ions were not made.

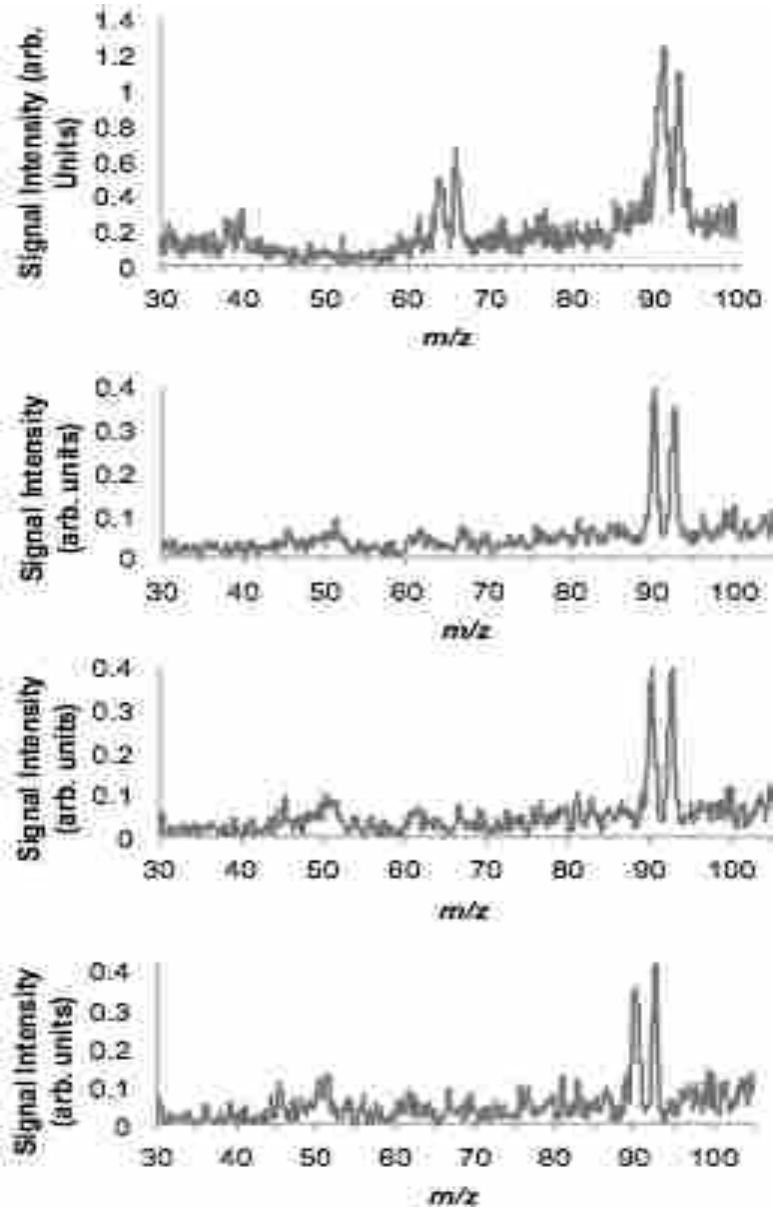

Figure 2-6: Four EI mass spectra of toluene using the planar electrode LIT with r_0 = 0.95 mm. The spectra were obtained under identical conditions, but the trap was disassembled and reassembled between each. Differences in the spectra may be due to small changes in plate alignment.

Figure 2.7 shows a spectrum of dichloromethane taken using the planar electrode LIT. This spectrum is an average of 200 individual scans. A different amplifier – with a significantly slower response time – was used in the results presented in Figure 2.7 from that used above, due to a failure in the original amplifier. Ions at m/z 49, 51, 84, 86, and 88 are observed, corresponding to the chlorine isotope peaks of the molecular ion and the Cl-loss fragment ion. The isotope ratios correspond with those expected. Several smaller peaks may be due to contamination. Similar to the toluene results, unit mass resolution or better is observed for all peaks, but the mass accuracy is off by as much as ±0.5 m/z units. As with toluene, the mass error in dichloromethane peaks was observed to be repeatable between scans.

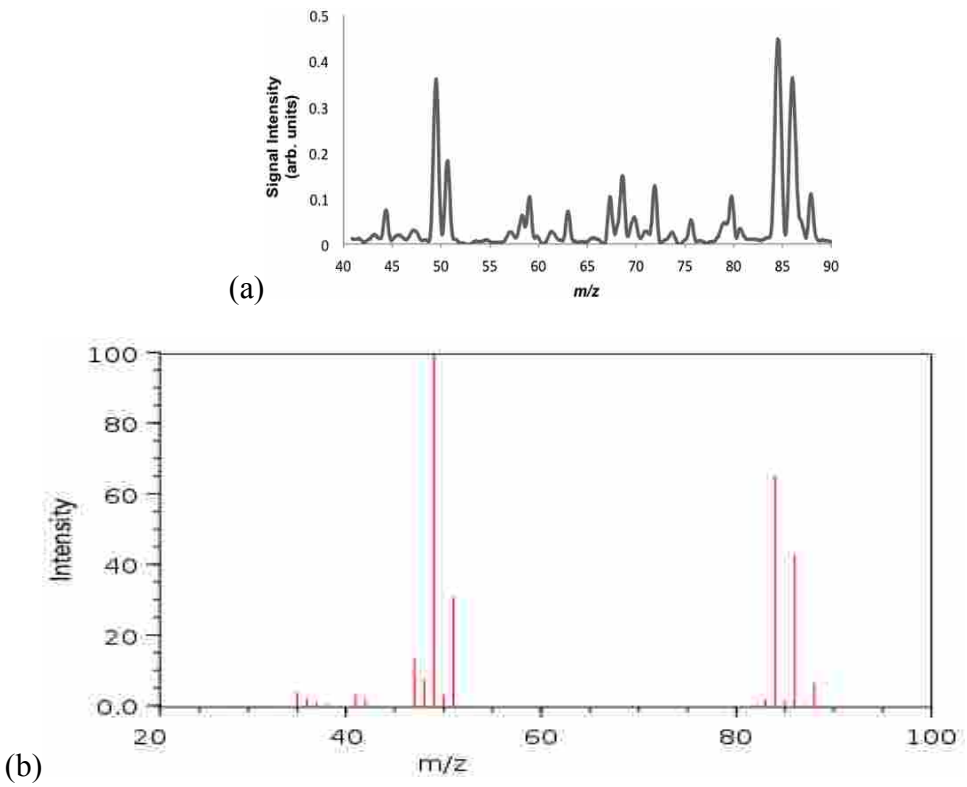

Figure 2-7: (a) EI mass spectrum of dichloromethane using the planar LIT with r_0 = 0.95 mm; (b) EI mass spectrum of dichloromethane from NIST database

The resolution of the LIT with plate spacing of r_0 = 0.95 mm is comparable to that of the LIT with r_0 = 2.19 mm plate spacing. Even though the 0.95 mm trap is smaller, the resolution was not greatly sacrificed by the reduced trapping volume. Several parameters affect the resolution, including RF frequency and amplitude, AC frequency and amplitude, end-bar voltage, electron gate voltage, DC off-set voltage, detector voltage, ionization time, cooling time, ramp time, sample pressure, helium pressure and scan averaging number. All of the parameters should be varied and optimized to generate signals and spectra with good resolution.

We have obtained the first experimental data from a linear ion trap with a half-spacing (r_0) of 0.95 mm by positioning two plates closer together from previous 2.19 mm without remaking the plates, which demonstrated the retained resolution as the larger LIT. The capacitive voltage dividers on PCB provided different RF amplitudes to each electrode and the capacitor values were adjusted to provide the correct electric field at this closer spacing. The length of the trapping region, 45 mm, is unchanged from the old device.

2.2.4 Calculating and Optimizing Electric Fields

In this work, the full RF amplitude was applied to Lines 2, 4, and 5, while 65% of this RF amplitude was applied to Line 3, and 16.1% of the RF magnitude was applied to Line 1. This potential distribution yields a field with the same monopole value as that in our previously published work.[45] These RF amplitudes were established by soldering small, surface-mount capacitors onto two PCBs, one behind each ceramic plate. Other than the values of the capacitors used, the PCBs were identical to those used with the larger plate spacing. The total capacitance of each plate was 25 pF. This value was chosen arbitrarily for convenience, and the values of individual capacitors were normalized to achieve this total capacitance. For a portable

instrument it would be desirable to minimize the capacitance of this device, and this will be pursued in future work.

As mentioned above, initial exploration of the planar electrode LIT was presented in previous work.[45] The plates were designed for a larger spacing – the slit width, electrode width, and electrode spacing were all selected to produce best results for an ion trap more than twice the size of the present device. It is not suggested that these same plates can be moved closer together indefinitely without any redesign, but rather that lithographically patterned plates in general are a viable option for miniaturization.

Table 2-1 shows the coefficients (not normalized) of the equations for the lowest multipole terms for each patterned line pair when the plates are spaced with r_0 value of 0.95 mm. For comparison, Table 2-2 shows the coefficients with the originally designed spacing with an r_0 value of 2.19 mm. The electrode encompassing the ejection slit was kept at zero potential during trapping and ejection. Note that the values of the higher-order fields on each line are significantly different between the two spacings. Because the size of the ejection slit and the plates did not change as the plates were moved closer together, the effects of the slit and plate edges were different between the two plate spacings. The optimized RF amplitudes applied to each electrode compensate for these slit and edge effects, which is why the RF amplitudes on each electrode are very different between the two spacings. A comprehensive treatment of this approach, and the effects of varying the trapping field by changing the RF amplitudes of individual electrodes, is given in the publications of Zhang et al.[51] and Austin et al.[41]

Table 2-1:
Multipole coefficients for each patterned electrode line with plate spacing r_0 = 0.95 mm

Line	A_0	A_2	A_4	A_6	A_8	A_{10}
1	222.4406	-114.182	128.112	-33.9923	228.3132	-781.927
2	139.3137	-149.506	-0.81321	8.377479	109.994	-446.437
3	75.08995	-90.7605	18.46099	-7.713	71.96953	-279.807
4	12.86505	-15.9104	3.936706	-2.38406	15.78186	-59.7109
5	1.007278	-1.24664	0.30418	-0.11435	0.785304	-3.05944

Table 2-2:
Multipole coefficients for each patterned electrode line with plate spacing r_0 = 2.19 mm

Line	A_0	A_2	A_4	A_6	A_8	A_{10}
1	168.4429	18.4	-2.525	2.06	-5.0509	4.389
2	185.4522	-7.0538	-6.2327	0.8457	-2.3571	2.1646
3	209.479	-34.6738	-3.8072	1.3366	-1.7502	1.62
4	108.4486	-25.6412	0.3638	0.567	-0.7763	0.7001
5	48.3397	-12.2671	0.4456	0.2134	-0.3428	0.3803

Tables 2-1 and 2-2 illustrate some specific effects that occur when the plates are more closely spaced. First, the monopole, or A_0 term, is generally much smaller as the plates are spaced closer together. This is because the central grounded electrode covering the slit occupies a larger solid angle as seen from the trapping center, and therefore becomes more dominant on the trapping field as the plates are moved together. To compensate for this effect, higher voltage must be applied to the outer electrodes.

In compensating for the loss in effective voltage in the trap, there is a loss of range in the tuning of the higher order multipoles. While the octopole (A_4/A_2) and the dodecapole (A_6/A_2) terms are comparable with the original 4.38 mm spacing, the even higher order terms are orders of magnitude different. This might explain the large voltage needed to accomplish resonant ejection compared with the voltage used in the larger trap. This problem can be addressed by using a narrower ejection slit and with a redesign of the electrode layout to be more appropriate

for the miniaturized spacing. It should be noted that the pattern used on these plates is far from optimal for this plate spacing, but nevertheless can produce reasonable results. This effect is in contrast to ion traps made using machined electrodes, where such a large displacement from the optimal trapping geometry would severely degrade performance.

2.3 Sub-mm Linear Ion Trap

2.3.1 Instrumentation

We have demonstrated the linear ion trap with r_0 = 2.19 mm and 0.95 mm plate spacing using toluene and dichloromethane, and obtained acceptable mass resolution. With the size reduction, the ion trap performance was still maintained. Since this project aims at developing the miniaturized linear ion trap, the size limit would be one of the important issues. The size reduction process should move forward in small steps to gradually solve unexpected problems. Therefore, the next step is to further miniaturize the linear ion trap.

A linear ion trap with characteristic trapping dimension of r_0 = 362 μm was created to test the possibilities of miniaturization using the two-plate approach. By reducing the size of LIT to sub-mm scale, the power consumption will be greatly reduced using lower voltages, and smaller and less electrodes allow less capacitance, which would be an efficient way to ion trap miniaturization.

The plate of the large linear ion trap (r_0 = 2.19 mm and 0.95 mm) demonstrated above consists of 8 RF electrodes and capacitive voltage dividers to apply RF amplitudes. The capacitor values were adjusted to provide the optimum electric field. However, if the capacitor value is too high, the instrument then requires high operating power, which may exceed the limit

of available power for portable applications. In addition, since the plate spacing is inversely proportional to the RF frequency in Mathieu equation, a high frequency RF power supply would be necessary for a small ion trap. It is difficult to manufacture such an RF power supply with both high voltage and frequency. Therefore, reducing the capacitance is important to reduce the power requirement of the further miniaturized mass spectrometers.

To overcome the capacitance problem in the sub-mm linear ion trap system, the electrode configuration was redesigned such that five electrodes were patterned on each ceramic plate (Figure 2-8). The plate spacing was reduced to 724 μm (r_0 = 362 μm), and the plate size was 2 cm × 4 cm. Compared with the large plate with ten RF electrodes, the small plate only consists of two RF electrodes applied with the same RF amplitude. Thus, no capacitive voltage divider is required in this ion trap, which efficiently reduced the capacitance and simplified the microfabrication process.

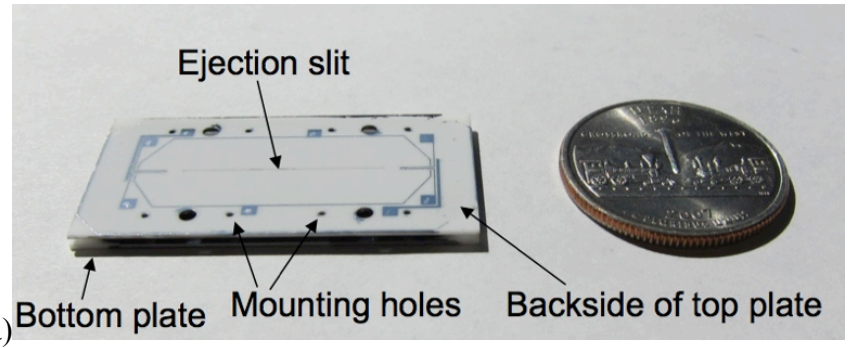

(a)

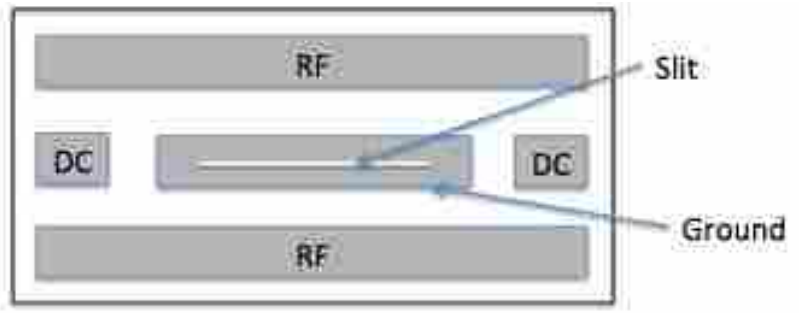

(b)

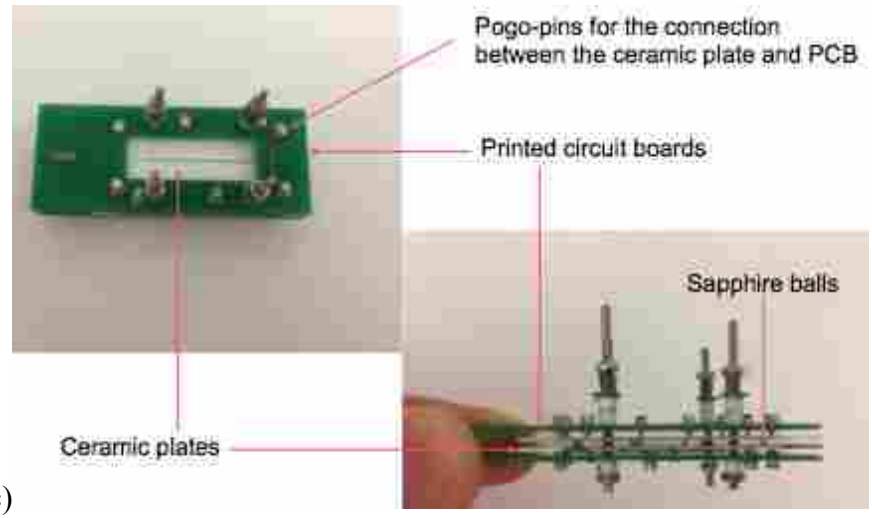

(c)

Figure 2-8: (a) Two ceramic plate facing together at r_0 = 362 µm; (b) electrode configuration on the ceramic plate; (c) assembled sub-mm linear ion trap.

2.3.2 Electric Field Determination

Prior to fabrication, the higher-order field effects were studied using software SIMION 8.0 to create a model for electrode configuration. The electrode configuration on the plate determines the electric field that affects the ion trap performance. Each electrode was designed and optimized in different sizes and positions, and the electric field in each case was determined via SIMION simulation. Higher-order field effects were studied to improve the ion trap performance. One of the electrode configurations with optimal quadrupole and higher-order fields was selected for microfabrication and subsequent use in the following experiment, which contains the electric field similar to that of the published rectilinear ion trap.[29] Theoretically, the two similar electric fields in the sub-mm linear ion trap and rectilinear ion trap would provide similar performance.

The slope of the potential distribution is straight close to the trapping center, which is indicative of a dominant quadrupole and small contributions of higher-order terms. The plot is curved closer to the slits, indicating more nonlinear electric field further away from the trapping center. The electric field was then calculated via subtracting a perfect quadrupole potential from the recorded electric potential. The electric field of the published rectilinear ion trap was studied for comparison (Figure 2-9 a). Hundreds of sub-mm linear ion trap designs were simulated for electric field optimization, and one design with a similar electric field with that of the rectilinear ion trap was obtained (Figure 2-9 b). All of the electric field calculations were normalized. The difference in noise may be due to the large step size.

(a)

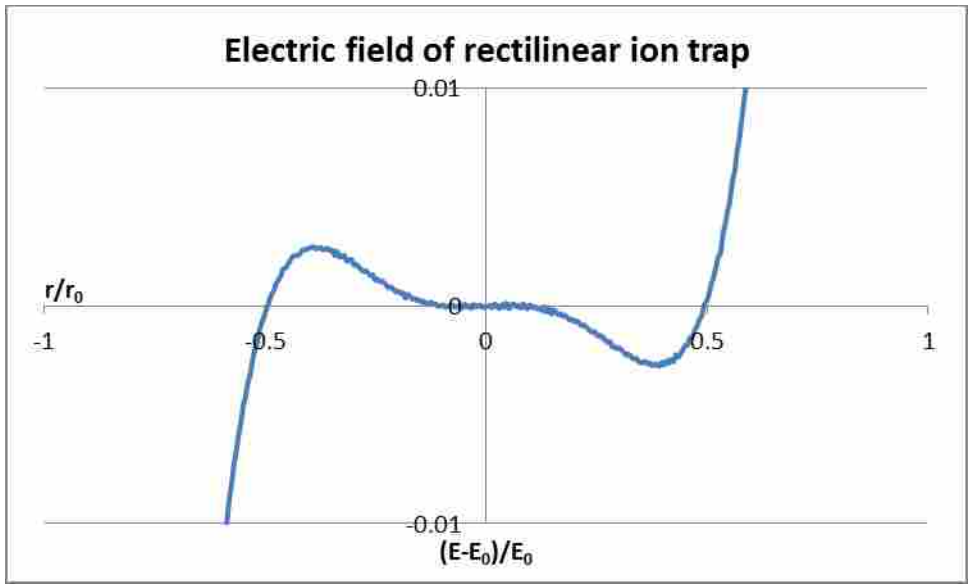

(b)

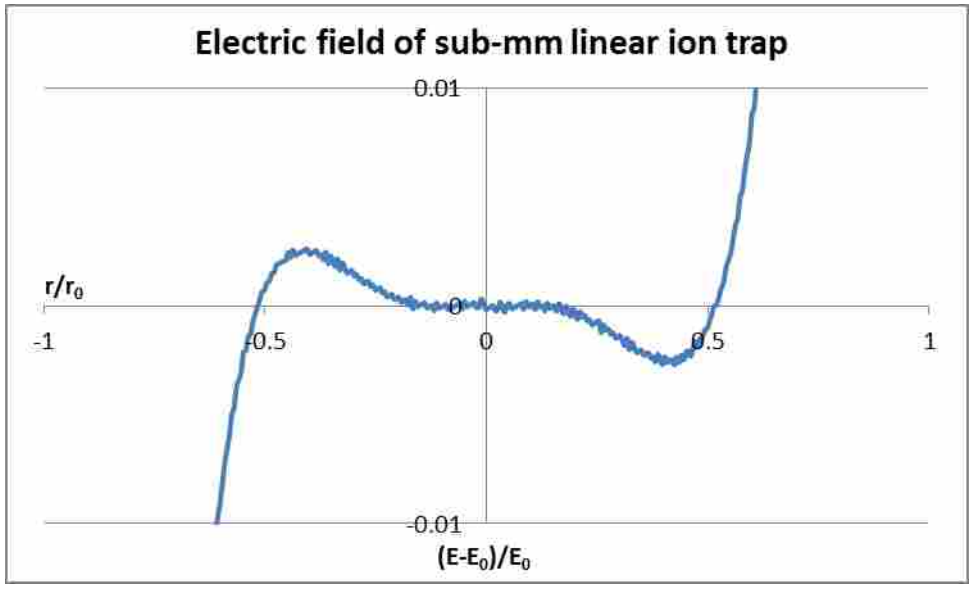

Figure 2-9: (a) Higher order non-linear electric trapping field of the published RIT.[29]; (b) Higher order non-linear electric trapping field of the LIT with r_0 = 362 µm. Differences in noise are not important—what matters is the shape of the overall curve.

2.3.3 Mass Analysis Methods

In most mass analysis experiments, mass-selective instability mode and mass-selective resonant ejection mode are the commonly used methods—these were discussed in Chapter 1. In this experiment, mass-selective resonant ejection was used at the beginning to collect the preliminary data. However, since the size reduction might cause a small trapping capacity and sacrificed resolution, the results may not be able to provide good mass resolution to demonstrate the ion trap performance. To address this problem, a digital waveform was applied as an alternative method to compensate for resolution loss.[52,53] One pair of high and low voltages was used to create trapping and excitation digital waveforms by rapidly switching between discrete voltages; a square wave chirp was used to sweep the trapping frequency. The quadrupolar trapping and excitation waveforms are generated using fast, low voltage electronics. As a consequence, mass spectra can be obtained via frequency sweep rather than the RF amplitude ramp, thereby significantly extending the mass range.

Compared with ramping the RF amplitude, digital waveform operation has been demonstrated to greatly enhance the mass resolution. J. A. Richards[54,55] first introduced the concept of the digital waveform method on a quadrupole mass filter in 1973. Recently, Ding et al.[56,57] presented a theoretical study on ion motion in a quadrupolar field driven using a digital waveform. The digital circuitry was used to produce the rectangular waveforms. By switching the circuits rapidly between discrete DC high voltage levels, a trapping waveform voltage is applied to the ring electrode. The timing of the switches can be precisely controlled by specially designed digital circuitry (Figure 2-10).

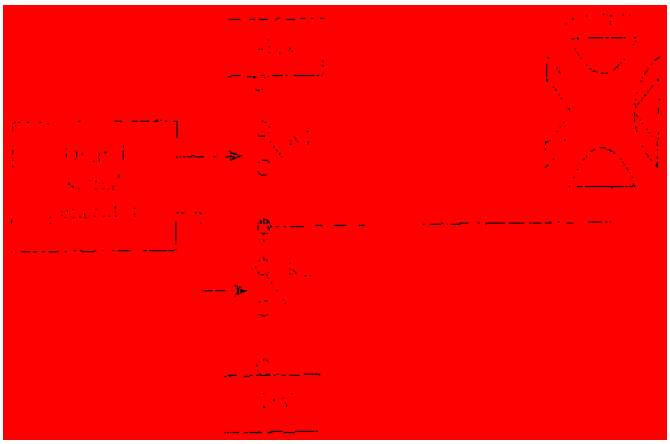

Figure 2-10: Schematic diagram of digital waveform circuitry. K_1 and K_2 are two switches.

For an ion of mass *m* and charge *e* moving in a trap driven by a periodic rectangular waveform (Figure 2-11), the stability parameters can be expressed as solutions of Mathieu equation

$$a_z = \frac{-8eU}{mr_0^2\Omega^2}; \qquad q_z = \frac{4eV}{mr_0^2\Omega^2} \qquad (2\text{-}1)$$

In the above equations, *U* is the DC voltage; *V* is the RF voltage; r_0 is the half-spacing between the two plate in the LIT; Ω is the frequency, where $\Omega = 2\pi/T$, and *T* is the period of the rectangular wave.

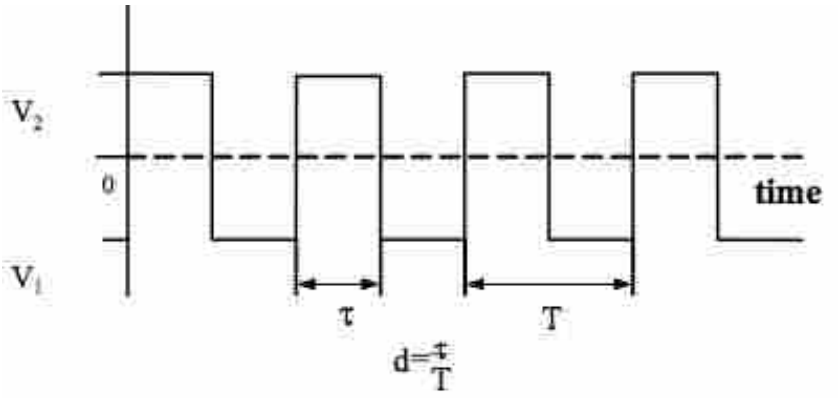

Figure 2-11: Rectangular wave voltages applied to the ion trap; V_1 and V_2 are the low and high discrete DC voltage, respectively; d is duty cycle; τ is the time of positive signal, and T is the period of the rectangular wave.

For the digital trapping waveform, both U and V are related to V_1, V_2 and the duty cycle (d), which can be calculated according to the equations

$$U=d\,V_1+(1-d)V_2 \qquad (2\text{-}2)$$

$$V=2(V_1-V_2)(1-d)d \qquad (2\text{-}3)$$

Parameters could be varied to generate different digital waveforms. For example, by varying the V_1, V_2 or d, U and V would change with time, which varies the a and q values. Alternatively, if only T is changed with time, Ω would be a variable in the analysis. Different waveforms would produce different ion motion and mass selectivity. There is an excitation waveform applied with the trapping waveform, working as 1/3 of the trapping frequency, since the 1/3 ratio of the excitation and trapping frequency has been demonstrated as optimal point in previously published papers.

The relationship among parameters used in digital trap operation is shown in Figure 2-12. An overall timing control is generated from a pulse generator (PNC), triggering the trapping waveform and excitation waveform, and switching the electron gate with time. The trapping waveform was generated from a function generator with a swept frequency from 5.0 to 1.0 MHz switched between -5 and +5 V. However, the required trapping voltages were -25 and +25 V, which were out of the limit of the function generator. A metal-oxide-semiconductor field-effect transistor (MOSFET) was introduced in the circuit design to amplify the amplitude of the trapping waveform. Another function generator was used to generate the excitation waveform with amplitude of -0.5 and +0.5 V at 1/3 of the trapping frequency. One side of the end-bar voltage was controlled using the pulse generator to switch the electron gate, which was opened and closed in expected time duration. The electronic signals were input into the ion trap in the vacuum chamber, and the detector signal was output from the vacuum chamber to the oscilloscope through a preamplifier.

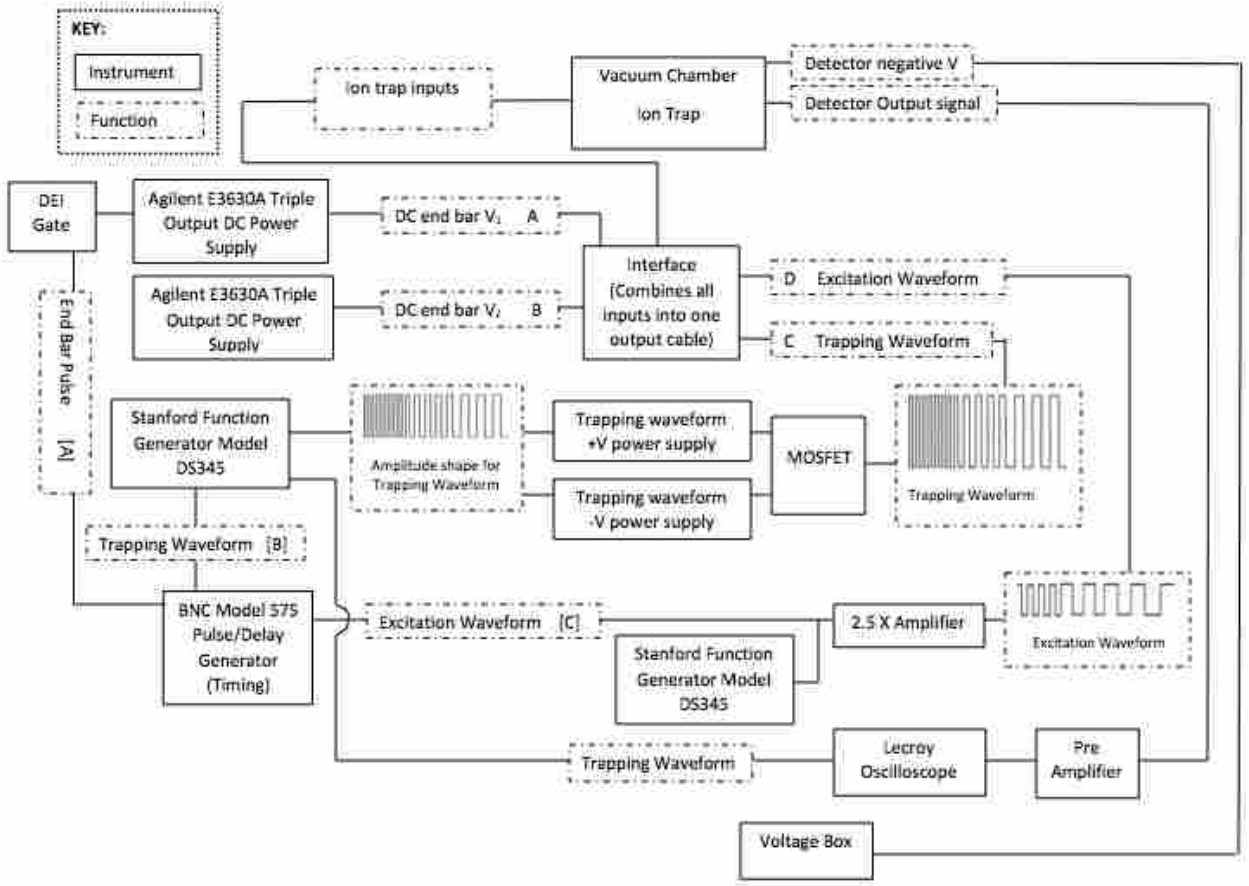

Figure 2-12: Circuit design for ion trap system using digital waveform analysis.

2.3.4 Ion Source Design

In the previous experiments on the planar linear ion trap, electron ionization was used as the ion source. The ion trap was operated in the vacuum chamber filled with sample gas for analysis and helium gas for collisional cooling. The electron gun (made by Torion, Inc.) was positioned close to one of the DC end-bar pointing to the center of the plate along the slit direction. When the electron gun directs a high-energy electron beam, the sample molecules between the two plates are ionized via colliding with electrons. However, with the decreased plate spacing of the miniaturized LIT, the electron beam might not reach to the plate center

completely. A slight deviation or defocusing would significantly reduce the ionization efficiency, which causes insufficient ionization and low sensitivity. To improve the ionization efficiency in the sub-mm LIT, three ionization sources were tested in the sub-mm linear ion trap, including glow discharge ionization, electrospray ionization (ESI) and electron ionization (EI).

A glow discharge ionization source was customized to improve the ionization efficiency due to its high-pressure resistance, low power consumption and long lifetime. The direct-current (DC) glow discharge was created by applying a high potential between two metal electrodes within a gas tube at low pressure (0.1–10 Torr). When the voltage exceeds a threshold named the striking voltage, the gas ionizes. Figure 2-13 is the cross section of a metal flange on the vacuum chamber, separates the air and vacuum at left and right, respectively. A grounded capillary tube is the sample inlet that passes through the vacuum chamber. On the vacuum side, a plastic annular tube with larger diameter enshrouds the capillary tube. A metal needle is fixed on the plastic tube applied with a high negative voltage. The sample molecules ionized via colliding with electrons are driven towards the cathode (needle) by the electric potential, and the electrons are driven towards the anode (capillary tube). Therefore, the sample gas and nitrogen background gas are ionized and inlet into the vacuum chamber by the pressure and voltage difference. The sample ions are filled in the vacuum chamber and trapped by the linear ion trap for mass analysis. Glow discharge ionization source is convenient, high-pressure resistive, low power consumption and robust. However, the background gas may cause high noise in the results, and ion fragmentation is easily influenced by pressure.

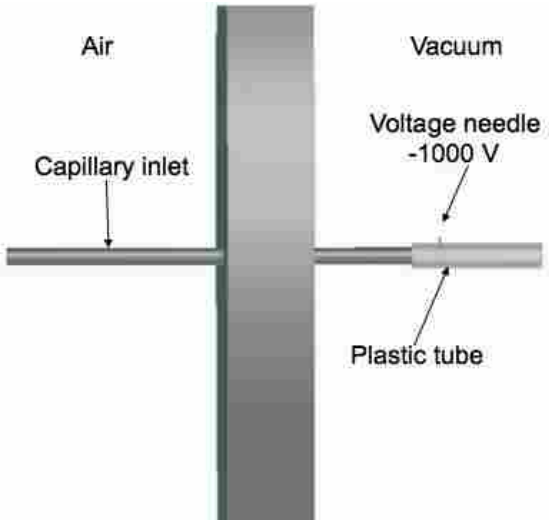

Figure 2-13: Customized glow discharge ionization source

In addition to glow discharge ionization, an electrospray ionization source was customized as the ion source (Figure 2-14). The capillary tube was used as sample inlet. A sample needle was positioned to align with the hole of the capillary tube outside the vacuum chamber. The sample solution was pumped using a syringe pump, then ionized and sprayed at the needle tip applied with -3000 V. At the needle tip, a Taylor cone was formed as the spray under the high voltage. An air curtain of nitrogen gas was used to accelerate solvent evaporation. In the ESI source, the ionization process may be explained by three mechanisms: the ion evaporation model (IEM), the charge residue model (CRM) and the chain ejection model (CEM).[58] The IEM suggests that the ions experience increased repulsive force during solvent evaporation, and continuously split to smaller droplets. When the Coulombic force is strong enough, the ion will be repulsed out of the droplet. Low molecular weight analytes usually follow the IEM. The CRM suggests that the droplet continuously evaporates, and the charge will finally remain on the ion with all the solvent evaporated out, which applies for large globular analytes. The CEM is for disordered polymers that the polymers leave out of the droplet and

take charge with them. The ESI source makes the sample inlet simple and efficient. However, some practical problems occurred during the experiment, such as high voltage discharge between the needle tip and capillary tube, instability due to improper position between the needle and capillary inlet, and clogging in the capillary due to improper syringe pumping speed. Moreover, some dry spots were found on the ceramic plates after the vacuum chamber was opened, indicating that the droplets were not completely evaporated before being inlet to the vacuum chamber.

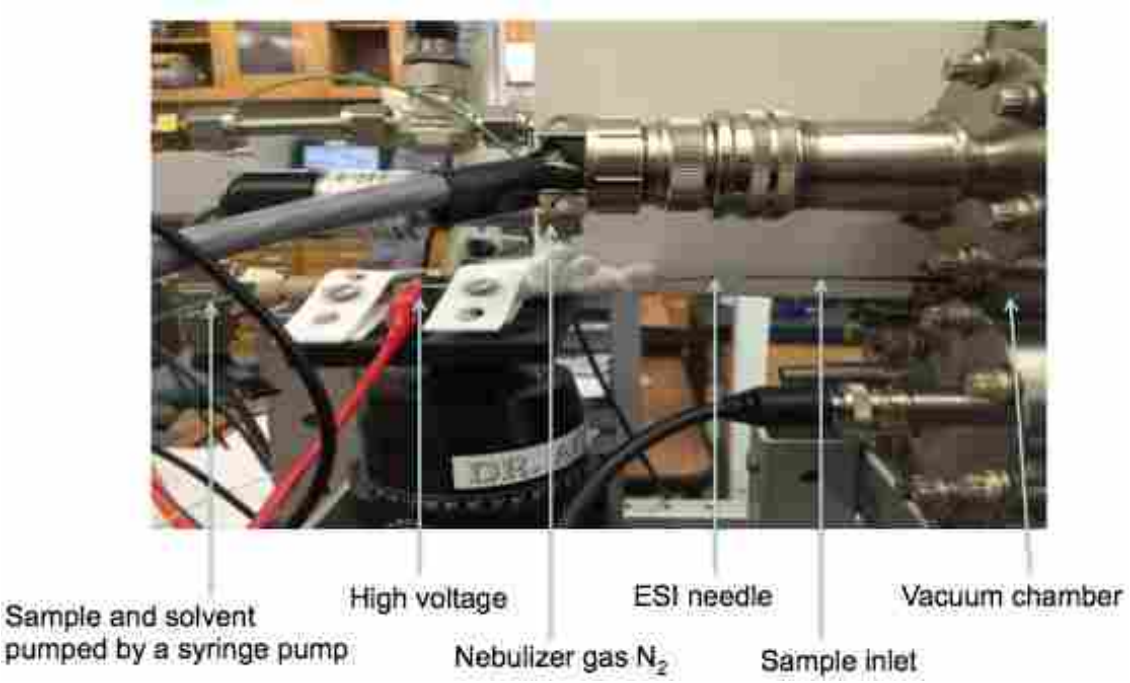

Figure 2-14: Customized electrospray ionization source

We next tested the electron ionization source, which was commonly used in our previous experiment. The tested electron gun was a commercial type, including an electron filament, a Pierce electrode, a chamber, a set of Einzel lens[59] elements and an electron beam outlet hole

(Figure 2-15). The tungsten filament coated with yttrium was applied with -60 V to generate electrons with energy of 60 eV. The Pierce electrode at back of the filament was applied with -61 V to push electrons toward the Einzel lens. The Einzel lens consists of three round electrodes applied with different voltages to focus the electron beam. The focused beam passes through the exit hole of the electron gun chamber and reaches the center of the two ceramic plates for ionization. If the electron beam is well focused, most electrons would reach the trap and the ionization efficiency would be higher.

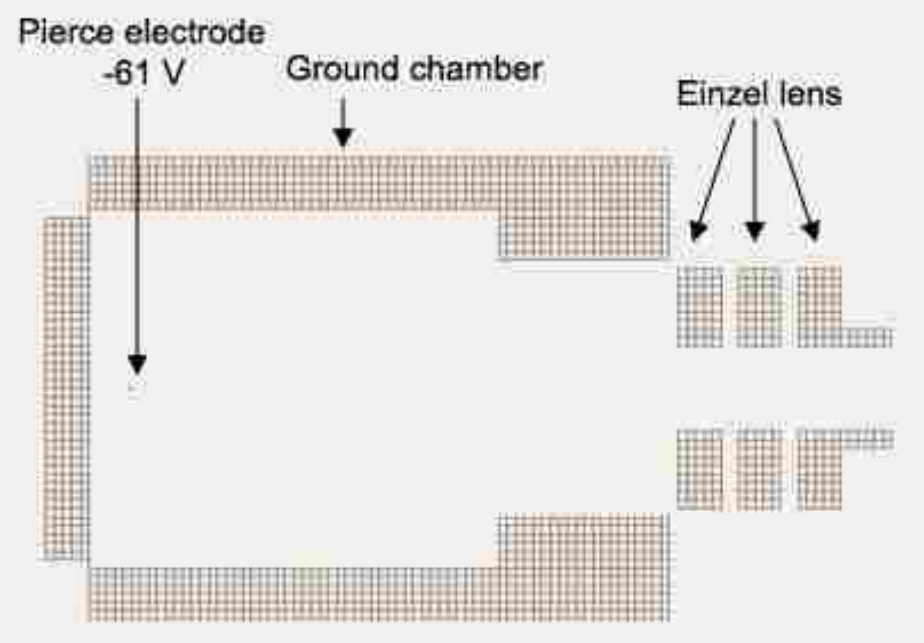

Figure 2-15: Einzel lens geometry of electron ionization source

However, no signal was observed using glow discharge ionization and ESI source, and only weak ionization signal was observed using the EI source. The reason why signals were not observed using both glow discharge and ESI source was not clear, but the low ionization signal from the EI source might be caused by poor beam focusing and thus low ionization efficiency of

the electron gun. To obtain higher signal intensity, the electron gun was redesigned to enhance the ionization efficiency.

Compared with the old electron gun, all parts of the new electron gun were revised (Figure 2-16). Several simulations were carried out with different electron gun geometries, especially on the shape, amount and position of the Einzel lens (Figure 2-17). The electron gun chamber was designed in a rectangular shape due to its better electron focusing and higher electron transmission rate than that of the round shape. The hole on each electrode was also enlarged to a long slit to enhance electron transmission. The curved filament in the old electron gun was replaced by a longer and straight filament to generate more electrons and match the slit. In addition, the geometry of the Einzel lens was redesigned and the electrode number was increased from three to five to achieve good focusing. The performance of the old and new electron guns were simulated and compared in SIMION 8.1 that showed different electron transmission rates, which is the percentage of the electrons passed through the hole/slit to the total number of the created electrons that were similar to each filament in the simulation.

(a) 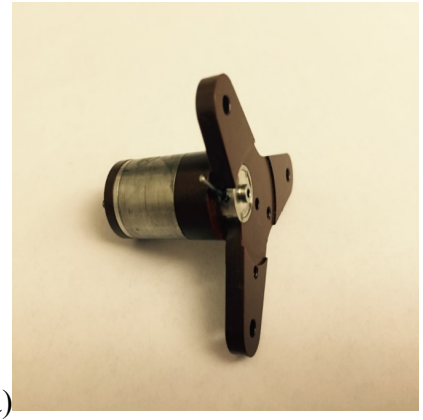 (b) 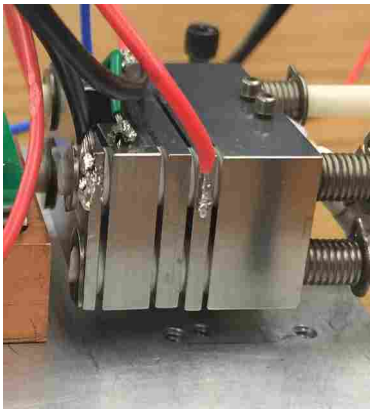

Figure 2-16: (a) Old version electron gun; (b) redesigned electron gun

(a) 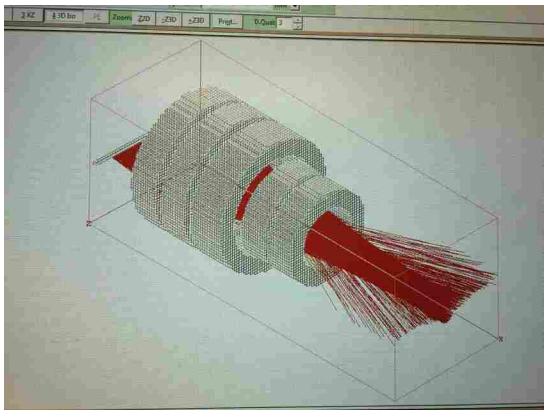 (b) 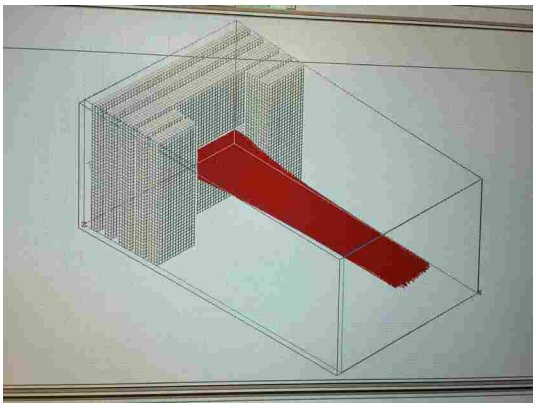

Figure 2-17: Two types of simulated Einzel lens: (a) Round-shape Einzel lens; (b) rectangular Einzel lens with two pairs of focusing electrodes.

The voltage on each Einzel lens electrode was optimized for electron focusing. The voltages on the first three electrodes from left to right are 0, -30 V, 0, which works as a normal Einzel lens. The other two electrodes at the end work as focusing electrodes. The highest electron transmission rate of the old (Torion) electron gun is 29%, while that of the new electron gun reaches 79% (Figure 2-18). The results indicate that the redesigned electron gun significantly improved the electron transmission rate. In a practical experiment, the new filament is longer than the old filament, so that the electrons created in the new electron gun should be more numerous than that in the old electron gun.

(a)

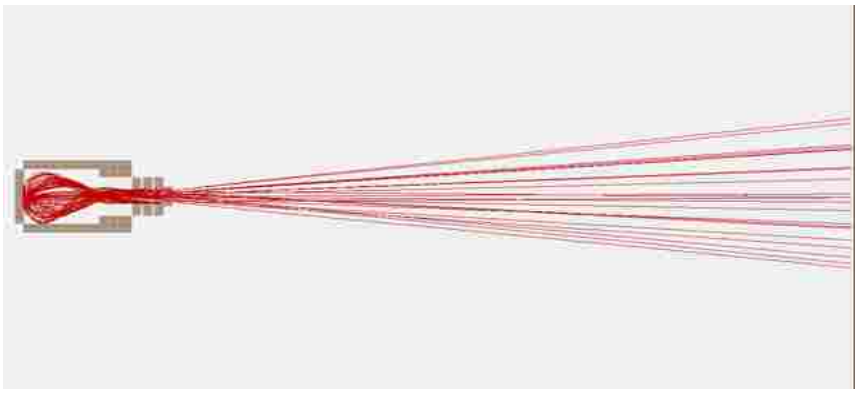

(b)

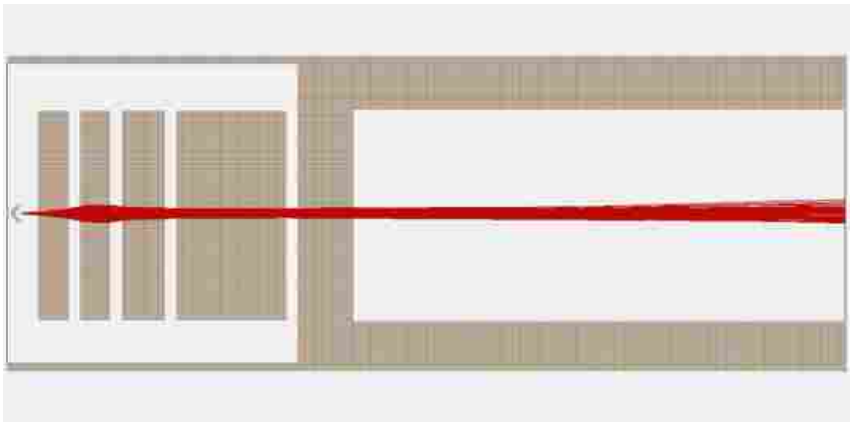

Figure 2-18: (a) Old electron gun with electron transmission rate of 29%; (b) the redesigned electron gun with electron transmission rate of 79%

The simulation results were tested in experiments. A similar trend was observed using a Faraday cup detector, the same ionization voltage and electrode focusing voltages (Figure 2-19). The two electron guns were independently pointed to a Faraday cup detector at the same distance with a mesh in between under vacuum. An ampere meter was connected to the Faraday cup, which measured the emission current received from the electron guns. As a result, the ion transmission efficiency was greatly improved by the redesigned electron gun.

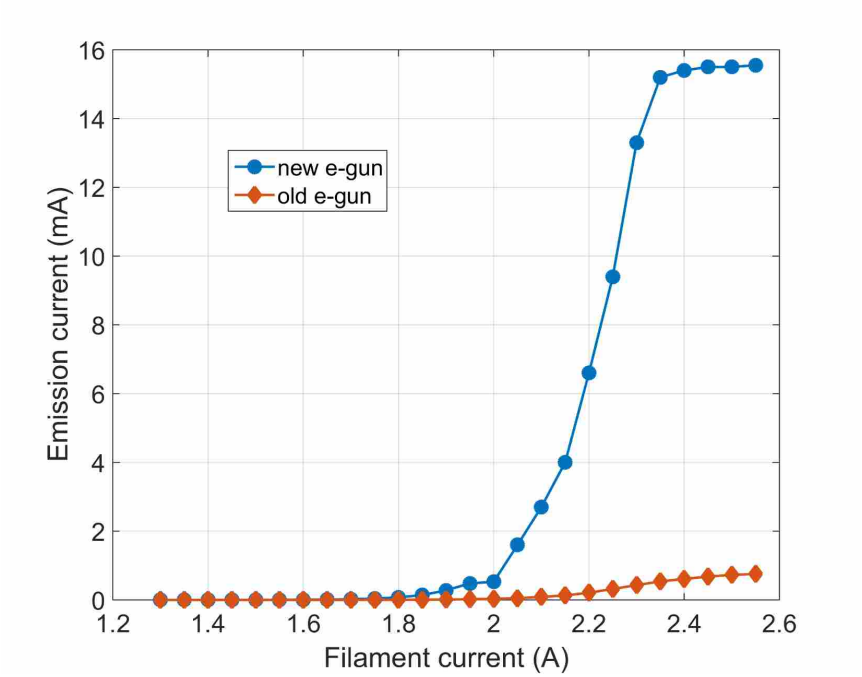

Figure 2-19: Emission current detected by Faraday cup detector. Filament voltage: -61 V

2.3.5 Results and Discussion

Although troubleshooting in the mass spectrometry system was made comprehensive, we were not able to observe any mass spectra with this setup. The feasibility of the sub-mm LIT design was reconsidered and a few drawbacks were revealed. One possible problem might be missing a ground electrode between the RF and AC electrode (Figure 2-20), which may cause interactions between high-frequency RF and AC waveform in such a small distance, so that ions would not be effectively trapped or resonantly ejected. Therefore, a ground electrode might be necessary as a shielding electrode for an effective electric field.

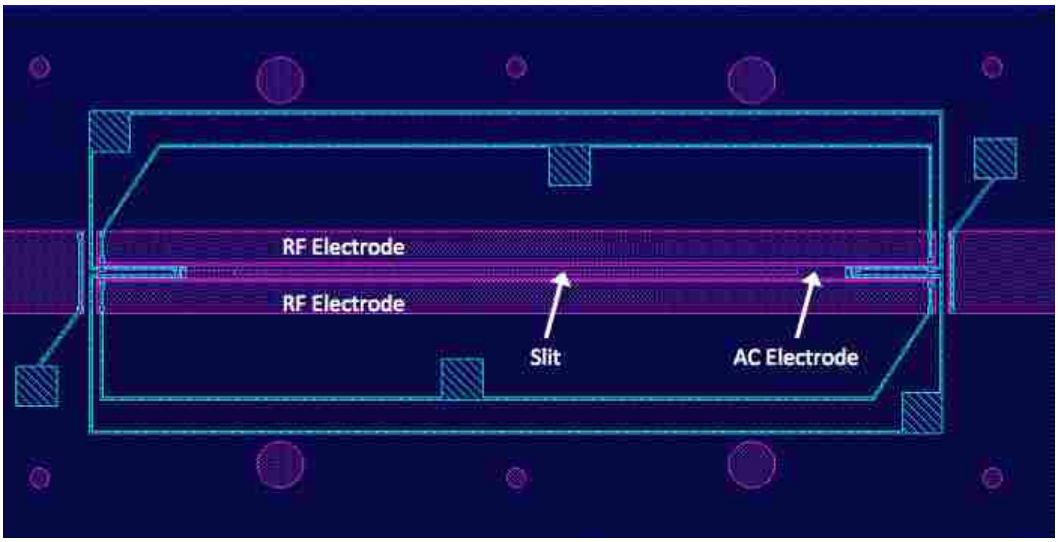

Figure 2-20: Electrode layout on the 724 µm-spacing LIT. A ground electrode should be considered between RF electrode and central AC electrode to avoid waveform interference.

In addition, the DC end-bar may be too small to keep a well-focused electron beam straightforward alone the slit direction, thus the ionization efficiency may be impacted even though the electron transmission efficiency was improved (Figure 2-21). The width of the AC electrode may also be a problem in ion ejection. The AC electrode is 215 µm wide, but a 100-µm slit is contained at inner side of the electrode, so the effective AC electrode may be too narrow to provide enough AC ion resonant ejection (Figure 2-22).

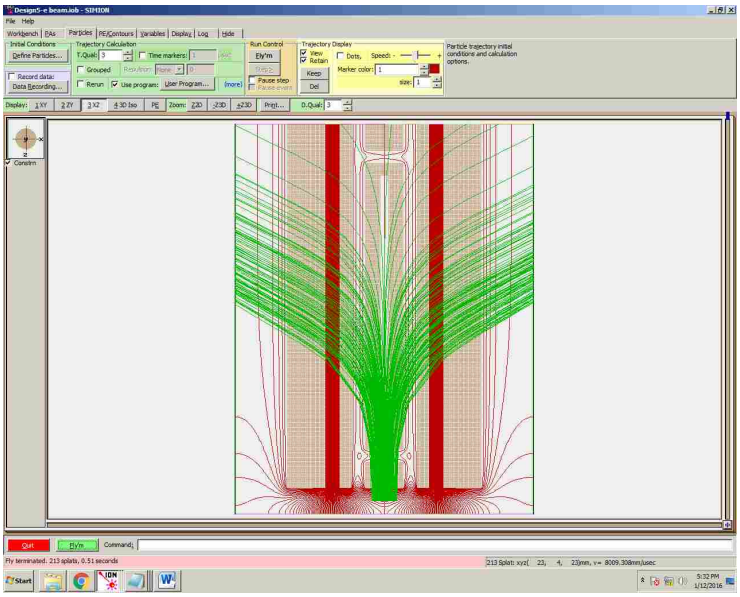

Figure 2-21: Electron beam path through the end-bar electrode in the SIMION simulation

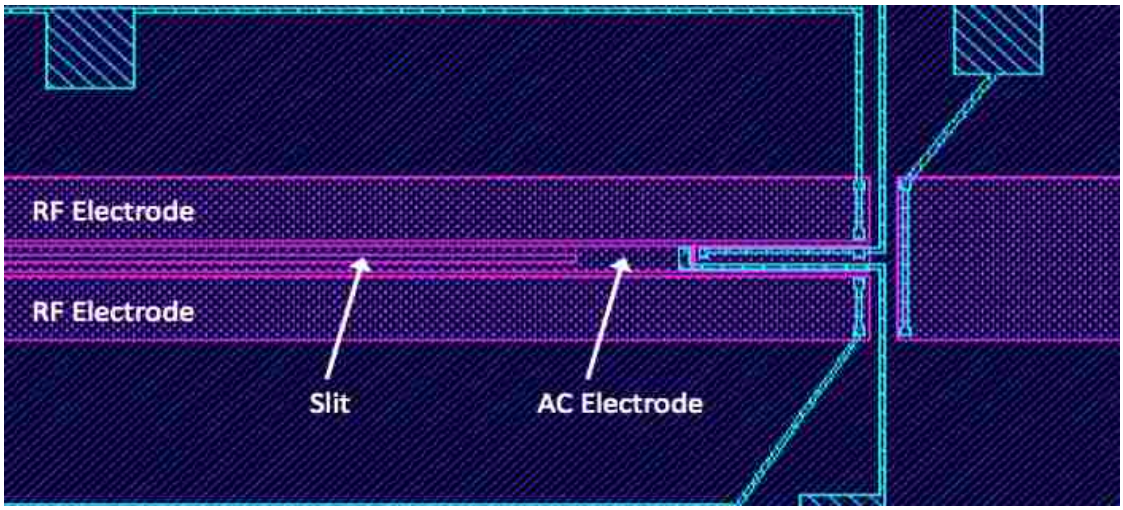

Figure 2-22: Electrode layout zoom-in from Figure 2-20

The most important issue is the aspect ratio of the ceramic plate. The aspect ratio of the large and sub-mm plate are compared in Figure 2-23. The plate spacing is 724 μm and the plate

thickness is 500 μm, however, the slit width is only 100 μm, which may be too narrow to eject ions out through the slit, so that most of the ions hit the edge of the slit before being ejected out. The resulting charge build-up hinders other ions from being ejected. These possible reasons may cause the failure of the sub-mm linear ion trap. Although this sub-mm LIT does not work, we could learn from the failure, which provides the reference for the follow-up ion trap development.

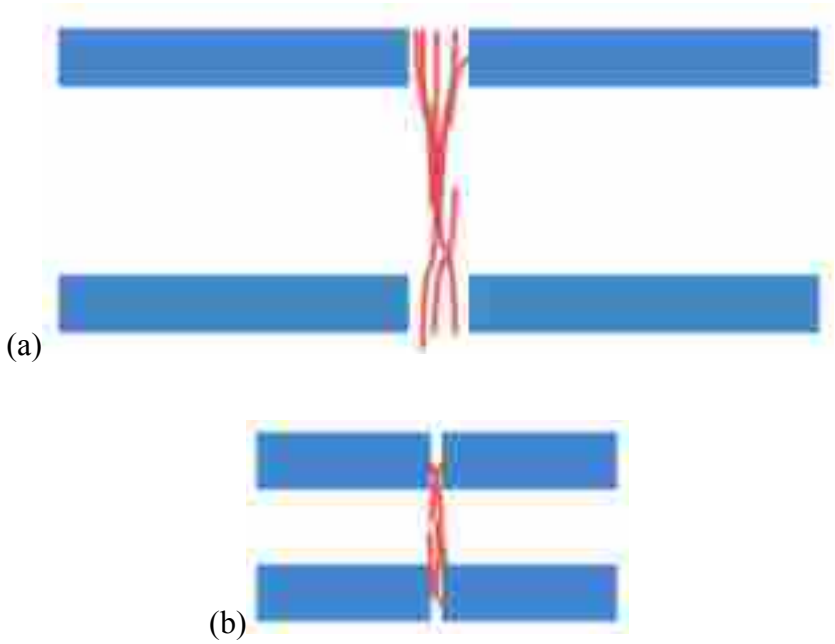

Figure 2-23: (a) Aspect ratio of the large plate; (b) aspect ratio of the sub-mm plate

2.4 Wire Linear Ion Trap

2.4.1 Instrumentation

In most linear ion traps, the geometry consists of solid metal electrodes that are fabricated with ion ejection slits. However, the ion ejection efficiency was limited by the narrow slits that

may reduce the sensitivity. An extreme problem of the ion ejection was described in the sub-mm linear ion trap that ions could not be ejected through the narrow slit with high aspect ratio. In other conditions, slits are not as small as that of the sub-mm linear ion trap, but some portion of the ions are still blocked by the solid electrodes. One immediate solution is to enlarge the slit width. However, a wider slit on the electrode would cause the more severe edge effects that significantly distort the electric field. Wang et al.[60] presented a mesh-electrode linear ion trap with a wide slit that could prevent electric field distortion, but creating a simplifier linear ion trap without using a slit while keeping a good electric field would be an ideal development. Our group created a new type of linear ion trap using fine metal wires instead of solid metal electrodes.[61] In this way, all the electrodes were in wire shape that greatly increased the ion ejection efficiency, and easily fabricated and assembled without using slits. It only requires two end-cap plates fixed on four supporting rods. Wires are run through the laser-drilled holes on the end-cap plates and the threads on each side are braided together. The distance between the two end-cap plates is slightly elongated by adjusting the fixing nuts to tighten the wires. The fabrication and assembling process can be easily achieved in the lab. In addition, it is easy to miniaturize the wire linear ion trap by reducing the spacing between the wires.

The wire linear ion trap consists of twenty-four wires held and positioned under tension by four supporting rods and two plastic end-cap plates (Figure 2-24). The end-cap plates were made of polyether ethyl ketone (PEEK) with 24 laser-drilled holes with 0.23 mm diameter in each plate. The position of the holes was optimized in the simulation and 24 wires with 0.2 mm diameter were fixed through the holes at four sides in a quadrupolar shape (Figure 2-25). The supporting rods and nuts were used to straighten the wires under tension, making a 62 mm length of the wire linear ion trap. The size of the wire linear ion trap was (H × W = 7.6 mm × 6.7 mm).

The trap height is defined as the distance between the top wire and bottom wire that are closest to the center. Similarly, the width is defined as the distance between the left wire and right wire that are closest to the center. An electron beam generated from the electron gun passes through the hole on one end-cap plate embedded with metal electrode. Electron gating was performed on the end-cap electrode to control ionization inside the trap. The ejected ions finally reach the electron multiplier detector through a shielding plate.

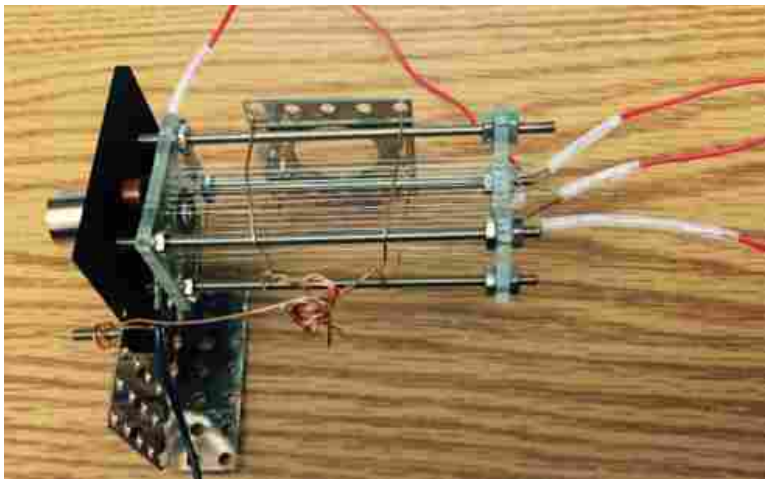

Figure 2-24: Wire ion trap with positioned electron gun. (Adapted from Wu, Q.; Li, A.; Tian, Y.; Zare, R.N.; Austin, D.E., Miniaturized Linear Wire Ion Trap Mass Analyzer. Anal. Chem. 2016, 88, 7800-7806.)

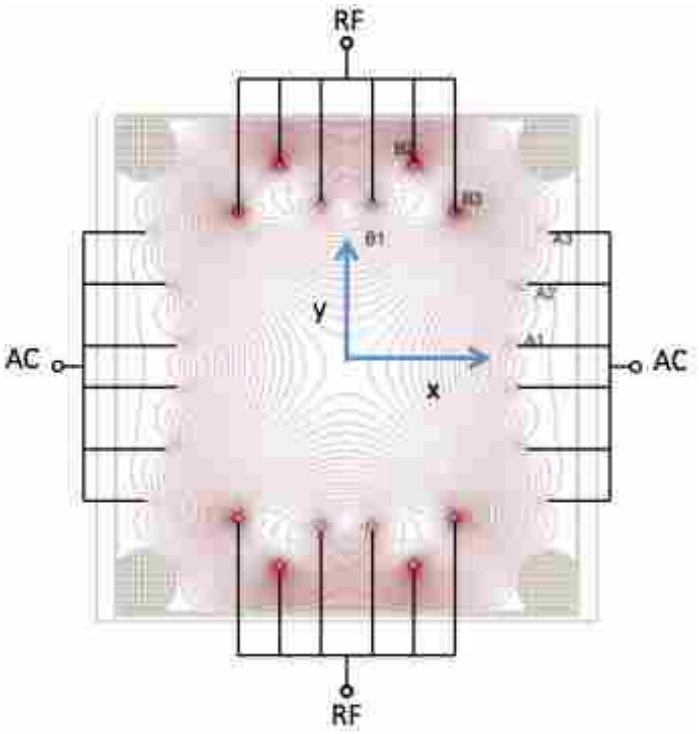

Figure 2-25: Wires position in quadrupolar shape

Mass-selective instability scan was used with a linear ramp of the RF amplitude and a constant additional AC signal. An RF waveform was applied on the wires of one opposite pair for ion trapping, while AC signals are on the other pair for resonant ejection. The RF trapping voltage was 175 $V_{0\text{-}p}$ at a fixed frequency of 1.42 MHz. A static potential of -60 V was applied on the electron gun filament with an ionization time of 150 ms. The RF voltage was ramped from 400 $V_{0\text{-}p}$ to 800 $V_{0\text{-}p}$ over a time period of 250 ms. The AC signal generated by an arbitrary waveform generator (SRS DS345, Stanford Research Systems, Sunnyvale, CA) was constant at a frequency of 180 kHz with amplitude of 4.3 $V_{0\text{-}p}$. The ions were detected using an electron multiplier with -1400 V and the signal was output by an oscilloscope through a preamplifier (Keithley 427 current amplifier, Beaverton, OR). Signal was averaged over 50 scans to produce a single spectrum. The uncorrected pressure of sample gasses in the vacuum chamber was 5.0 ×

10^{-5} Torr measured with an ion gauge (FRG-720, Agilent, Santa Clara, CA), and the uncorrected pressure of background helium buffer gas was 2.6×10^{-3} Torr.

2.4.2 Results and Discussion

Two compounds were analyzed using the wire linear ion trap – toluene and a mixture of toluene and deuterated toluene (toluene-D_8) with a ratio close to 1:1 (Figure 2-26 (a)(b)). The peaks of m/z 91 and 92 of toluene sample shown in Figure 2-26(a) were separated, which presented unit mass resolution. However, the peaks from the mixture of toluene and deuterated toluene in Figure 2-26(b) were not completely resolved. A slight mass shift was observed on both mass spectra possibly due to wire misalignment, space charge effects or low precision of fabrication. The results demonstrated the feasibility of the wire linear ion trap. The follow-up experiments for ion trap optimization and improvement have been done.

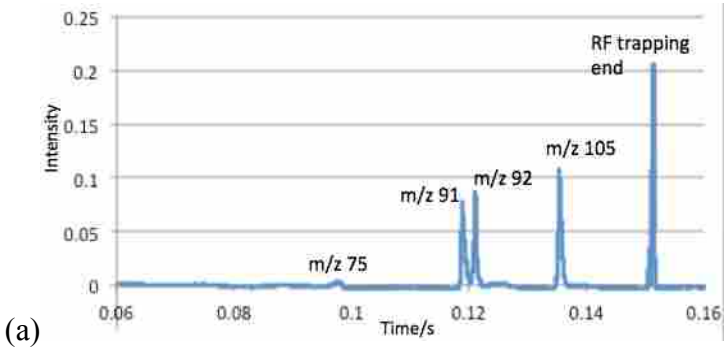

(a)

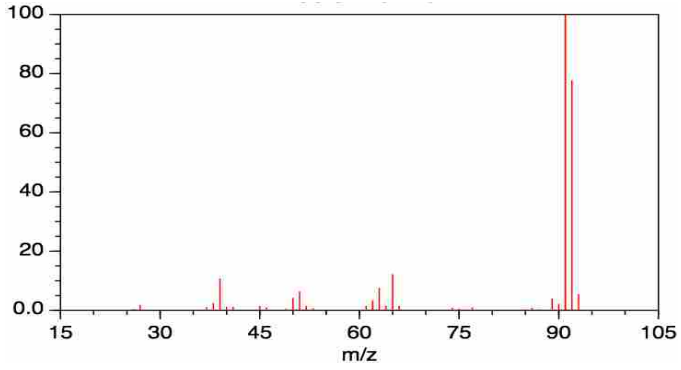

(b)

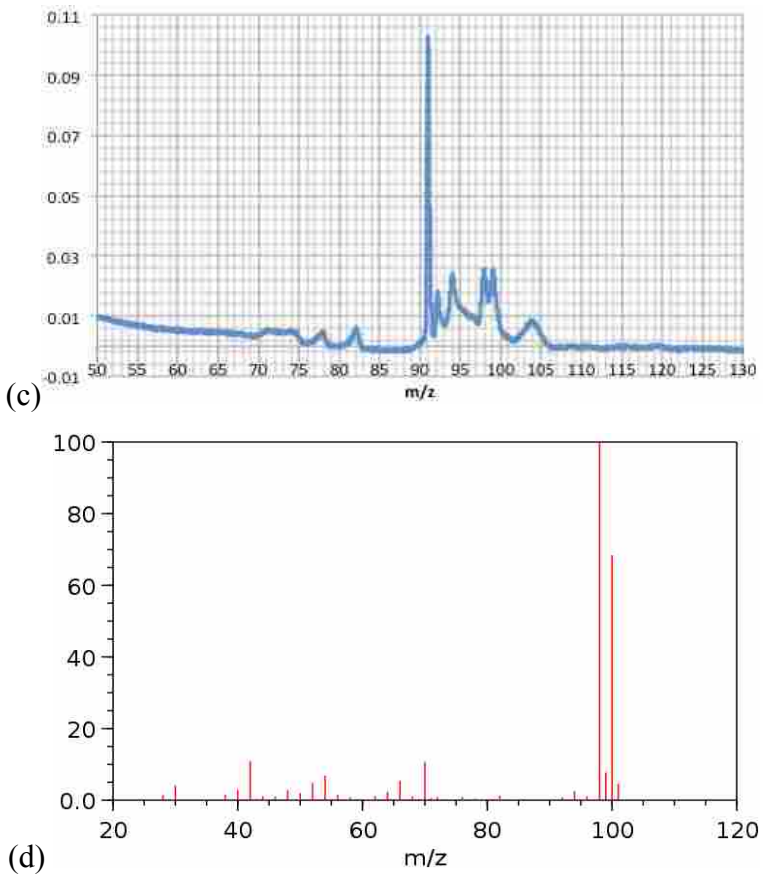

Figure 2-26: (a) Mass spectrum of toluene from wire linear ion trap; (b) EI mass spectrum of toluene from NIST database; (c) mass spectrum of toluene and deuterated toluene (D_8) mixture; (d) EI mass spectrum of deuterated toluene (D_8) from NIST database

2.5 Conclusion

The experiments demonstrated the feasibility of ion trap miniaturization using lithographically patterned planar electrodes. The 1.90 mm spacing ion trap in the present work has a higher aspect ratio than that with the larger plate spacing (4.38 mm), increasing the theoretical trapping capacity compared with a device with all three dimensions scaled by the same amount. The 1.90 mm spacing LIT can be made without remaking the ceramic plate by only changing the capacitive voltage dividers on the PCBs, which provides a simpler way for ion

trap miniaturization. We have also demonstrated an interesting property of such ion traps, which is that the germanium coating at the inner side of the plate might affect the mass resolution.

A further miniaturized sub-mm LIT with plate spacing of 724 μm was created and tested in both mass-selective resonant ejection mode and digital waveform method. Several improvements and troubleshooting were made in the ion source customization, electron-gun redesign and simulation. Some drawbacks in the LIT design were found that might cause the failure of the ion trap operation. These experiments have provided guidance with regard to the electrode and slit layout on future miniaturized designs.

A linear ion trap made of 24 wires supported between two plates was studied and demonstrated experimentally. Unit mass resolution was obtained in the toluene sample, but the mixture of toluene and deuterated toluene (toluene-D_8) was not resolved. Mass shift was observed in the results, which may be caused by wire misalignment of untightened wires. The parameters were adjusted to generate the mass spectra. More optimization work on the ion trap performance improvement is necessary in the following experiments.

2.6 References

1. Careri, M.; Mangia, A., Trends in analytical atomic and molecular mass spectrometry in biology and the life sciences. *Anal. Bioanal. Chem*. **2011**, *399*, 2585-2595.

2. Lee, M.S.; Zhu, M.; Jian, W.; Yao, M.; Wen, B.; Jones, E.B., Use of triple quadrupole–linear ion trap mass spectrometry as a single LC–MS platform in drug metabolism and pharmacokinetics studies, in Mass Spectrometry in Drug Metabolism and Disposition: Basic Principles and Applications. John Wiley, Hoboken, NJ, USA, 2011, chap. 15.

3. Curcuruto, O.; Guidugli, F.; Traldi, P.; Sturaro, A.; Tagliaro, F.; Marigo, M., Ion-trap mass spectrometry applications in forensic sciences. I. Identification of morphine and cocaine in hair extracts of drug addicts. *Rapid Commun. Mass Spectrom*. **1992**, *6*, 434-437.

4. Johnson, R.D.; Botch, S.R., The screening of forensic blood, urine, and tissue specimens for xenobiotics using ion-trap liquid chromatography-tandem mass spectrometry. *J. Anal. Toxicol*. **2011**, *35*, 65-74.

5. Leshin, L.A.; Mahaffy, P.R.; Webster, C.R.; Cabane, M.; Coll, P.; Conrad, P.G.; Archer Jr, P.D.; Atreya, S.K.; Brunner, A.E.; Buch, A.; Eigenbrode, J.L.; Flesch, G.J.; Franz, H.B.; Freissinet, C.; Glavin, D.P.; McAdam, A.C.; Miller, K.E.; Ming, D.W.; Morris, R.V.; Navarro-González, R.; Niles, P.N.; Owen, T.; Pepin, R.O.; Squyres, S.; Steele, A.; Stern, J.C.; Summons, R.E.; Sumner, D.Y.; Sutter, B.; Szopa, C.; Teinturier, S.; Trainer, M.G.; Wray, J.J.; Grotzinger, J.P.; MSL Science Team. Volatile, isotope, and organic analysis of Martian Fines with the Mars Curiosity Rover. *Science* **2013**, DOI: 10.1126/science.1238937.

6. Gao, L.; Song, Q.; Patterson, G.E.; Cooks, R.G.; Ouyang, Z., Handheld rectilinear ion trap mass spectrometer. *Anal. Chem*. **2006**, *78*, 5994-6002.

7. Malcolm, A.; Wright, S.; Syms, R.R.A.; Dash, N.; Schwab, M.-A.; Finlay, A., Miniature mass spectrometer systems based on a microengineered quadrupole filter. *Anal. Chem*. **2010**, *82*, 1751-1758.

8. Syms, R.R.A.; Tate, T.J.; Ahmad, M.M.; Taylor, S., Fabrication of a microengineered quadrupole electrostatic lens. *Electron. Lett.* **1996**, *32*, 2094-2095.

9. Syms, R.R.A.; Tate, T.J.; Ahmad, M.M.; Taylor, S., Design of a microengineered electrostatic quadrupole lens. *IEEE Trans. Electron Dev*. **1998**, *45*, 2304-2311.

10. Taylor, S.; Tindall, R.; Syms, R., Silicon based quadrupole mass spectrometry using microelectromechanical systems. *J. Vac. Sci. Tech. B*. **2001**, *19*, 557-562.

11. Taylor, S.; Tunstall, J.J.; Syms, R.R.A.; Tate, T.J.; Ahmad, M.M., Initial results for a quadrupole mass spectrometer with a silicon micromachined mass filter. *Electron. Lett.* **1998**, *34*, 546-547.

12. Geear, M.; Syms, R.R.A.; Wright, S.; Holmes, A.S., Monolithic MEMS quadrupole mass spectrometers by deep silicon etching. *J. Microelectromech. Syst*. **2005**, *14*, 1156-1166.

13. Velasquez-Garcia, L.F.; Akinwande, A.I., An out-of-plane MEMS quadrupole for a portable mass spectrometer. *Proceedings of the Solid State Sensors, Actuators and Microsystems Conference*, Cite Centre Des Congres Lyon, France, **2007**, pp. 2215-2320.

14. Velasquez-Garcia, L.F.; Cheung, K.; Akinwande, A.I., An application of 3-D MEMS packaging: out-of-plane quadrupole mass filters. *J. Microelectromech. Syst*. **2008**, *17*, 1430-1438.

15. Chiaverini, J.; Blakestad, R.B.; Britton,J.; Jost, J.D.; Langer, C.; Leibfried, D.; Ozeri, R.; Wineland, D.J., Surface-electrode architecture for ion-trap quantum information processing. *Quantum Inf. Comput*. **2005**, *5*, 419-441.

16. Seidelin, S.; Chiaverini, J.; Reichle, R.; Bollinger, J.J.; Leibfried, D.; Britton, J.; Wesenberg, J.H.; Blakestad, R.B.; Epstein, R.J.; Hume, D.B.; Itano, W.M.; Jost, J.D.; Langer, C.; Ozeri, R.; Shiga, N.; Wineland, D.J., Microfabricated surface- electrode ion trap for scalable quantum information processing. *Phys. Rev. Lett*. **2006**, *96*, 253003.

17. Riter, L.S.; Peng, Y.; Noll, R.G.; Patterson, G.E.; Aggerholm, T.; Cooks, R.G., Analytical performance of a miniature cylindrical ion trap mass spectrometer. *Anal. Chem*. **2002**, *74*, 6154-6162.

18. Patterson, G.E.; Guymon, A.J.; Riter, L.S.; Everly, M.; Raming, J.G.; Laughlin, B.C.; Ouyang, Z.; Cooks, R.G., Miniature cylindrical ion trap mass spectrometer. *Anal. Chem*. **2002**, *74*, 6145-6153.

19. Wu, G.; Cooks, R.G.; Ouyang, Z., Geometry optimization for the cylindrical ion trap: field calculations, simulations and experiments. *Int. J. Mass Spectrom*. **2005**, *241*, 119-132.

20. Yang, M.; Kim, T.; Hwang, H.; Yi, S.; Kim, D., Development of a palm portable mass spectrometer. *J. Am. Soc. Mass Spectrom.* **2008**, *19*, 1442-1448.

21. Blain, M.G.; Riter, L.S.; Cruz, D.; Austin, D.E.; Wu, G.; Plass, W.R.; Cooks, R.G., Towards the hand-held mass spectrometer: design considerations, simulation, and fabrication of micrometer-scaled cylindrical ion traps. *Int. J. Mass Spectrom*. **2004,** *236*, 91-104.

22. Austin, D.E.; Cruz, D.; Blain, M.G., Simulations of ion trapping in a micrometer-sized cylindrical ion trap. *J. Am. Soc. Mass Spectrom*. **2006**, *17*, 430-441.

23. Ouyang, Z.; Badman, E.R.; Cooks, R.G., Characterization of a serial array of miniature cylindrical ion trap mass analyzers. *Rapid Commun. Mass Spectrom*. **1999**, *13*, 2444-2449.

24. Badman, E.R.; Johnson, R.C.; Plass, W.R.; Cooks, R.G., A miniature cylindrical quadrupole ion trap: simulation and experiment. *Anal. Chem*. **1998**, *70*, 4896-4901.

25. Tabert, A.M.; Griep-Raming, J.; Guymon, A.J.; Cooks, R.G., High-throughput miniature cylindrical ion trap array mass spectrometer. *Anal. Chem*. **2003**, *75*, 5656-5664.

26. van Amerom, F.H.W.; Chaudhary, A.; Cardenas, M.; Bumgarner, J.; Short, R.T., Microfabrication of cylindrical ion trap mass spectrometer arrays for handheld chemical analyzers. *Chem. Eng. Comm*. **2007**, *195*, 98-114.

27. Chaudhary, A.; van Amerom, F.; Short, R.T., Development of microfabricated cylindrical ion trap mass spectrometer arrays. *J. Microelectromech. Syst*. **2009**, *18*, 442-448.

28. Song, Y.; Wu, G.; Song, Q.; Cooks, R.G.; Ouyang, Z.; Plass, W.R., Novel linear ion trap mass analyzer composed of four planar electrodes. *J. Am. Soc. Mass Spectrom*. **2006**, *17*, 631-639.

31. Ouyang, Z.; Wu, G.; Song, Y.; Li, H.; Plass, W.R.; Cooks, R.G., Rectilinear ion trap: concepts, calculations, and analytical performance of a new mass analyzer. *Anal. Chem*. **2004**, *76,* 4595.

30. Maas, J.D.; Hendricks, P.I.; Ouyang, Z.; Cooks, R.G.; Chappell, W.J., Miniature monolithic rectilinear ion trap arrays by stereolithography on printed circuit board. *J. Microelectromech. Syst*. **2010**, *19*, 951-960.

31. Li, X.; Jiang, G.; Luo, C.; Xu, F.; Wang, Y.; Ding, L.; Ding, C., Ion Trap Array Mass Analyzer: Structure and Performance. *Anal. Chem*. **2009**, *81*, 4840-4846.

32. Wang, L.; Xu, F.; Ding, C., Performance and geometry optimization of the ceramic-based rectilinear ion traps. *Rapid Commun. Mass Spectrom*. **2012**, *26*, 2068-2074.

33. Pau, S.; Pai, C.S.; Low, Y.L.; Moxom, J.; Reilly, R.T.A.; Whitten, W.B.; Ramsey, J.M., Microfabricated quadrupole ion trap for mass spectrometer applications. *Phys. Rev. Lett*. **2006**, *96*, 120801.

34. Ouyang, Z.; Cooks, R.G., Miniature mass spectrometers. *Annu. Rev. Anal. Chem*. **2009**, *2*, 187-214.

35. Orient, O.J.; Chutjian, A., A compact, high-resolution Paul ion trap mass spectrometer with electron-impact ionization. *Rev. Sci. Instrum*. **2002**, *73*, 2157-2160.

36. Hager, J.M., A new linear ion trap mass spectrometer. *Rapid Commun. Mass Spectrom*. **2002**, *16*, 512.

37. Schwartz, J.C.; Senko, M.W.; Syka, J.E.P., A two-dimensional quadrupole ion trap mass spectrometer. *J. Am. Soc. Mass Spectrom*. **2002**, *13*, 659-669.

38. Lammert, S.A.; Plass, W.R.; Thompson, C.V.; Wise, M.B., Design, optimization and initial performance of a toroidal rf ion trap mass spectrometer. *Int. J. Mass Spectrom*. **2001**, *212*, 25-40.

39. Austin, D.E.; Peng, Y.; Hansen, B.J.; Miller, I.W.; Rockwood, A.L.; Hawkins, A.R.; Tolley, S.E., Novel ion traps using planar resistive electrodes: implications for miniaturized mass analyzers. *J. Am. Soc. Mass Spectrom*. **2008**, *19*, 1435-1441.

40. Zhang, Z.; Peng, Y.; Hansen, B.J.; Miller, I.W.; Wang, M.; Lee, M.L.; Hawkins, A.R.; Austin, D.E., Paul trap mass analyzer consisting of opposing microfabricated electrode plates. *Anal. Chem*. **2009**, *81*, 5241-5248.

41. Austin, D.E.; Hansen, B.J.; Peng, Y.; Zhang, Z., Multipole expansion in quadrupolar devices comprised of planar electrode arrays. *Int. J. Mass Spectrom*. **2010**, *295*, 153-158.

42. Austin, D.E.; Wang, M.; Tolley, S.E.; Maas, J.D.; Hawkins, A.R.; Rockwood, A.L.; Tolley, H.D.; Lee, E.D.; Lee, M.L., Halo ion trap mass spectrometer. *Anal. Chem*. **2007**, *79*, 2927-2932.

43. Wang, M.; Quist, H.E.; Hansen, B.J.; Peng, Y.; Zhang, Z.; Hawkins, A.R.; Rockwood, A.L.; Austin, D.E.; Lee, M.L., Performance of a halo ion trap mass analyzer with exit slits for axial ejection. *J. Am. Soc. Mass Spectrom*. **2011**, *22*, 369-378.

44. Peng, Y.; Hansen, B.J.; Quist, H.E.; Zhang, Z.; Wang, M.; Hawkins, A.R.; Austin, D.E., Coaxial ion trap mass spectrometer: concentric toroidal and quadrupolar trapping regions. *Anal. Chem*. **2011**, *83*, 5578-5584.

45. Hansen, B.J.; Niemi, R.J.; Hawkins, A.R.; Lammert, S.A.; Austin, D.E., A lithographically patterned discrete planar electrode linear ion trap mass spectrometer. *J. Microelectromech. Syst*. **2013**, *22*, 876-883.

46. Xu, W.; Chappell, W.J.; Cooks, R.G.; Ouyang, Z., Characterization of electrode surface roughness and its impact on ion trap mass analysis. *J. Mass Spectrom*. **2009**, *44*, 353-360.

47. Douglas, D.J.; Frank, A.J.; Mao, D., Linear ion traps in mass spectrometry. *Mass Spectrom. Rev.* **2004**, *24*, 1-29.

48. Lammert, S.A.; Rockwood, A.A.; Wang, M.; Lee, M.L.; Lee, E.D.; Tolley, S.E.; Oliphant, J.R.; Jones, J. L.; Waite, R.W., Miniature toroidal radio frequency ion trap mass analyzer. *J. Am. Soc. Mass Spectrom*. **2006**, *17*, 916-922.

49. Tian, Y.; Higgs, J.M.; Li, A.; Barney, B.; Austin, D.E., How far can ion trap miniaturization go? Parameter scaling and space- charge limits for very small cylindrical ion traps. *J. Mass Spectrom*. **2014**, *49*, 233-240.

50. R. E. March, J. F. J. Todd. Quadrupole Ion Trap Mass Spectrometry. John Wiley, Hoboken, NJ, USA, 2005, pp. 106–112.

51. Zhang, Z.; Quist, H.E.; Peng, Y.; Hansen, B.J.; Wang, M.; Hawkins, A.R.; Austin, D.E., Effects of higher-order multipoles on the performance of a two-plate quadrupole ion trap mass analyzer. *Int. J. Mass Spectrom*. **2011**, *299*, 151-157.

52. Ding, L.; Sudakov, M.; Kumashiro, S., A simulation study of the digital ion trap mass spectrometer. *Int. J. Mass Spectrom*. **2002**, *221*, 117-138.

53. Bandelow, S.; Marx, G.; Schweikhard, L., The 3-state digital ion trap. *Int. J. Mass Spectrom.* **2013**, *353*, 49-53.

54. Richards, J.A.; Huey, R.M.; Hiller, J., A new operating mode for the quadrupole mass filter. *Int. J. Mass Spectrom*. *Ion Phys.***1973,** *12*, 317-339.

55. Richards, J.A., Quadrupole mass filter spectrum control using pulse width modulation. *Int. J. Mass Spectrom. Ion Phys.* **1977**, *24*, 219-224.

56. Ding, L.; Sudakov, M.; Brancia, F.L.; Giles, R.; Kumashiro, S., A digital ion trap mass spectrometer coupled with atmospheric pressure ion sources. *J. Mass Spectrom.* **2004**, *39*, 471-484.

57. Ding, L.; Kumashiro, S., Ion motion in the rectangular wave quadrupole field and digital operation mode of a quadrupole ion trap mass spectrometer. *Rapid Commun. Mass Spectrom*. **2006**, *20*, 3-8.

58. Konermann, L.; Ahadi, E.; Rodriguez, A.D.; Vahidi, S., Unraveling the mechanism of electrospray ionization. *Anal. Chem*. **2013**, *85*, 2-9.

59. Rashid, M.H., Simple analytical method to design electrostatic einzel lens. *Proceedings of the DAE Symp. on Nucl. Phys.* **2011**, *56*, 1132-1133.

60. Wang, L.; Xu, F.; Dai, X.; Fang, X.; Ding, C., Development and Investigation of a Mesh-Electrode Linear Ion Trap (ME-LIT) Mass Analyzer. *J. Am. Soc. Mass Spectrom*. **2014**, *25*, 548-555.

61. Wu, Q.; Li, A.; Tian, Y.; Zare, R.N.; Austin, D.E., Miniaturized Linear Wire Ion Trap Mass Analyzer. *Anal. Chem*. **2016**, *88*, 7800-7806

3 SIMULATION STUDY OF CHAOTIC ION MOTION IN A TOROIDAL ION TRAP MASS ANALYZER*

3.1 Introduction

3.1.1 Toroidal Ion Trap Development

Ion trap mass spectrometers are widely used for identifying and quantifying compounds and analyzing mixtures in fields of study as diverse as biochemistry,[1] environmental monitoring,[2] forensics,[3] petrology[4] and planetary science.[5,6] In a 3-D quadrupole ion trap, a radiofrequency (RF) waveform and three hyperboloidal electrodes—two end-caps and one ring electrode—create the quadratically varying electric potential needed to trap and mass-analyze ions.[7,8] Similarly, the quadrupole mass filter employs four hyperbolic rods, trapping ions in two dimensions and allowing a subset of ions to pass through the length of the device.[9] Many geometrical variants have been designed to facilitate miniaturization or otherwise modify some aspect of trap performance. For instance, the cylindrical ion trap (CIT) utilizes cylindrical electrodes, which are simpler to manufacture and miniaturize than those of the quadrupole ion trap.[10,11] The linear ion trap (LIT) is derived from the quadrupole mass filter but with added axial trapping.[12,13] The LIT has the advantage that ions are not confined to a small volume at the trap center, but rather are confined along a line, allowing more ions to be trapped for a given frequency and RF amplitude.[12-14] The rectilinear ion trap is derived from the LIT, but with flat-rectangular electrodes.[15,16] In 2001, Lammert et al. created the toroidal ion trap, in which the

* This chapter is from a published paper "Li, A.; Higgs, J.M.; Austin, D.E., Chaotic motion of single ions in a toroidal ion trap mass analyzer. *Int. J. Mass Spec*. **2017**, *in press*", in which I performed all the simulation experiments except for the β value calculation.

cross section of a quadrupole ion trap is rotated along an axis located outside of the trapping region. The toroidal ion trap consists of a central electrode, an outer ring electrode, and two end-caps, all based on hyperbolic surfaces of revolution. Analogous to the LIT, the toroidal trap exhibits a larger trapping capacity—ions are trapped in a torus or ring and ejected through slits in the endcap electrodes.[17,18] A miniaturized version of this toroidal ion trap is currently used in a commercial, portable GC-MS instrument.[19] Taylor and Austin presented a simplified electrode geometry in which the toroidal trapping region is made using cylindrical electrodes and ions are ejected radially to a detector located at the center.[20]

3.1.2 Ion Motion in Ion Traps

Although the electrode geometry may be simplified, the ion motion in all RF trapping devices is rather complex. Ion motion consists of several components (Figure 3-1), including micromotion (small-amplitude motion at the same frequency and phase as the applied RF) and secular motion (large-amplitude, harmonic motion with frequencies corresponding to the position of the ion as plotted on a stability diagram).[21] Secular motion consists of several frequencies, with the dominant frequency typically a fraction of the frequency of the driving RF. Secular motion is often resonantly excited by a supplementary applied signal for ion excitation, fragmentation, isolation, or ejection.[22-26]

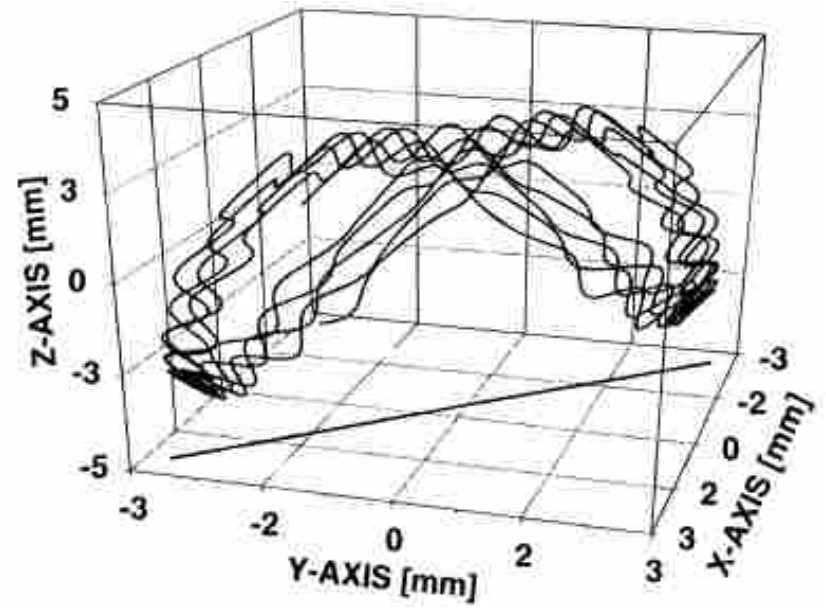

Figure 3-1: Ion motion in the electric field. (Adapted from Nappi, M,; Weil, M.; Cleven, C.D.; Horn, L.A.; Wollnic, H.; Cooks, G.R. Visual representations of simulated three-dimensional ion trajectories in an ion trap mass spectrometer, Int. J. Mass Spec. and Ion Pro., 1997, 161, 77–85)

The complex motion of trapped ions is commonly studied using a combination of mathematical models and computer simulations. These studies seek to optimize ion trap design and performance or to understand specific observations. For instance, Berkeland et al. discussed the ion micromotion in a quadrupole ion trap, and described three methods to detect and minimize adverse micromotion.[27] Londry et al. discussed mass selective axial ion ejection from a linear quadrupole ion trap via studying the ion motion to obtain optimal electric fields.[26] Higgs et al. studied the ion motion in three different types of toroidal ion traps.[28] Huo et al. presented a SIMION simulation study of the slit impact on the miniature rectilinear ion trap in which the trap performance was optimized via adjusting the slit geometry.[29] Yang et al. optimized the performance of a toroidal ion trap with triangular electrode geometry via SIMION simulation.[30] Wu et al. studied the electrode misalignment of the planar linear ion trap via simulating the

electric field and ion trapping.[31] Blain et al. discussed design considerations for a micrometer-scaled cylindrical ion trap relying on SIMION simulations of ion motion.[32]

3.1.3 Electric Field in Ion Traps

The motion of trapped ions is due primarily to the shape and magnitude of the time-varying electric potentials and fields within the trap. The electric potential distribution within a perfect quadrupole ion trap is purely quadratic, and the resulting field perfectly linear, but in practice this cannot be achieved due to electrode truncation, slits and/or holes, and imperfections in electrode fabrication and positioning. These factors lead to distortions of the potential distribution. For distortions with the same symmetry as the trap itself, the distortions are conveniently modelled using higher-order solutions to the Laplace equation. For instance, small amounts of hexapole, octopole, decapole, dodecapole, and other higher-order terms superimpose onto the dominant quadrupole and make the resulting electric field non-linear. Even small contributions of these nonlinear terms can have a significant effect on the ion motion. The nonlinear field is either detrimental or in some cases beneficial to ion excitation and ejection. Non-linear fields can cause undesirable and unexpected ion ejection (black holes or black canyons) that make ions eject at undesirable times, but can also be used to contain ions during excitation and improve ion ejection and mass analysis.[33-37] Numerous studies have focused on optimizing trap performance via adjusting the higher order field terms. For instance, the original Finnigan quadrupole ion trap was stretched by 10.8% in the ejection direction to improve mass accuracy and resolution.[12] Other groups including Wu et al.[12], Ouyang et al.[15] and Bruker-Franzen[38] instruments also optimized higher order fields in ion traps by modifying the geometric structures. A "-10% compensation rule" was presented for field optimization, suggesting that an

optimal field for a boundary or linear resonance ejection mass scan should contain a sum of -10% of the relative strengths of octopole and dodecapole.[39]

Compared to the electric fields in other ion traps, the electric field in the toroidal ion trap has additional complexities due to the curvature of the trapping region. Lammert et al. demonstrated that a pure quadrupole field cannot be achieved in the toroidal ion trap due to the radius of curvature of the trapping region.[17] Wang also noted that, for the same reason, none of the conventional higher-order multipoles are strictly applicable to this device.[40] The trapping center of a toroidal trap is not co-located with the rotational axis, so electric potentials increasing with any polynomial form from the trapping center will of necessity have a "cusp" or discontinuity at the rotational axis. While they may be useful to first order, they do not completely describe the potentials or the ion behavior in the device. Kotana and Mohanty have developed mathematical models to describe the potential distribution in the toroidal ion trap.[41] They also presented a computation method on the stability diagram in the toroidal ion trap and observed features similar to what we observed.[42]

Higgs et al. conducted SIMION simulations exploring motion of ions in toroidal ion traps,[28] and also in a potential representing a mathematically pure, quadrupole-like toroidal harmonic.[43] Among other findings is that a centripetal effect shifts the center of ion motion outward from the saddle-point of the trapping potential. In addition, the pure toroidal harmonic shows a strong, fairly broad chasm or black canyon running through the stability region. We subsequently conducted simulations on these toroidal systems to understand mass analysis through boundary ejection, including characterizing the direction of ion ejection under different conditions. In doing so we have observed an interesting and unusual behavior. On many portions of the stability diagram, including black canyons and expected non-linear resonance

lines, the direction of ion ejection shows fractal-like behavior. The direction of ion ejection is extremely sensitive to initial conditions of the simulation, and zooming in to a specific feature shows finer details with similar pattern. In other words, the ion ejection demonstrates classical chaotic behavior.

3.1.4 Chaos in Non-linear Electric Fields

Classical chaotic motion is a deterministic but unpredictable long-term state in a nonlinear dynamic system that is highly sensitive to initial conditions. A common example is the double pendulum (a pendulum is attached to the bottom of another pendulum). The motions of the pendula do not follow simple, predictable patterns. Using appropriate equations of motion, it is possible to calculate any future state, but the calculation must be done iteratively—calculation of a given future state requires knowing the immediately preceding state.[44,45] The motion of chaotic systems is generally represented by a set of nonlinear equations of motion. Because of the nonlinearity, it is impossible to calculate the (n)th step state without knowing the information of the (n-1)th step. Therefore, it is unpredictable in the long-term, but deterministic. Small differences in the initial state will cause diverse results. A chaotic system contains many "decision" points where small differences in the current state lead to different paths. In some cases rounding errors in calculations can have a similar effect.

Chaos is defined as an irregular and disordered motion. However, if every step of the chaotic motion is recorded, we can see the locus follows an orbit, which is called the strange attractor (Figure 3-2). The strange attractor can be observed in any chaotic motion, and the interesting thing is that the structure of the strange attractor is similar to the ion motion in the ion

trap (Figure 3-1). It is possible that there may be some relationship among the strange attractor, chaotic motion and non-linear electric fields in the ion trap.

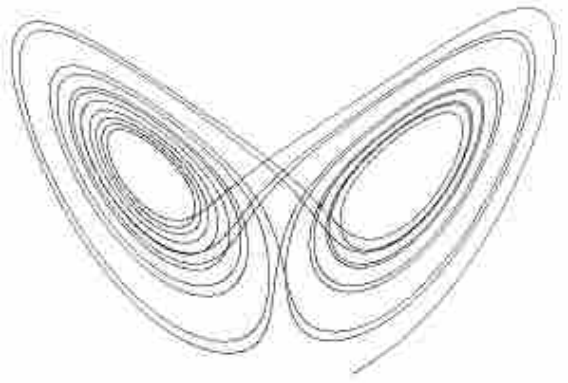

Figure 3-2: Strange attractor reflects the orbit of chaotic motion.

3.1.5 Two-ion and Single-ion Chaotic Motion

Chaotic motion of ions in traps has been studied from the standpoint of the two-ion effect, which is different from what is reported in the present study. With two ions in a trap, the position and charge of one ion affect the motion of the other ion, analogous to the effect one pendulum has on the other in the double pendulum example. Blümel showed that two or more ions in a quadrupole ion trap demonstrate chaotic motion due to Coulombic repulsion, and argued that this chaotic motion is responsible for RF heating of trapped ions.[46] Baumann et al. also studied the regular and chaotic motion of two ions in a quadrupole ion trap, and provided integrals of ion motion and critical parameters that can cause chaotic behaviors.[47] Hoffnagle et al. investigated an order-chaos transition of two ions in a quadrupole ion trap, and presented the Mathieu-Coulomb equations to interpret a boundary transition.[48] Hasegawa et al. demonstrated the nonlinear equations of two-ion motion in a quadrupole ion trap using a discrete Fourier

expansion method that predicts a bistability between the regular and chaotic state.[49] In each case, the motion of a given ion is perturbed by the other ion.

Trapped ions also exhibit chaotic behavior in a quantum mechanical context, including transitions of excited states. These quantum effects have been widely studied, but are of a fundamentally different nature than the chaotic behavior in the present study. For instance, Walther characterized quantum chaos-order transitions of single ions in a quadrupole ion trap using polarization gradient laser cooling, and obtained relevant parameters for phase transitions.[50] Berman et al. introduced a quantum model for a single-ion transition to quantum chaos in a linear ion trap, and compared with the classical dynamic system in different dimensionless driving forces.[51]

In our simulations of toroidal ion traps, we have observed that individual ions exhibit chaotic motion due entirely to the trapping fields and the resulting simulations of motion. This paper focuses on chaotic behavior of single ion ejection in the cylindrical toroidal ion trap. We present the stability diagram for this device. Fractal-like patterns appear in a series of zoomed-in regions of the stability diagram, including nonlinear resonance lines. We also discuss the implications for other ion trap geometries and the effect on mass analysis.

3.2 Methods

3.2.1 Simulation Study of Stability Diagram

Ion trajectory simulations using SIMION 8.1 (Scientific Instrument Services, Inc., Ringoes, NJ) were carried out on the toroidal ion trap composed of cylindrical electrodes.[20] Figure 3-3 shows the design of this ion trap. The SIMION model contains a 2-D array rotated about an axis.

The dimensions as published and as used in these simulations are R = 36.15 mm, r_0 = 5.91 mm, z_0 = 5.81 mm, slit width = 1.6 mm with a reported hexapole component of -2.3%, octopole of +0.8%, and decapole of -3.6%. The size of the SIMION potential array was 600 × 600 grid units (gu) with cylindrical symmetry. All simulations used double-precision values for all parameters to minimize the effect of rounding errors.

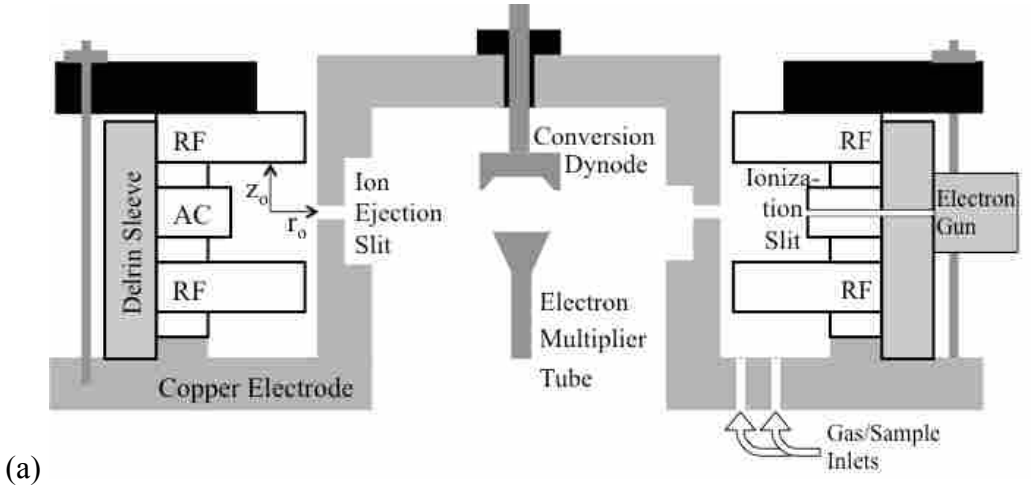

(a)

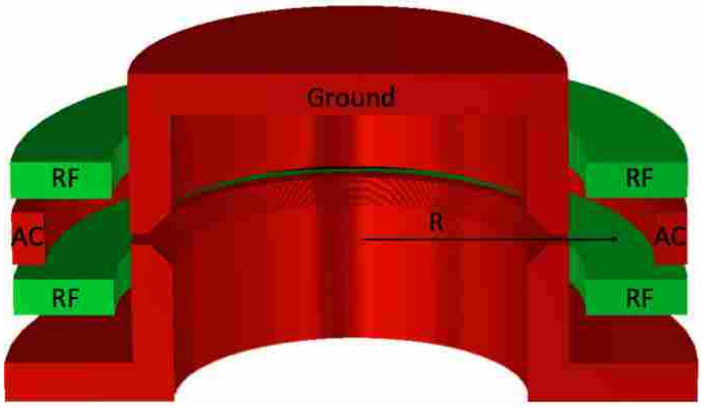

(b)

Figure 3-3: (a) Geometry of the published cylindrical-electrode toroidal ion trap (R = 36.15 mm, r_0 = 5.91 mm, z_0 = 5.81 mm, slit width = 1.6 mm). The dimension r_0 is the distance from the trapping center to the surface of the ejection slit. (Adapted from ref 20); (b) 3-D representation of the cylindrical-electrode toroidal ion trap. The dimension R is the distance from the trapping center to the rotational axis.

The simulated trap was operated with an RF frequency of 1.14 MHz and an RF amplitude that ranged from 0 to 1000 $V_{0\text{-}p}$, applied to both RF electrodes. A DC offset was also applied to both the RF electrodes with a voltage that ranged from -150 to 150 V. In some simulations, an AC signal was applied on the electrode opposite the ejection slit to examine resonant ejection behavior. In these cases the AC frequency was 380 kHz, or one-third the RF frequency, with 1.75 $V_{0\text{-}p}$ amplitude and 3.25 V offset, as in ref [20]. The AC signal was phase-locked with the RF, with the zero-crossing of the RF coinciding with the zero-crossing of the AC. The mass-to-charge ratio of the ions was 100 Th.

To create the stability diagram, ion stability was simulated for all possible combinations of RF amplitude and DC offset within the above ranges, with step sizes of 1 $V_{0\text{-}p}$ (RF) and 0.3 V (DC). Zoomed in regions included ever-smaller subsets of the DC and RF ranges and smaller step sizes, with the smallest RF step size being 10 μV. Data were processed using Excel (Microsoft, Redmond, WA).

Except where noted, for each value of RF and DC, ions had identical initial parameters: RF phase = 0, zero initial kinetic energy, located at a position 0.2 mm away from the trapping center (offset 0.15 mm in r, 0.15 mm in z). The small offset from center corresponds to 0.01 eV per 100 V applied to the RF electrodes, and was kept small to avoid effects due to large ion excursion from the trapping center. For each simulation with a given value of RF and DC, only a single ion was used. The initial state of the ion was identical in each run—no random variables or distributions were used. The simulation did not include any ion-neutral collisions. The potential surface was updated every 0.05 μs to provide a smooth RF waveform. The ion was considered stable if it remained in the trap after 5 ms. If the ion hit an electrode within 5 ms, the position of the ion's demise was recorded. This information established which of the four

electrodes was hit—designated herein as the inner radial, outer radial (AC), or either of the axial (RF) electrodes. The "inner radial" electrode includes the ejection slit.

3.3 Results and Discussion

3.3.1 Chaotic and Fractal Behaviors

For the full stability diagram, the RF and DC voltages had a step of 1 $V_{0\text{-}p}$ and 0.3 V, respectively, over the full voltage ranges given above. For each data point, the RF and DC were held constant and the ion trajectory simulated for that point. No supplementary AC was applied. The results are shown in Figure 3-4. Blue points designate ions considered stable (>5 ms). Red points indicate ions that impacted on the inner radial electrode, including the ejection slit. Yellow points indicate ions that struck the RF electrodes (ejection in the direction of the rotational axis). Grey points show conditions under which ions impacted the outer radial electrode. Most of the plot area consists of large regions with a single color. However, the blue stable region is crossed by a prominent line of instability at $\beta r + 2\beta z = 2$ that corresponds to the hexapole resonance in conventional quadrupole ion traps. A narrower unstable band runs most of the way through the stability region and also corresponds to the hexapole $\beta r = 2/3$ resonance. Both top and bottom apices show additional lines of instability originating at the apex, as is common in other types of ion traps.[50] Above and to the right, and below and to the left of the stability region, ions are unstable and ejected in the axial direction. In the other two regions of instability, ions are unstable and ejected radially. For values of RF and DC above and to the left, all ions are ejected inwardly. However, the region below and to the right consists of bands alternating between inward and outward radial ejection, with the bands generally becoming narrower as they approach the region of stability.

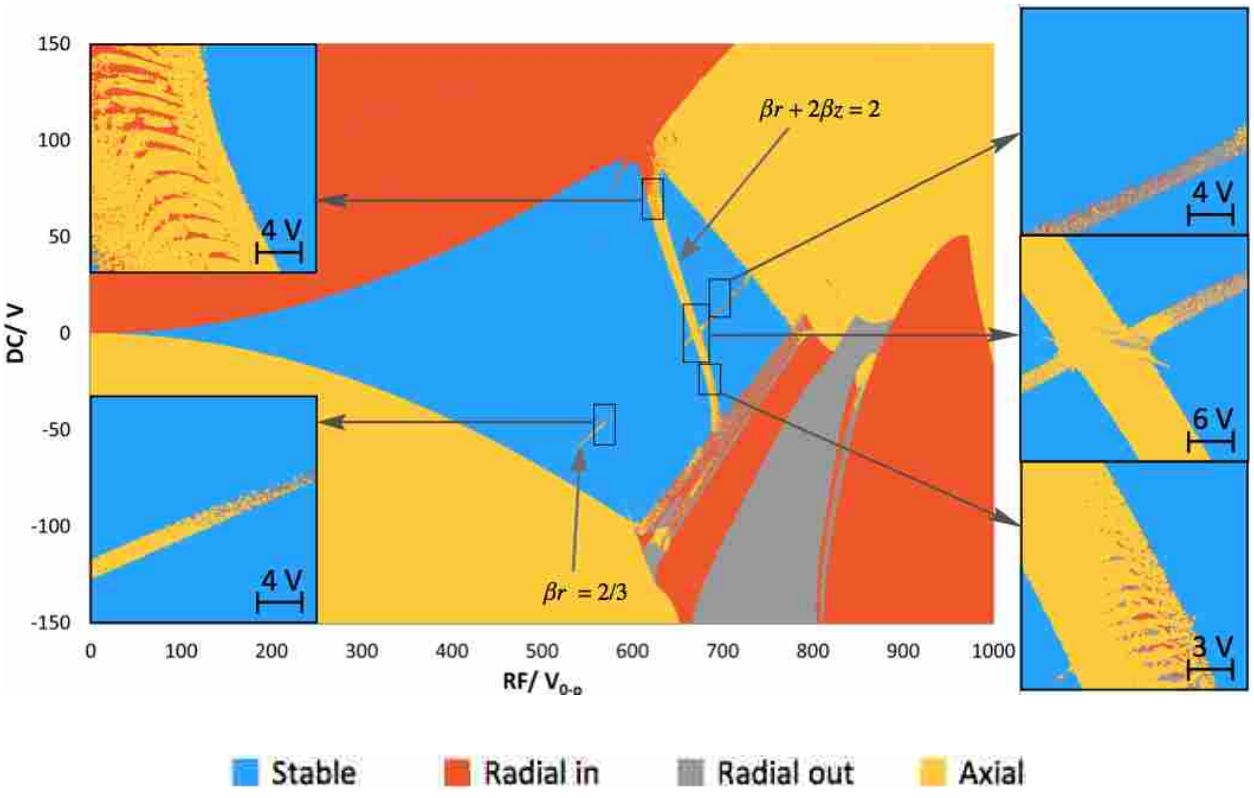

Figure 3-4: Stability diagram of cylindrical-electrode toroidal ion trap without applied AC. Colors represent the direction with which the ion is ejected at each combination of RF and DC voltages. Insets show zoomed in regions as indicated.

Figure 3-4 also shows several zoomed-in subsets. In these cases, the step size between points is 0.1 V. Sections from the more prominent unstable line ($\beta r + 2\beta z = 2$) show interesting banding and other patterns at this scale. To be consistent with the convention for plotting ion trap stability diagrams, the DC and RF are scaled differently in the main stability diagram. However, zoomed-in areas are plotted with the same scaling between RF and DC. Because of this, rectangular sections from the main stability diagram appear as square zoomed-in sections. In each inset, the scale bar shows the dimension of both $RF_{0\text{-}p}$ and DC voltage.

The complete stability diagram was also determined with the addition of a small AC signal applied to the outer electrode, as described above. All other parameters were the same as the stability diagram from Figure 3-4. The results of these simulations are shown in Figure 3-5a. Notable differences from the diagram without AC are: 1) the hexapole resonant line ($\beta r = 2/3$) is wider and spans the whole width of the stability region; 2) the stability region has several new, faint lines of instability; and 3) the upper left region of instability now has several small features with outward radial ejection. Two subsets of this diagram, labelled b and c, were zoomed in for further study using a 0.1 V step size. From these, two interesting regions (d, e) were selected and zoomed in to a step size of 0.01 V. This process continued down to a step size of 0.00001 V.

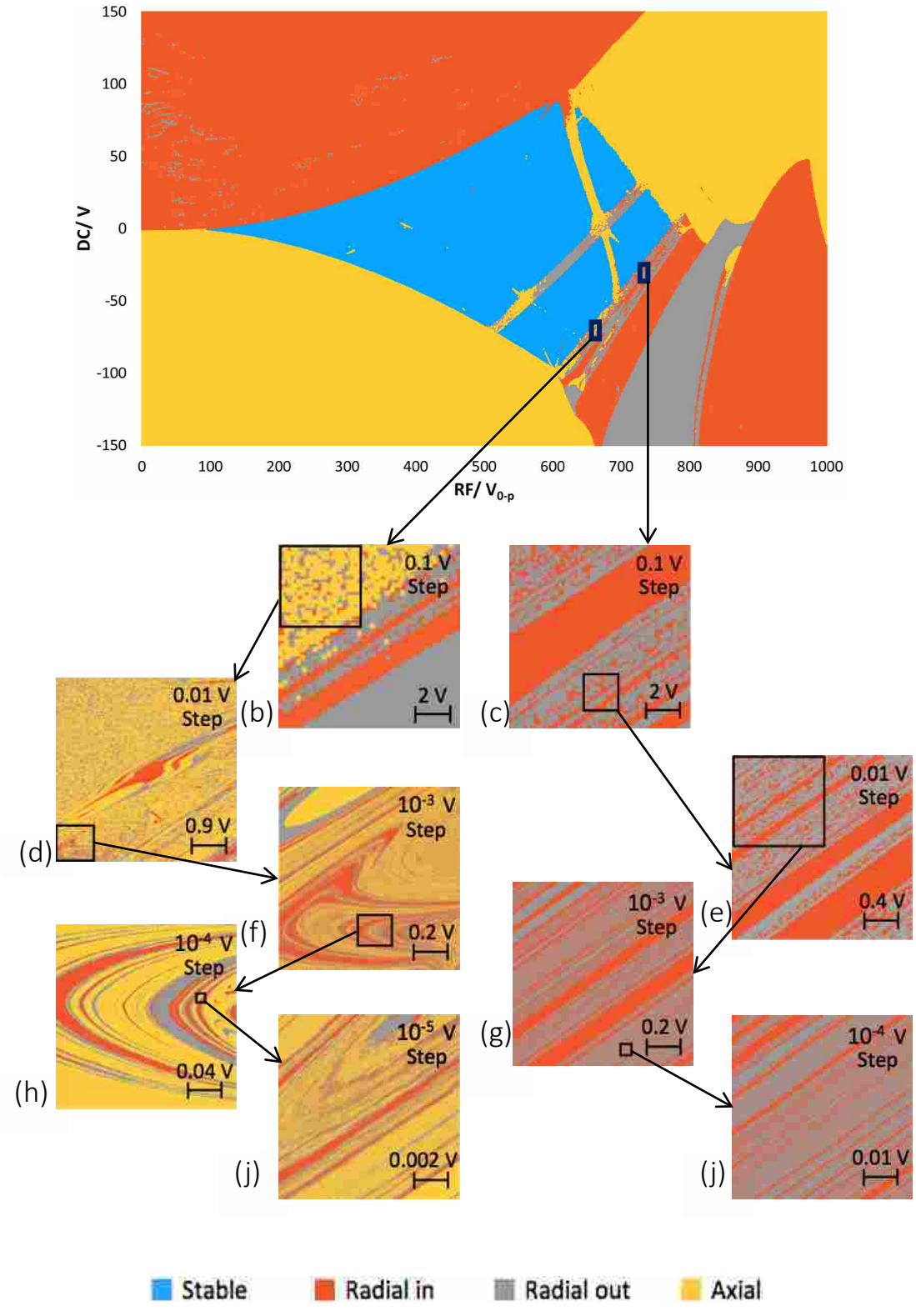

Figure 3-5: Stability diagram of cylindrical-electrode toroidal ion trap with applied AC. Colors represent the direction with which the ion is ejected at each combination of RF and DC voltages. Insets show zoomed in regions as indicated.

These regions show chaotic behavior: the ejection direction is very sensitive to small changes in the operating voltages of the trap. Further, the patterns obtained at one scale are qualitatively repeated (self-similar) at all smaller scales. Figures 3-5d, f, h and j show particularly interesting and intricate patterns as the ion alternates between axial, radial inward, and radial outward ejection. Rounding errors would give random patterns, particularly at smaller scales, and would not give the structures observed in these figures; hence we conclude that the observed chaotic behavior is not due to rounding errors in the simulation.

The simulation yielding Figure 3-5f was re-run several times using a different initial position and velocity vector of the ion (Table 3-1). These simulations explored whether the ion motion is also sensitive to these initial parameters. The results (Figure 3-6) show that the observed chaotic patterns are also sensitive to the choice of ion starting conditions in the simulations.

Table 3-1:
Ion initial conditions used for Figure 3-6a, 3-6b and 3-6c.

Figure 3-6	*Kinetic Energy*	*Velocity Vector*	*Starting Position*	*RF Phase at Ion Birth*
(a)	0.05 eV	(2,0,0)	0.1 mm offset in r	0
(b)	0.1 eV	(0,1,0)	0.2 mm offset in r	0
(c)	0.1 eV	(0,1,0)	0.3 mm offset in r	0

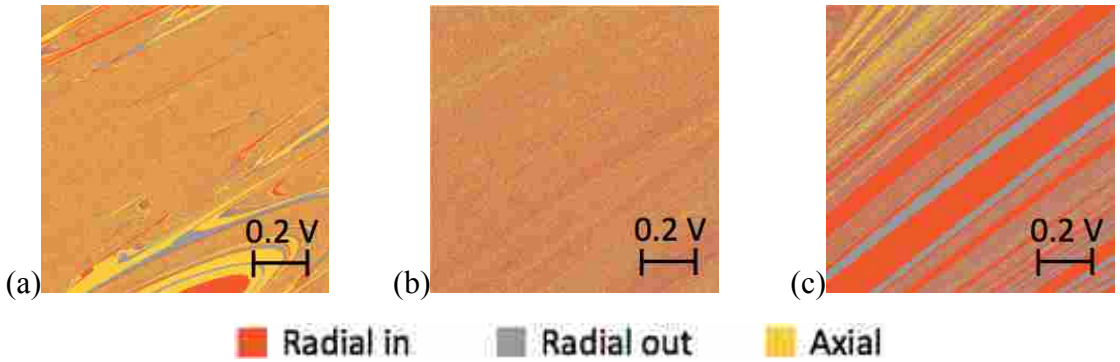

Figure 3-6: Re-run of the simulation in Figure 3-5f using three sets of different initial conditions of the ion. The initial conditions are shown in Table 3-1.

As expected, ions with nearly identical starting conditions have similar trajectories initially, but these trajectories diverge at some point prior to ion ejection. To illustrate this, a simulation of two trajectories for the same ion with nearly the same initial conditions (differing by 0.0001 mm in starting position) is presented in Figure 3-7. The results show that the two ions started at very close position and have almost the same trajectory initially, then deviated from each other over time, and are eventually ejected to opposite directions. Ion repulsion was not considered in this simulation.

Ion traps in practice are usually operated with some amount of buffer gas or background gas. Ion-neutral collisions cool ions and improve mass analysis. These collisions also scramble information about an ion's starting conditions in the trap. Another simulation was run (Figure 3-8) with buffer gas to investigate the influence of collisions on the direction of ion ejection. The ion initial condition was same as that of the Figure 3-6c, but with helium buffer gas at 3 mTorr. Collisions randomize ion ejection among several possible directions, but with preference for outward radial ejection. In experiments this result means that ions would be lost

to non-detection directions just as they would be without collisions. However, the chaotic pattern is obscured by the collisional randomization.

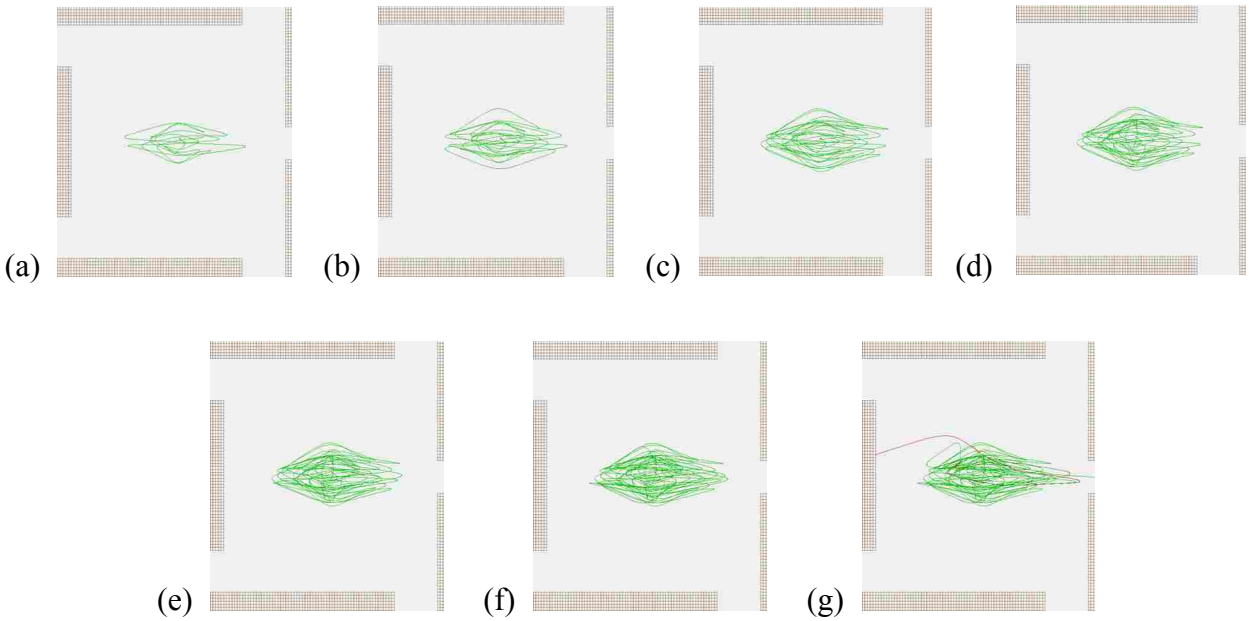

Figure 3-7: The ion time-of-flight increases with figure number. Two ions are created with nearly the same initial conditions (differing by 0.0001 mm in starting position). Ion #1 is red, and ion #2 is green.

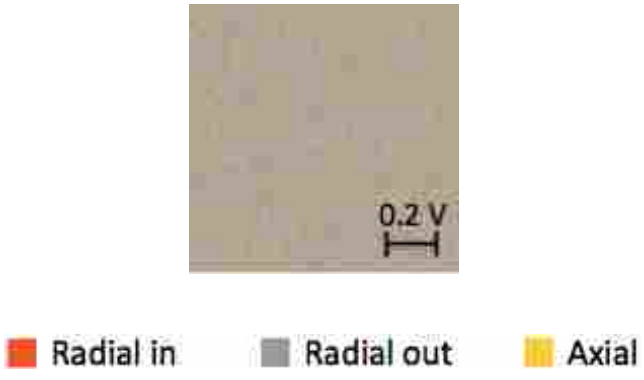

Figure 3-8: Re-run of the simulation in Figure 3-6c using the same initial conditions but with helium buffer gas at 3 mTorr.

We next ran simulations to determine whether the chaotic behavior also affected the position or other properties of the stability boundary, as this may affect boundary ejection of ions. A subset close to the bottom right boundary was zoomed in using a 0.1 V step voltage between each point in both RF and DC axes. The same region was recalculated using different initial conditions including ion-starting position, velocity vector, initial kinetic energy and the RF phase at ion formation (Table 3-2). The subset contains a portion of the stable trapping region and part of the chaotic boundary. Similar to the results seen in Figure 3-6, these simulations (Figure 3-9(a)-(h)) showed different chaotic patterns outside of the boundary. However, the position of the boundary shifts with each set of variables. Within this small sample set, the location of the boundary in terms of RF amplitude spans a range of 30 V, which would correspond to a large uncertainty in the m/z of ions ejected at that portion of the boundary.

Table 3-2:
Ion initial conditions of Figure 3-9a-h

Figure 3-6	*Kinetic Energy*	*Velocity Vector*	*Starting Position*	*RF Phase at Ion Birth*
(a)	0.1 eV	(3,0,0)	0.3 mm offset in r	0.8 π
(b)	0.5 eV	(3,0,0)	0.3 mm offset in r	0.8 π
(c)	0.05 eV	(2,0,0)	0.1 mm offset in r	0
(d)	0	(1,0,0)	0.4 mm offset in r	0
(e)	0	(1,0,0)	0.2 mm offset in z	0.56 π
(f)	0.3 eV	(1,0,0)	0.2 mm offset in z	0.56 π
(g)	0	(1,0,0)	0.4 mm offset in z	0
(h)	0	(1,0,0)	0.2 mm offset in z	0

(a) 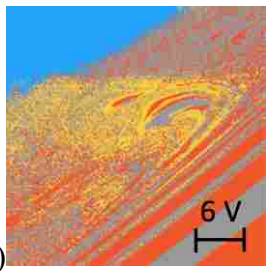

(b) 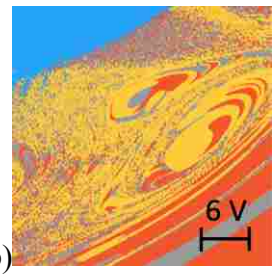

(c) 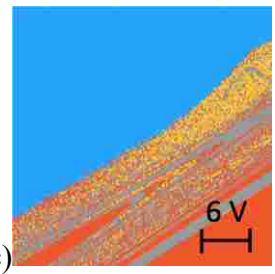

(d) 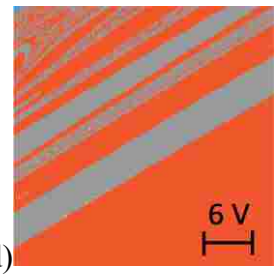

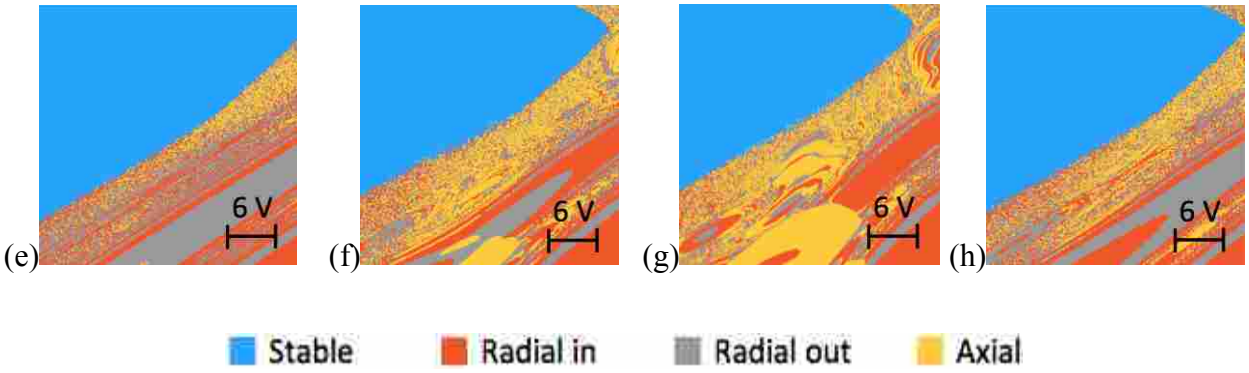

Figure 3-9: Simulation with 0.1 V step voltage of the subset close to the bottom right boundary using different initial conditions of the ion (Table 3.2). Note that in a-d, the ion starting position is offset in the r-direction; in e-h the ion starting position is offset in the z-direction.

In Figure 3-9, an obvious boundary shift was observed due to an offset of ion starting position in the r-direction. Ions in Figure 3-9a and 3-9b were created at the same position (0.3 mm offset in r) and the boundary position was approximately the same, even though their initial kinetic energy was different. In Figure 3-9c, the ions were created closer to the trapping center (0.1 mm offset in r) and the boundary shifted to right. In Figure 3-9d, the ions were created further away from the trapping center (0.4 mm offset in r), the boundary shifted significantly to left and only a small stable region was observed at the upper left corner of the figure. In Figure 3-9g and 3-9h, ions were created at same initial conditions but different offset position in z-direction and a slight boundary shifted was observed. The observation may indicate that the ion starting position in r-direction has more influence on the boundary shift than z-direction. However, it is not predictable from this small sample set whether the boundary shift is chaotic (i.e., small change in initial conditions gives large difference in outcome), or whether there may be some predictive relationship or function relating the boundary shift to the initial conditions.

Another subset close to the other boundary at upper right was zoomed in using 0.1 V step voltage and different initial conditions as well (Figure 3-10 and Table 3-3). With other parameters constant, varying the RF phases at ion formation caused a slight boundary shift.

Table 3-3:
Ion initial conditions of Figure 3-9a-h

Figure 3-6	*Kinetic Energy*	*Velocity Vector*	*Starting Position*	*RF Phase at Ion Birth*
(a)	0.1 eV	(1,0,0)	Trapping center	0.28 π
(b)	0.1 eV	(1,0,0)	Trapping center	0.8 π
(c)	0.1 eV	(1,0,0)	Trapping center	1.25 π
(d)	0.1 eV	(1,0,0)	Trapping center	1.8 π
(e)	0.1 eV	(1,0,0)	0.15 mm offset in r and z	0
(f)	0.1 eV	(1,0,0)	0.15 mm offset in r and z	0.5 π
(g)	0.1 eV	(1,0,0)	0.15 mm offset in r and z	0.8 π
(h)	0.1 eV	(1,0,0)	0.15 mm offset in r and z	1.5 π

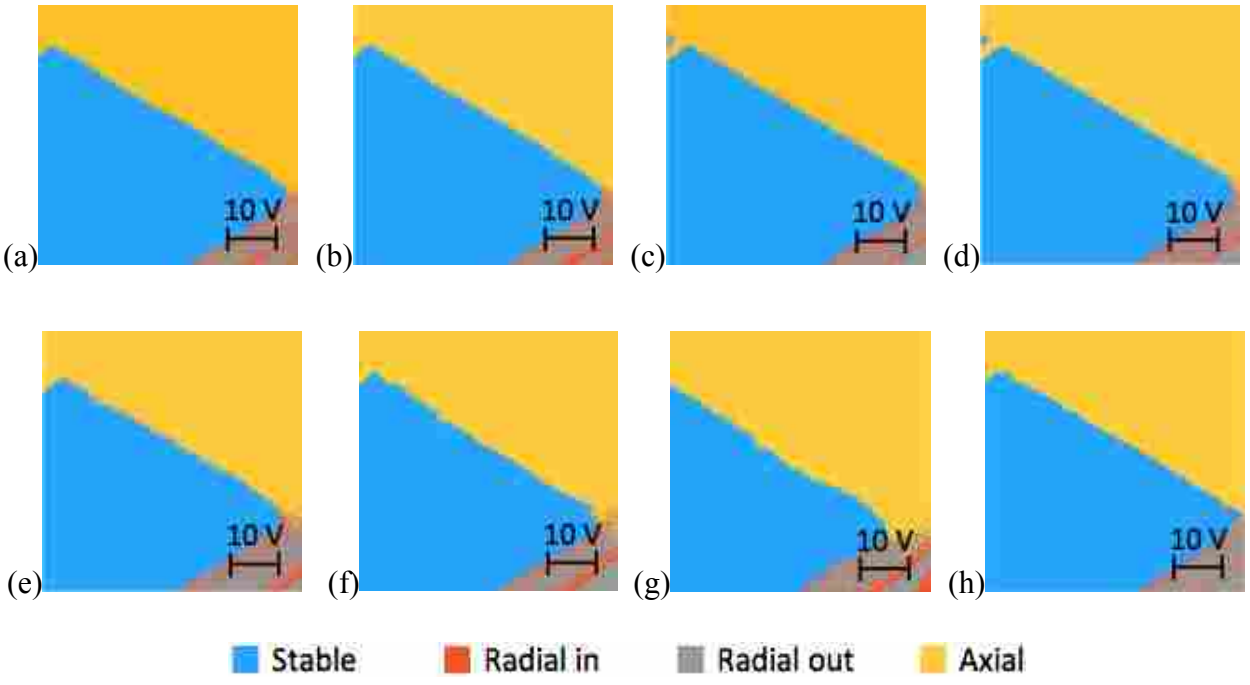

Figure 3-10: 0.1 V step voltage simulation of the subset close to the upper right boundary using different initial conditions of the ion (Table 3.3); Figure 3.10a-d The ion starting position is at the center of the trap and the RF phase difference were varied; Figure 3.10e-h The ion starting position is 0.15 mm offset in both r and z-direction and the RF phase difference were varied.

In these simulations, the position of the stability boundary was sensitive to the initial conditions of the ions. In addition, the boundary itself is somewhat diffuse, and therefore sensitive to the trap operating conditions. Somewhat similar observations were made by Ding[52] in simulations and experiments on quadrupole mass filters in which the electrodes consisted of two different diameters of rods. In this case, the higher-order terms of the trapping field were modified with the physical geometry of the filter. Different filter geometries showed shifted stability boundaries relative to the ideal filter. However, boundary shifts in the present work are observed without any change to the physical electrodes nor to the shape of the trapping fields. Ding also observed what were called "diffuse" boundaries near the apex of the stability region, and these may be similar to the effect reported in the present work. Konenkov et al.[53] presented simulations of stability boundaries and calculated peak shapes for quadrupole mass filters to which higher-order multipoles had been added. They found a predictable shift in the boundaries as a function of higher-order fields. They also reported an increase in peak width under such conditions, which may be a result of the diffuse boundary we have observed.

We next examined the resonant lines crossing the stability regions, which may play a role in ion isolation, ion losses, or resonant excitation and ejection. Zoomed-in regions are shown in Figure 3-11. The step voltage in each inset is 0.1 $V_{0\text{-p}}$. The ion ejection along the $\beta r + 2\beta z = 2$ line shows banding at this scale, similar to what was observed without applied AC. The hexapole resonant line ($\beta r = 2/3$) also shows patterns. The comparison between the two stability diagrams indicates that the applied AC waveform may change the specific details of the ion motion, but it does not cause the chaotic aspect of the motion.

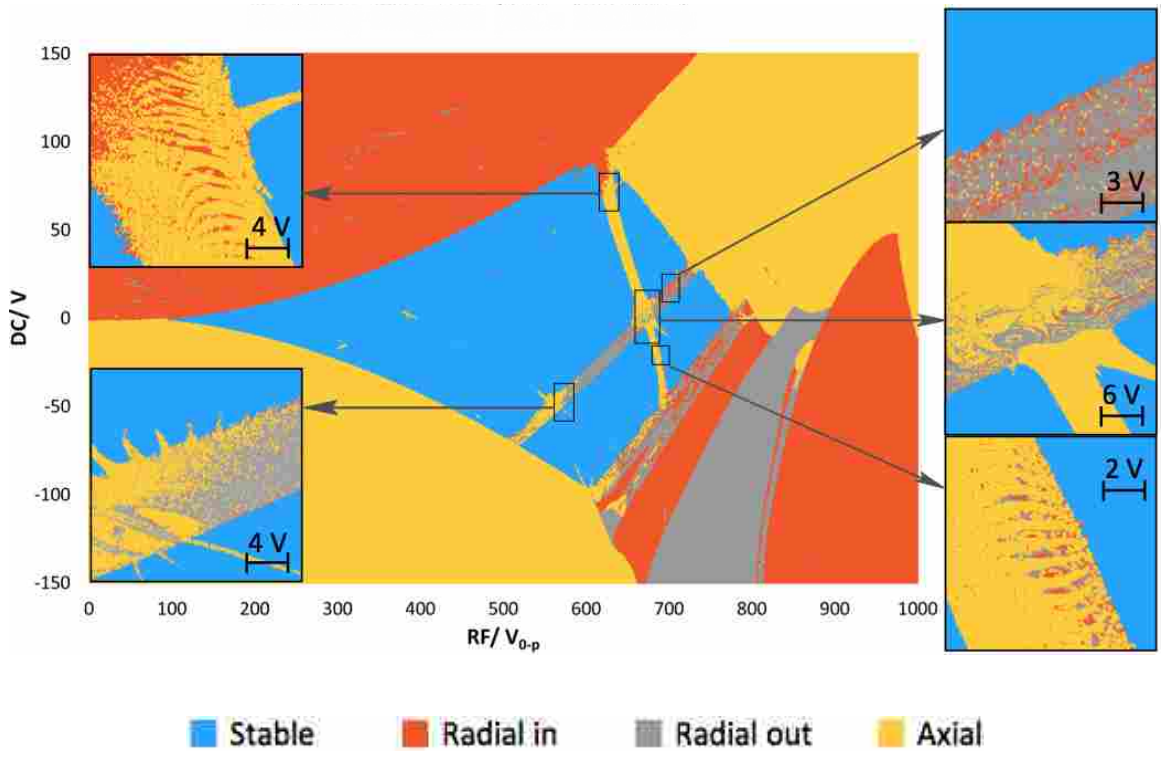

Figure 3-11: Stability diagram of cylindrical-electrode toroidal ion trap with applied AC. Insets show zoomed in regions from the resonant features crossing the stability region.

While the familiar black canyons of ion traps result from non-linear field components, ion losses typically appear when ions are far from the trapping center, such as ion introduction, activation, and fragmentation.[38] In contrast, non-linear ejection in the present work appears with ions located close to the center (trapped with "thermal" energies). Along a ring corresponding to the trapping center of a toroidal-type trap, the electric field is still curved around the torus.[28] This additional curvature may cause the observed ion instability. It may also be that non-linear effects are more pronounced in toroidal traps for other reasons.

3.3.2 Influence on Ion Trap Operation

Franzen noted[38] that ion traps made entirely of higher-order potential distributions (e.g., a hexapole-only trap) are not capable of mass analysis because ion motion is sensitive to initial ion conditions. However, our results show that this principle applies more broadly, and (at least in the present case) also applies to ion traps with relatively small amounts of higher-order terms. Nonetheless, the cylindrical-electrode toroidal ion trap is capable of mass analysis with resolving power comparable to other types of ion traps[20] using resonant ejection, and yet also exhibits chaotic ion motion. It has previously been noted that the diffuse features of stability boundaries of toroidal traps[42] complicates ejection along those boundaries. In addition, the observation in the present work of strong resonance lines and associated ejection indicates a possible limitation to the operational mass range in a toroidal trap.

Franzen[38] also noted that a variety of coupling effects accompany higher-order terms. These include coupling of kinetic energy among different coordinate axes (r and z) and pick-up of energy from the applied RF. The observed chaotic behavior may have a related underlying mechanism, as coupling may be position dependent. However, at this point there is insufficient information to explain the relationship between these effects.

We have presented only one output variable in the above simulations, specifically the ejection direction. Chaotic motion may also be present in other forms among ions that are stably trapped, but would not have been noticed in these simulations. The non-linear components of the electric field that lead to chaotic motion are present at all points in the stability diagram, including regions identified as “stable”. Of course, in practical applications, chaotic motion resulting from Coulombic forces from other trapped ions may be a greater effect than—or at least a different effect from—that resulting from the electric field.

Higgs et al. [43] noted patterns in nonlinear resonance bands of a toroidal harmonic field that are similar to the patterns observed in the present device, although they did not attribute these to chaotic behavior. However, the presence of these patterns indicates that the chaotic behavior in the present study is not limited to this specific electrode configuration, but may be general to toroidal ion traps. Whether chaotic trajectories also play a role in other types of ion traps remains to be seen. The asymmetry of the electrodes in toroidal traps makes it easy to observe chaotic motion. Specifically, the three ejection directions – radial inward, radial outward, and axial – have similar pseudopotential well depths but very different field shapes. Nonlinear terms are present in the electric fields of all realizable ion trap designs, so likely chaotic motion is an element in ion trajectories in other devices as well.[52] Due to the symmetry of other trap types, chaotic motion may not be observed as differences in ejection direction, but may be expressed in other aspects of ion motion. Other types of traps do, however, exhibit black canyons and black holes,[33-35] similar to the regions examined in the present work. Likely chaotic motion is a general condition resulting from nonlinear fields in quadrupole-type ion traps, although it may not play a significant role in mass analysis and performance.

3.4 Conclusion

Non-linear terms in the electric field of ion traps result in several effects on trap performance, including mass accuracy, mass resolution, and trapping capabilities. These terms also give rise to chaotic motion of the trapped ions. This effect is shown in the ejection direction of ions within resonance bands of a cylindrical-electrode toroidal ion trap. While Coulombic forces of neighboring ions can cause chaotic motion, we show that the effect is also present for individual ions, and is due only to the shape of the trapping fields. Although ion motion is strongly sensitive to initial ion parameters and trap voltages, high-resolution mass analysis (peak

widths of less than 1 amu) has been demonstrated in this specific trap. Future studies will explore the extent to which chaotic motion exists in other types of ion traps.

3.5 References

1. Jonscher, K.R.; Yates, J.R., The quadrupole ion trap mass spectrometer—A small solution to a big challenge. *Anal. Biochem*. **1997**, *244*, 1-15.

2. Gros, M.; Petrovic, M.; Barcelo, D., Tracing pharmaceutical residues of different therapeutic classes in environmental waters by using liquid chromatography/quadrupole-linear ion trap mass spectrometry and automated library searching. *Anal. Chem*. **2009**, *81* 898-912.

3. Kevin, J.J.; Crowley, J.; Hamilton, B.; Lehane, M.; Skulberg, O.; Furey, A., Anatoxins and degradation products, determined using hybrid quadrupole time-of-flight and quadrupole ion-trap mass spectrometry: forensic investigations of cyanobacterial neurotoxin poisoning. *Rapid Commun. Mass Spectrom*. **2005**, *19*, 1167-1175.

4. Philp, R.P.; Lewis, C.A.; Campbell, C.; Johnson, E., The ion trap detector as an aid to analytical chemists in the oil industry. *Org. Ceochem*. **1989**, *14*, 183-187.

5. Todd, J.J.; Barber, S.J.; Wright, I.P.; Morgan, G.H.; Morse, A.D.; Sheridan, S.; Leese, M.R.; Maynard, J.; Evans, S.T.; Pillinger, G.T.; Drummond, D.L.; Heys, S.C.; Huq, S.E.; Kent, B.J.; Sawyer, E.C.; Whalley, M.S.; Waltham, N.R., Ion trap mass spectrometry on a comet nucleus: the Ptolemy instrument and the Rosetta space mission. *J. Mass Spectrom*. **2007**, *42*, 1-10.

6. Nguyen, T.E.; Becker, L.; Doroshenko, V.; Cotter, R.J., Development of a low power, high mass range mass spectrometer for Mars surface analysis. *Int. J. Mass Spectrom*. **2008**, *278*, 170-177.

7. Paul, W.; Steinwedel, H., Apparatus for separating charged particles of different specific charges, German Patent 944,900 (1956); U.S. Patent 2,939,952 (1960)

8. Paul, W.; Steinwedel, H., A new mass spectrometer without a magnetic field, Z. *Naturforsch.* **1953**, *8a*, 448–450.

9. Knewstubb, P.F., Mass spectrometry and ion-molecule reactions, *Cambridge University Press*, Cambridge (1969)

10. Bonner, R.F.; Fulford, J.E.; Hamilton, G.F., March, R.E.: The cylindrical ion trap. Part I. General introduction. *Int. J. Mass Spectrom. Ion Processes* **1977**, *24*, 255-269.

11. Wu, G.; Cooks, R.G.; Ouyang, Z., Geometry optimization for the cylindrical ion trap: field calculations, simulations and experiments. **2005**, *24*, 119-132.

12. Schwartz, J.C.; Senko, M.W.; Syka, J.E.P., A two-dimensional quadrupole ion trap mass spectrometer. *J. Am. Soc. Mass. Spectrom.* **2002**, *13*, 659-669.

13. Hager, J.W., A new linear ion trap mass spectrometer. *Rapid Commun. Mass Spectrom.* **2002**, *16*, 512-526.

14. Li, A.; Hansen, B.J.; Powell, A.T.; Hawkins, A.R.; Austin, D.E., Miniaturization of a planar-electrode linear ion trap mass spectrometer. *Rapid Commun. Mass Spectrom.* **2014**, *28*, 1338-1344.

15. Ouyang, Z.; Wu, G.; Song Y.; Li, H.; Plass, W.R.; Cooks, R.G., Rectilinear ion trap: Concepts, calculations, and analytical performance of a new mass analyzer. *Anal. Chem*. **2004**, *76*, 4595-4605.

16. Gao, L.; Song, Q.; Patterson, G.E.; Cooks, R.G.; Ouyang, Z., Handheld rectilinear ion trap mass spectrometer. *Anal. Chem.* **2006**, *78*, 5994-6002.

17. Lammert, S.A.; Plass, W.R.; Thompson, C.V.; Wise, M.B., Design, optimization and initial performance of a toroidal rf ion trap mass spectrometer. *Int. J. Mass Spectrom.* **2001**, *212*, 25-40.

18. Austin, D.E.; Wang, M.; Tolley, S.E.; Maas J.; Hawkins, A.R.; Rockwood, A.L.; Tolley, H.D.; Lee, E.D.; Lee, M.L., Halo ion trap mass spectrometer. *Anal. Chem*. **2007**, *79*, 2927-2932.

19. Contreras, J.A.; Murray, J.A.; Tolley, S.E.; Oliphant, J.L.; Tolley, H.D.; Lammert, S.A.; Lee, E.D.; Later, D.W.; Lee, M.L., Hand-portable gas chromatograph-toroidal ion trap mass spectrometer (GC-TMS) for detection of hazardous compounds. *J. Am. Soc. Mass. Spectrom.* **2008**, *19*, 1425-1434.

20. Taylor, N.; Austin, D.E., A simplified toroidal ion trap mass analyzer. *Int. J. Mass Spectrom.* **2012,** *321-322*, 25-32.

21. March, R.E.; Todd, J.F.J., Quadrupole ion trap mass spectrometry (2nd ed.). *John Wiley & Sons*, New York (2005)

22. March, R.E.; McMahon, A.W.; Londry, F.A.; Alfred, R.J.; Todd, J.F.J.; Vedel, F., Resonance excitation of ions stored in a quadrupole ion trap. Part 1. A simulation study. *Int. J. Mass Spectrom. Ion Processes* **1989**, *95*, 119–156.

23. March, R.E.; Londry, F.A.; Alfred, R.L.; Penman, A.D.; Todd, J.F.J.; Vedel, F.; Vedel, M., Resonance excitation of ions stored in a quadrupole ion trap. Part 2. Further simulation studies. *Int. J. Mass Spectrom*. *Ion Processes* **1991**, *110*, 159–178.

24. Londry, F.A.; Collings, B.A.; Stott, W.R., Fragmentation of ions by resonant excitation in a high order multipole field, low pressure ion trap, U.S. Patent Application No. 2003/0189171 (2003).

25. Schwartz, J.C.; Jaardine, L., High resolution parent-ion selection/isolation using a quadrupole ion-trap mass spectrometer. *Rapid Commun. Mass Spectrom.* **1992**, *6*, 313-317.

26. Londry, F.A.; Hager, J.W., Mass selective axial ion ejection from a linear quadrupole ion trap. *J. Am. Soc. Mass. Spectrom.* **2003**, *14*, 1130-1147.

27. Berkeland, D.J.; Miller, J.D.; Bergquist, J.C.; Itano, W.M.; Wineland, D.J., Minimization of ion micromotion in a Paul trap. *J. Appl. Phys*. **1998**, *83*, 5025-5033.

28. Higgs, J.; Austin, D.E., Simulation of ion motion in toroidal ion traps. *Int. J. Mass Spectrom.* **2014**, *363*, 40-51.

29. Huo, X.; Tang, F.; Chen, J.; Zhang, X.; Wang, X., Characterization of the impact of the ejection slit on miniature rectilinear ion trap analysis. *Int. J. Mass Spectrom* **2016**, **399-400**, 44-50.

30. Yang, H.; Xu, C.; Yue, L.; Mikhail, S.; Pan, Y.; Ding, C., Optimization of Performance of Toroidal Ion Trap with Trianglar Electrode by Theoretical Simulation. *Chinese J. Anal. Chem*. **2016**, *44*, 482-488.

31. Wu, Q.; Tian, Y.; Li, A.; Austin, D.E., Simulations of electrode misalignment effects in two-plate linear ion traps. *Int. J. Mass Spectrom.* **2015**, *393*, 52-57.

32. Blain, M.G.; Riter, L.S.; Cruz, D.; Austin, D.E.; Wu, G.; Plass, W.R.; Cooks, R.G., Towards the hand-held mass spectrometer: design considerations, simulation, and fabrication of micrometer-scaled cylindrical ion traps. *Int. J. Mass Spectrom.* **2004**, *236*, 91-104.

33. Alheit, R.; Hennig, C.; Morgenstern, R.; Vedel, F.; Werth, G., Observation of instabilities in a Paul trap with higher-order anharmonicities. *J. Appl. Phys. B*. **1995**, *61*, 277-283.

34. Eades, D.M.; Yost, R.A.; Cooks, R.G., Black canyons for ions stored in an ion-trap mass spectrometer. *Rapid Commun. Mass Spectrom.* **1992**, *6*, 573-578.

35. Guidugli, F.; Traldi, P., A phenomenological description of a black hole for collisionally induced decomposition products in ion‐trap mass spectrometry. *Rapid Commun. Mass Spectrom.* **1991**, *5*, 343-348.

36. Michaud, A.L.; Frank, A.J.; Ding, C.; Zhao, X.; Douglas, D.J., Ion Excitation in a Linear Quadrupole Ion Trap with an Added Octopole Field. *J. Am. Soc. Mass. Spectrom.* **2005**, *16*, 835-849.

37. Eades, D.M.; Johnson, J.V.; Yost, R.A., Nonlinear resonance effects during ion storage in a quadrupole ion trap. *J. Am. Soc. Mass. Spectrom.* **1993**, *4*, 917-929.

38. Franzen, J.; Gabling, R.H.; Schubert, M.; Wang, Y., Non-linear ion traps. In: March, R.E.; Todd, J.F.J. (eds.) Practical aspects of ion trap mass spectrometry (Vol. I), p. 49. CRC Press, Boca Raton, NY, (1995)

39. Wu, G.; Cooks, R.G.; Ouyang, Z., Geometry optimization for the cylindrical ion trap: field calculations, simulations and experiments. *Int. J. Mass Spectrom.* **2005**, *241*, 119-132.

40. Wang, M.; Quist, H.E.; Hansen, B.J.; Peng, Y.; Zhang, Z.; Hawkins, A.R.; Rockwood, A.L.; Austin, D.E.; Lee, M.L., Performance of a halo ion trap mass analyzer with exit slits for axial ejection, *J. Am. Soc. Mass Spectrom.* **2011**, *22*, 369–378.

41. Kotana, A.N.; Mohanty, A.K., Determination of multipole coefficients in toroidal ion trap mass analysers. *Int. J. Mass Spectrom.* **2016**, *408*, 62-76.

42. Kotana, A.N.; Mohanty, A.K., Computation of Mathieu stability plot for an arbitrary toroidal ion trap mass analyser. *Int. J. Mass Spectrom.* **2017***, 414*, 13-22.

43. Higgs, J.M.; Petersen, B.V.; Lammert, S.A.; Warnick, K.F.; Austin, D.E., Radiofrequency trapping of ions in a pure toroidal potential distribution. *Int. J. Mass Spectrom.* **395**, 20-26 (2016)

44. Schuldberg, D., Chaos Theory and Creativity. *Encyclopedia of Creativity (2nd ed.). Academic Press*, Massachusetts, 183-191 (2011)

45. Weber, H.; Arfken, G.B., Nonlinear methods and chaos (Chapter 19). *Essentials of Math Methods for Physicists, Academic Press*, Massachusetts (2013)

46. Blümel, R., A introduction to chaos in dynamic ion traps. *Phys. Scripta*. **1995**, *T59*, 126-130.

47. Baumann, G.; Nonnenmacher, T.F., Regular and chaotic motions in ion traps: A nonlinear analysis of trap equations. *Phys. Rev. A*. **1992**, *46*, 2682-2692.

48. Hoffnagle, J.A.; Brewer, R.G., Two-ion chaos. *Phys. Scripta*. **1995**, *T59*, 380-386.

49. Hasegawa, T.; Uehara, K., Nonlinear dynamics of two particles in the RF trap. *Prog. Crystal Growth and Charact*. **1996**, *33*, 401-404.

50. Walther, H., From a single ion to a mesoscopic system - crystallization of ions in Paul traps. *Phys. Scripta*. **1995**, *T59*, 360-368.

51. Berman, G.P.; James, D.F.V.; Hughes, R.J.; Gulley, M.S.; Holscheiter, M.H.; Lopez, G.V., Dynamical stability and quantum chaos of ions in a linear trap. *Phys. Rev. A*. **2000**, *61*, 023403.

52. Ding, C.; Konenkov, N.V.; Douglas, D.J., Quadrupole mass filters with octopole fields. *Rapid Commun. Mass Spectrom*. **2003,** *17*, 2495-2502.

53. Konenkov, N.V.; Londry, F.; Douglas; D.J.; Ding, C., Linear quadrupoles with added hexapole fields, *J. Am. Soc. Mass Spectrom.* **2006**, *17*, 1063–1073.

4 MINIATURIZED CYLINDRICAL TOROIDAL ION TRAP MASS ANALYZER

4.1 Toroidal Ion Trap

In ion trap development, the toroidal ion trap was directly derived from the 3D quadrupole ion trap by rotating the cross section of a quadrupole ion trap along an axis located outside of the trapping region.[1,2] The toroidal ion trap consists of a central electrode, an outer ring electrode, and two end-caps, all based on hyperbolic surfaces of revolution (Figure 4-1). Analogous to the LIT, the toroidal trap exhibits a larger trapping capacity—ions are trapped in a torus or ring region and ejected through slits in the end-cap electrodes.

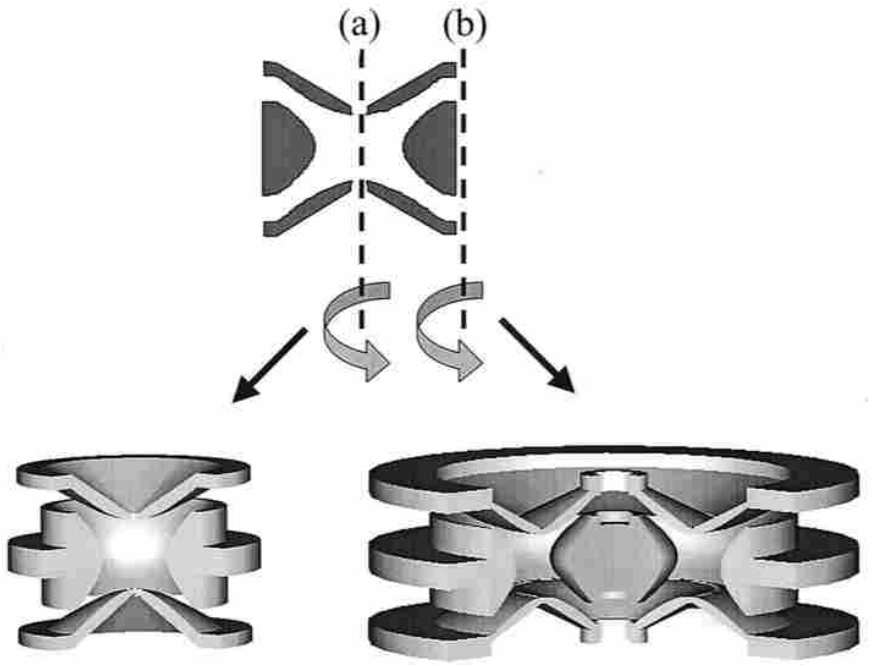

Figure 4-1: The result of rotating a conventional 3D ion trap cross-section. Rotation on an axis that intersects at the intersection of the hyperbolae (a) gives the conventional 3D ion trap geometry. Rotation on an axis that is placed at some distance away from the intersection of the hyperbolae (b) gives a toroidal trapping geometry.[1]

As mentioned in Chapter 3, the electric field is more complicated in the toroidal ion trap than other types of ion traps due to the curvature generated from the torus geometry. In the original design of the torodial ion trap, the electric field trapping center is slightly off, toward the ejection slit, due to the curvature (Figure 4-2). Therefore, the ejected ion would easily hit the electrode close to the slit, which would significantly reduce the ion ejection efficiency. To address this problem, Taylor and Austin developed a cylindrical toroidal ion trap (CTIT) by rotating 360 degrees along an axis that is out of the cross section of a cylindrical ion trap, which makes the ejection direction different from the original toroidal ion trap (Figure 1-9, Figure 3-3). In this way, the curvature did not move the trapping center, and the electrode geometry of the toroidal ion trap was simplified from the hyperbolic to cylindrical (Figure 4-3).

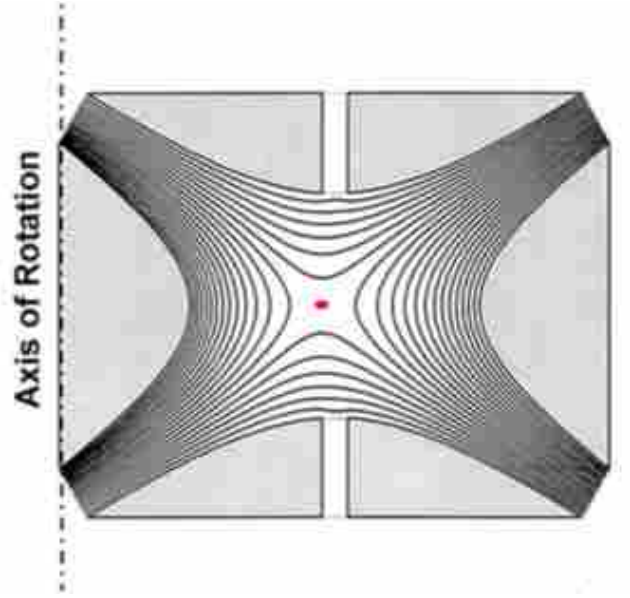

Figure 4-2: Electric field distortion (misaligned trapping center and ejection slit) of toroidal ion trap caused by curvature.

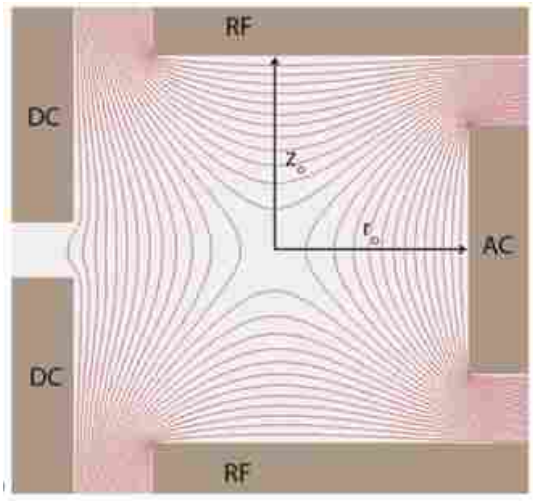

Figure 4-3: Electric field in cylindrical toroidal ion trap. Movement of the trapping center due to curvature is not relevant to ion ejection; ion ejection is always aligned with the ejection slit.[4]

4.2 Miniaturized Cylindrical Toroidal Ion Trap

The miniaturized cylindrical toroidal ion trap developed by Taylor and Austin has been demonstrated.[8] The electric field was also studied and discussed in Chapter 3. Here, we further miniaturized the cylindrical toroidal ion trap to 1/3 of its original published size to demonstrate its feasibility and performance.

4.2.1 Instrumentation

Figure 3-3 (previous chapter) shows the design of the original cylindrical toroidal ion trap. The dimensions of the published trap are R = 36.15 mm, r_0 = 5.91 mm, z_0 = 5.81 mm and slit width = 1.6 mm, with a reported hexapole component of -2.3%, octopole of +0.8%, and decapole of -3.6%. In this experiment, the dimensions of the miniaturized ion trap, scaled at 1/3 of the original size, are R = 12.05 mm, r_0 = 1.97 mm, z_0 = 1.94 mm, slit width = 0.53 mm.

4.2.2 Mass Analysis

The mass-selective instability scan in both forward and reverse mode was initially used with a linear ramp of the RF amplitude with a constant additional AC signal. The RF frequency was 3.405 MHz, which is ~3 times the frequency used in the published trap. The RF voltage ramp was varied each time using different trapping, starting, and ending voltages to obtain and optimize the signal. The AC frequency and amplitude were also varied to determine the resonant ejection point. The signals from 100 scans were averaged to produce a single spectrum. The uncorrected pressure of sample gasses in the vacuum chamber was 5.0×10^{-5} Torr, and the uncorrected pressure of the background helium buffer gas was 3.0×10^{-3} Torr, measured with a Pfeiffer DPG-202 wide range vacuum gauge. Toluene, deuterated toluene (D_8-toluene), benzene, n-heptane and isobutylbenzene were separately analyzed with the electron ionization source.

4.3 Results and Discussion

Peaks from all the samples were observed using a mass-selective instability forward scan. The mass spectrum of benzene is shown in Figure 4-4. However, the peak position did not move when varying the AC frequency and the mass resolution was not acceptable. In an RF voltage ramp, the q value of the ions increases with the increased RF voltage. When an AC signal is applied, a resonant line would be created at the stability diagram. The ions approach the resonant line with an increased q value, and are eventually resonantly ejected at the resonant point. When the AC frequency is changed, the position of the resonant line should be changed as well, so that the same peak should be ejected at a different times when varying AC frequencies, but the peaks stayed constant position through this experiment. Therefore, we may conclude that the peaks might not be caused by AC resonant ejection.

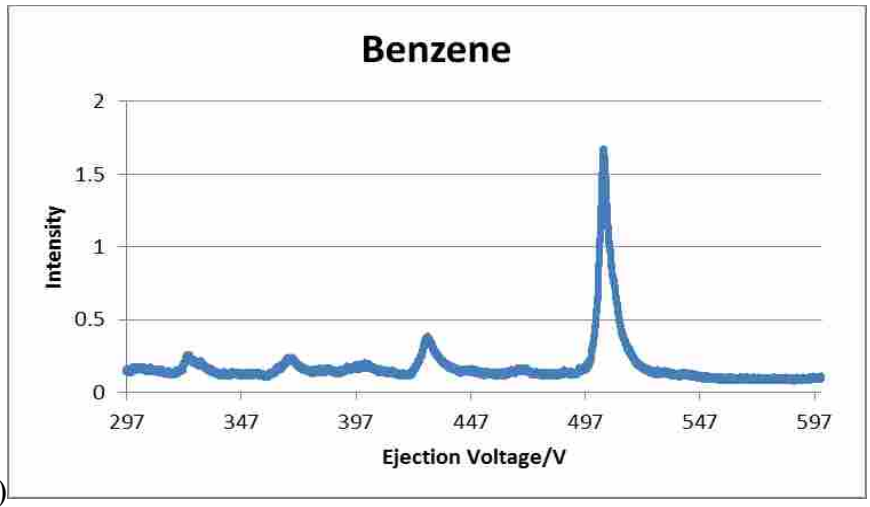

(a)

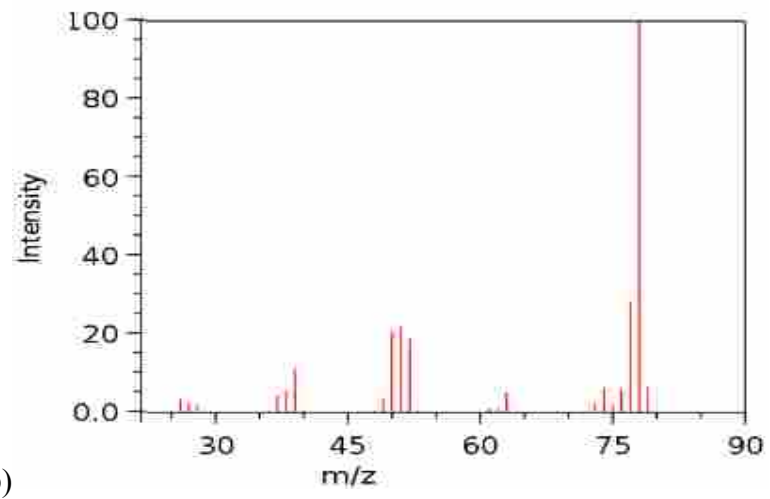

(b)

Figure 4-4: (a) Forward scan mass spectrum of benzene with applied AC waveform; (b) EI-mass spectrum of benzene from NIST database

The RF was used, while the AC waveform was turned off, to determine the ejection mode. The peaks were the same with the applied AC waveform, which may be due to boundary ejection. However, peaks can also be observed in the reverse scan without applying the AC waveform (Figure 4-5). Theoretically, boundary ejection could not occur in the reverse scan, since ions would not be trapped initially outside of the stable region. Therefore, a possible explanation is that the peaks were ejected from black canyons.

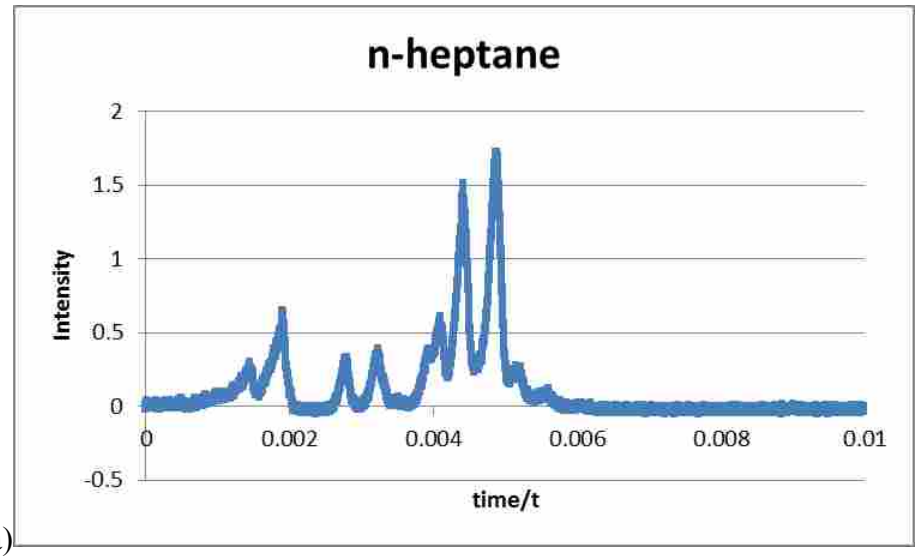
n-heptane
Intensity
time/t
2
1.5
1
0.5
0
-0.5
0
0.002
0.004
0.006
0.008
0.01

(a)

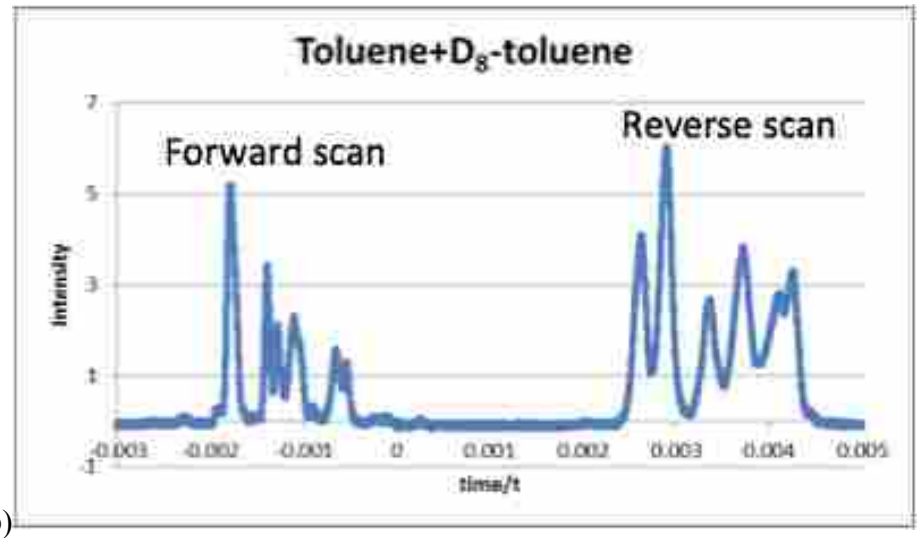
Toluene+D8-toluene
Forward scan
Reverse scan
Intensity
time/t

(b)

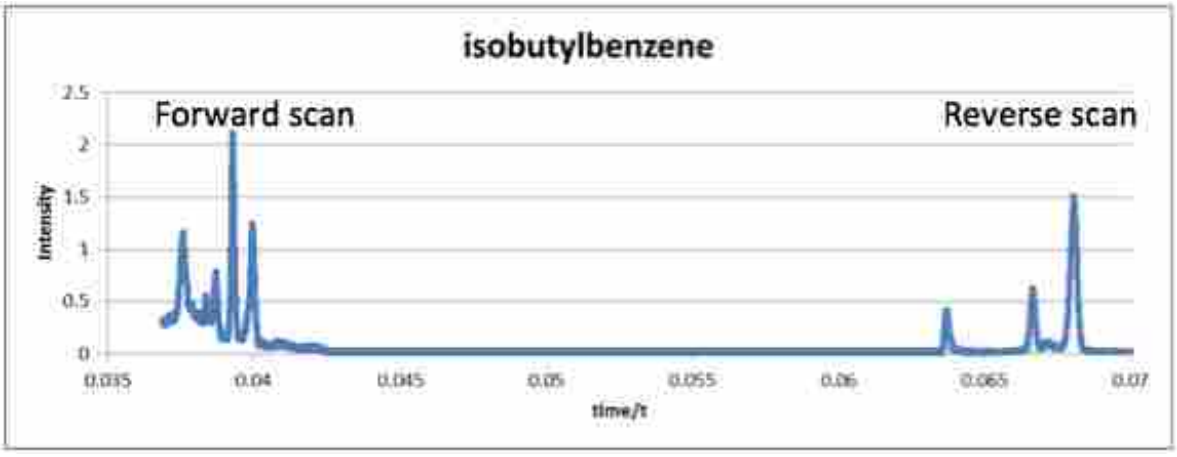
isobutylbenzene
Forward scan
Reverse scan
Intensity
time/t
2.5
2
1.5
1
0.5
0
0.035
0.04
0.045
0.05
0.055
0.06
0.065
0.07

(c)

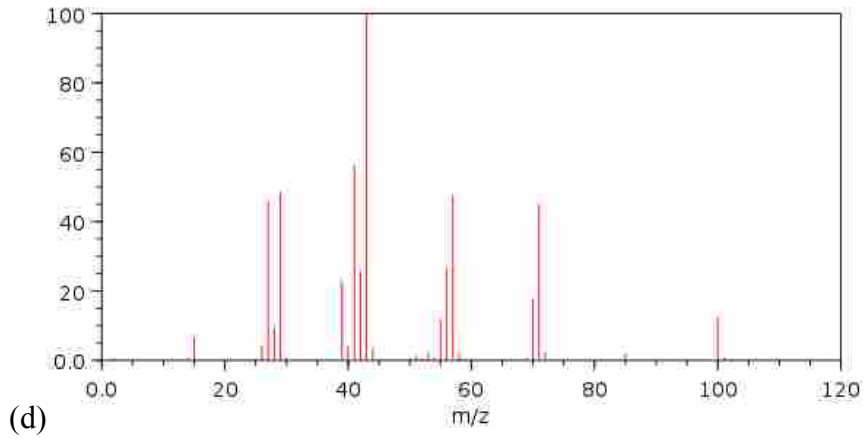

(d)

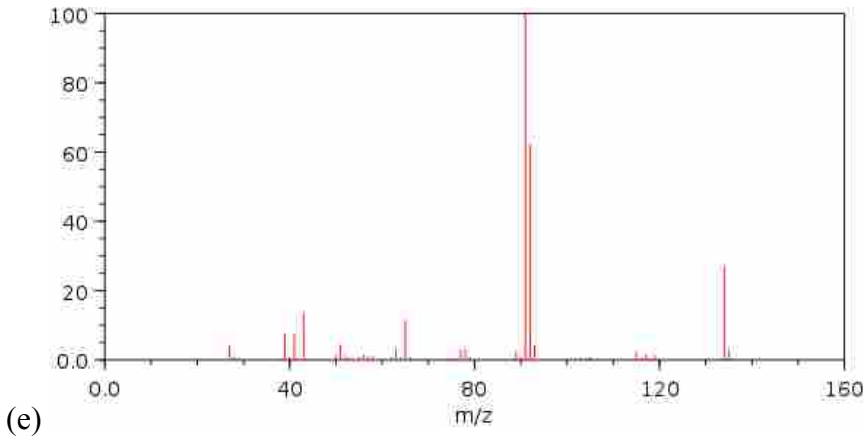

(e)

Figure 4-5: (a) Reverse scan mass spectrum of n-heptane without AC waveform; (b) RF waveform consists of both forward and reverse scans - mass spectrum of n-heptane without AC waveform; (c) RF waveform consists of both forward and reverse scans - mass spectrum of isobutylbenzene without AC waveform; (d) EI-mass spectrum of heptane from NIST database; (e) EI-mass spectrum of isobutylbenzene from NIST database

In the simulation study in Chapter 3, several black canyons were observed in the stable region, which would cause unexpected ion ejection during mass analysis.[7] When ions approach a black canyon, they pick up as much energy as they would from a resonant line directly made by the AC. Then, the ion excursion would increase for ion ejection. Unlike the AC resonant line, black canyons can only provide a small amount of energy for ion excursion and non-linear resonant ejection. Thus, the mass resolution of the peaks observed from a black canyon ejection

is much lower than that of an AC ejection, an important reason why black canyon ejection should be avoided.

Ions with the same mass-to-charge ratio should be ejected at the same q value, at the same time. However, if the stable region contains complex non-linear resonant lines (black canyons), ions with the same mass-to-charge ratio would reach the black canyons successively when the q value increases or decreases during mass analysis, and only a small portion of the ions would be ejected at each black canyon. Therefore, the mass spectrum would be reflected as multi-peaks for the same ions. The only solution to this problem without optimizing the trap geometry is to restrict the q value of the ions within a small range, in which the stable area is clear of any black canyons.

As shown in Figure 4-4 and 4-5, there are peaks that do not follow current theories, and could not be assigned at this time. If the peaks are the ions ejected at only one black canyon, the converted mass-to-charge ratio of the ions should be linear as a function of the ejection voltage, but the calculated result was nonlinear. If the peaks were the ions ejected at multiple black canyons, it would be impossible to assign the mass-to-charge ratio of the ions.

Therefore, the electric field of the miniaturized cylindrical toroidal ion trap may not be efficient for mass analysis due to the strong black canyon effect. The next step on this experiment would be electric field optimization that a calculated portion of nonlinear higher order terms could be added into the electric field to compensate the black canyon in the stable region. After determining the portion of higher order terms, the electrode shape or position of the cylindrical toroidal ion trap would be adjusted to obtain the expected electric field.

4.4 Conclusion

The mass analysis performance of the one-third scale miniaturized cylindrical toroidal ion trap was studied, which was impacted by the black canyon effect. Several peaks were observed at a fixed time with varied AC frequency, many of which could not be assigned due to random ejections. In addition, the mass resolution of the peaks was not acceptable, due to the black canyon effect. The black canyon effect was caused by a distorted electric field, which may be optimized in a follow-up experiment. The higher order nonlinear terms of the electric field would be studied and optimized for electrode repositioning and redesign, which might eliminate the black canyon effect in the stable region and improve the ion trap performance.

4.5 References

1. Lammert, S.A.; Plass, W.R.; Thompson, C.V.; Wise, M.B., Design, optimization and initial performance of a toroidal rf ion trap mass spectrometer. *Int. J. Mass Spectrom*. **2001**, *212*, 25-40.

2. Lammert, S.A.; Rockwood, A.A.; Wang, M.; Lee, M.L.; Lee, E.D.; Tolley, S.E.; Oliphant, J.R.; Jones, J. L.; Waite, R.W., Miniature toroidal radio frequency ion trap mass analyzer. *J. Am. Soc. Mass Spectrom*. **2006**, *17*, 916-922.

3. Higgs, J.M.; Petersen, B.V.; Lammert, S.A.; Warnick, K.F.; Austin, D.E., Radiofrequency trapping of ions in a pure toroidal potential distribution. *Int. J. Mass Spectrom.* **395**, 20-26 (2016)

4. Higgs, J.M.; Austin, D.E., Simulation of ion motion in toroidal ion traps. *Int. J. Mass Spectrom.* **2014**, *363*, 40-51.

5. Kotana, A.N.; Mohanty, A.K., Determination of multipole coefficients in toroidal ion trap mass analysers. *Int. J. Mass Spectrom.* **2016**, *408*, 62-76.

6. Kotana, A.N.; Mohanty, A.K., Computation of Mathieu stability plot for an arbitrary toroidal ion trap mass analyser. *Int. J. Mass Spectrom.* **2017***, 414*, 13-22.

7. Li, A.; Higgs, J.M.; Austin, D.E., Chaotic motion of single ions in a toroidal ion trap mass analyzer. *Int. J. Mass Spectrom.* **2017**, *In Press*.

8. Taylor, N.; Austin, D.E., A simplified toroidal ion trap mass analyzer. *Int. J. Mass Spectrom*. **2012,** *321-322*, 25-32.

5 PERSPECTIVE AND FUTURE WORK

5.1 Summary

Three types of miniaturized ion trap mass analyzers were presented in this dissertation. These include the 1/3 scale cylindrical toroidal ion trap; the wire linear ion trap[3]; and both the sub-mm spacing planar linear ion trap, and large-plate planar linear ion trap with dual spacing.[1,2] The planar linear ion traps consist of two ceramic substrates that are lithographically patterned aluminum electrodes coated with a thin layer germanium. The two plates are aligned using sapphire balls and contact, with a printed circuit board (PCB) on the backside. The PCBs also connect to electric power supplies that provide different voltages to each electrode on the ceramic plates. A quadrupolar electric field is then generated via applying the voltages on the electrodes, and the electric field can also be adjusted and optimized by changing the voltage distribution on the electrodes. In the miniaturization of the large spacing linear ion trap, spacing was moved closer together without remaking the ceramic plates and electric fields were redesigned via changing the capacitive voltage dividers on the PCBs. In the wire linear ion trap, twenty-four stainless steel wires are aligned and held tight between two plates. A quadrupolar electric field is created via applying different RF and AC waveforms on each electrode. The electric field can be adjusted by changing the wire position. In the miniaturized cylindrical toroidal ion trap, the electrodes are miniaturized to 1/3 of the original cylindrical toroidal ion trap. By adjusting the position of the RF electrodes of the cylindrical toroidal ion trap, the electric field could be slightly changed.

5.2 Future Work

5.2.1 Sub-mm Linear Ion Trap

The feasibility of the 724 μm-spacing LIT was not demonstrated due to the electrode and plate design problems mentioned in Chapter 3, which have been used as the guide to the following linear ion trap design. The next generation plate has a tapered shape at the slit area, so that the ions can be ejected out of the narrow slit instead of hitting the slit edge (Figure 5-1).

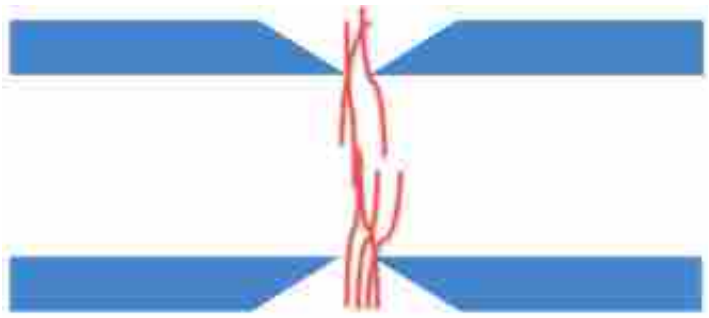

Figure 5-1: Tapered LIT plate

An alternative plan is proposed for the sub-mm LIT, which is to design a linear ion trap using only PCBs instead of using both PCBs and ceramic plates. All the electrodes are patterned on the PCBs and applied with electronic signal directly from the power supply. Compared to the ceramic plate, PCB is less expensive, more rugged and easily fabricated. Three-month fabrication time and $200 price for each ceramic plate would be greatly reduced to three days and $20 for each PCB. Since the precision of PCB is not as good as that of ceramics, the linear ion trap using PCBs would be studied at a larger plate spacing than the sub-mm spacing. In addition, the PCBs would be fabricated with a tapered plate, as seen in Figure 5-1.

By using a PCB-based linear ion trap, a two-plate PCB quadrupole-quadrupole-LIT (Q-Q-LIT) system could be completed, which consists of two PCB plates patterned with electrodes to generate two quadrupole ion guides and a linear ion trap in series (Figure 5-2). The first quadrupole is used to guide ion or perform collision induced dissociation (CID) in rough vacuum. The second quadrupole ion guide in high vacuum will axially transfer the ions into the LIT. Mass analysis can be performed in the LIT. There is an end-bar wall with an injection hole between each component. Electrospray ionization (ESI) will be used instead of EI. Mass-selective instability and digital waveform methods would be used for mass analysis. This two-plate mass spectrometry system would become a novel method for portable-MS development.

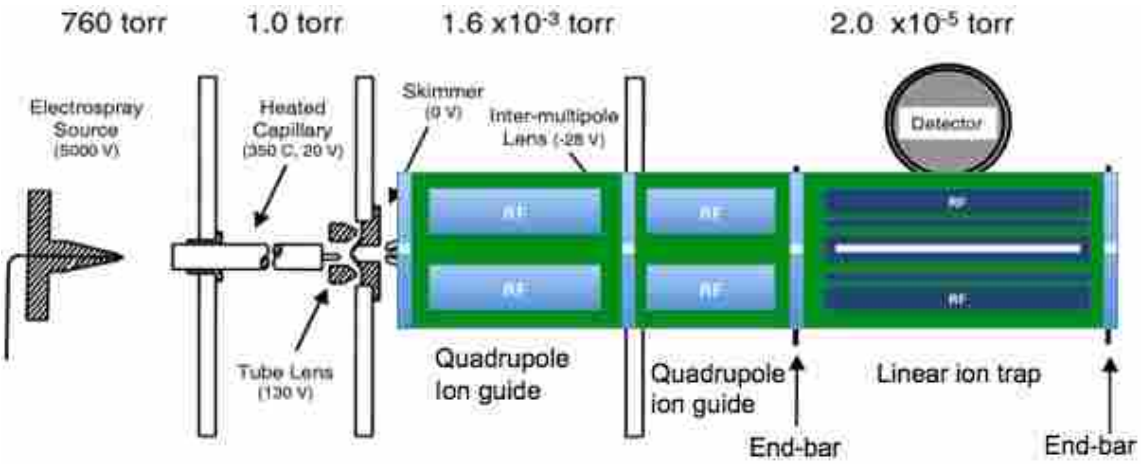

Figure 5-2: Two-plate PCB quadrupole-quadrupole-LIT (Q-Q-LIT) system.

5.2.2 One-third Scale Cylindrical Toroidal Ion Trap

In the previous experiment on the one-third scale cylindrical toroidal ion trap, the black canyon effect significantly affected the mass analysis. The electric field should be optimized to

eliminate the black canyon effect. The direct way is to adjust the position and distance between the two RF electrodes without remaking the electrodes, which may partially eliminate the black canyon effect. However, it is not deterministic since slight change in the electrode position may not eliminate the black canyon completely. Another method to solve this problem is to redesign the electrode configuration. The electric field would be optimized and studied in a simulation by adding different portion of nonlinear higher order terms. The optimized electric field may not contain black canyons in the stable region, which would lead to performing a more efficient mass analysis.

5.3 Development of the Miniaturized Mass Analyzers

Four miniaturized ion trap mass analyzers were discussed and studied here, including miniaturized linear ion trap with spacing of 4.38 mm and 1.9 mm, sub-mm linear ion trap, wire linear ion trap and cylindrical toroidal ion trap in both original and 1/3 miniaturized sizes. Each of them has unique capabilities with different advantages and drawbacks. In the future, miniaturized ion traps would experience continuous evolution and improvement. The next step for the linear ion trap would be developing sub-mm mass analyzer with good mass resolution and larger trapping capacity compared to the other traps in the same size. Although there are many challenges to the size reduction, they would be revealed and addressed in this process. For the wire linear ion trap, the characteristics of simple-made and robust make it promising for the trap miniaturization, especially working in the harsh environments. For the cylindrical toroidal ion trap, the trap at original size has been commercialized to provide outstanding performance, so it is also worthy to be further miniaturized. However, the complex electric field would be a challenge to the miniaturization, which should be effectively addressed in the future.

5.4 References

1. Hansen, B.J.; Niemi, R.J.; Hawkins, A.R.; Lammert, S.A.; Austin, D.E., A lithographically patterned discrete planar electrode linear ion trap mass spectrometer. *J. Microelectromech. Syst*. **2013**, *22*, 876-883.

2. Li, A.; Hansen, B.J.; Powell, A.T.; Hawkins, A.R.; Austin, D.E., Miniaturization of a Planar-Electrode Linear Ion Trap Mass Spectrometer. *Rapid Commun. Mass Spectrom*. **2014**, *28*, 1338-1344.

3. Wu, Q.; Li, A.; Tian, Y.; Zare, R.N.; Austin, D.E., Miniaturized Linear Wire Ion Trap Mass Analyzer. *Anal. Chem*. **2016**, *88*, 7800-7806.